



HAL
open science

On the Study of Large-Dimension Reconfigurable Cable-Driven Parallel Robots

Dinh Quan Nguyen

► **To cite this version:**

Dinh Quan Nguyen. On the Study of Large-Dimension Reconfigurable Cable-Driven Parallel Robots. Automatic. UNIVERSITE MONTPELLIER 2, 2014. English. NNT : . tel-02409262

HAL Id: tel-02409262

<https://theses.hal.science/tel-02409262>

Submitted on 13 Dec 2019

HAL is a multi-disciplinary open access archive for the deposit and dissemination of scientific research documents, whether they are published or not. The documents may come from teaching and research institutions in France or abroad, or from public or private research centers.

L'archive ouverte pluridisciplinaire **HAL**, est destinée au dépôt et à la diffusion de documents scientifiques de niveau recherche, publiés ou non, émanant des établissements d'enseignement et de recherche français ou étrangers, des laboratoires publics ou privés.

THÈSE

Pour obtenir le grade de
Docteur

Délivré par **UNIVERSITE MONTPELLIER 2**

Préparée au sein de l'école doctorale : **Information,
Structures, Systèmes**

Et de l'unité de recherche : **Laboratoire d'Informatique de
Robotique et de Microélectronique de Montpellier**

Spécialité : **Génie Informatique, Automatique et Traitement
du Signal**

Présentée par **Dinh Quan NGUYEN**

**On the Study of Large-Dimension
Reconfigurable Cable-Driven Parallel Robots**

Soutenue le 18/12/2014 devant le jury composé de

Mr. Jacques GANGLOFF, Professor, University of Strasbourg, France	Reviewer
Mr. Andreas POTT, Professor, University of Stuttgart, Germany	Reviewer
Mr. Cédric BARADAT, Director of Technology, Tecnalia France	Examiner
Mr. François PIERROT, Research Director, LIRMM/CNRS, France	Supervisor
Mr. Marc GOUTTEFARDE, Researcher, LIRMM/CNRS, France	Joint Supervisor

ACADÉMIE DE MONTPELLIER

UNIVERSITÉ MONTPELLIER II

Sciences et Techniques du Languedoc

PH.D THESIS

présentée au Laboratoire d'Informatique de Robotique
et de Microélectronique de Montpellier pour
obtenir le diplôme de doctorat

Spécialité : **Génie Informatique, Automatique et Traitement du Signal**
Formation Doctorale : **Systèmes Automatiques et Microélectroniques**
École Doctorale : **Information, Structures, Systèmes**

On the Study of Large-Dimension Reconfigurable Cable-Driven Parallel Robots

by

Dinh Quan NGUYEN

Soutenance on 18 December 2014, before the jury composed of :

President

Mr. Jacques GANGLOFF, Professor University of Strasbourg, France

Reviewers

Mr. Andreas POTT, Professor University of Stuttgart, Germany

Examiners

Mr. Cédric BARADAT, Director of Technology Tecnalía France

Supervisor

Mr. François PIERROT, Research Director LIRMM/CNRS, France

Joint Supervisor

Mr. Marc GOUTTEFARDE, Researcher LIRMM/CNRS, France

ACKNOWLEDGEMENT

First and foremost, my utmost appreciation to my thesis supervisor, Dr. Marc Gouttefarde, whose invaluable advice, guidance, patience, sincerity, encouragement I will never forget. My gratitude for his kind and constant support is beyond words.

I would like to express my thanks to all the partners involved in the CableBOT project: from CNRS LIRMM (Mr. Marc Gouttefarde, Mr. François Pierrot,...), from Tecnalía (Ms. Mariola Rodríguez, Mr. Micaël Michelin, Mr. Cédric Baradat), from INRIA (Mr. Jean-Pierre Merlet, Mr. Laurent Blanchet), from IPA Germany (Mr. Andreas Pott, Mr. Philipp Miermeister), from UDE Germany (Mr. Tobias Bruckmann, Mr. Christopher Reichert, Ms. Katharina Müller), from EADS France (Mrs. Marie-Paule Guillou), from ACCIONA Spain (Mr. Manuel Palomino), from VICINAY CEMVISA Spain (Mr. Jesús Canãda, Mr. José Ignacio Olmos) and from the European commission (Mr. Vincenzo Nicoló). It was my great pleasure to work with them during the 3 years of CableBOT project. I have learnt a lot and gain a lot of invaluable experience in cable robots, in robotics. During this time, I have the opportunities of meeting with many great people in various robotic fields all around the world.

I would also like to thank my friend and colleague, Johann Lamaury, with whom I had the pleasure of working in the same laboratory and sharing ideas on cable robots during my first two years. My great thanks to Pierre-Elie Herve, with whom I have spent days of exciting experiments on the CoGiRo prototype. Without his help I may get lost on the theoretical highway. Special thanks to Samah Shayya my neighbor colleague (his desk is right next to mine in the lab room), a workaholic and very academic friend. His comments and arguments on various topics related to kinematics and dynamics of parallel robots are greatly appreciated. I used to find myself ashamed before his tenacity of doing research. Thanks to that sometimes it boosts me more energy to work harder during my PhD life.

Many thanks to all general staffs at LIRMM who helped me complete my thesis. Special thanks to Mr. Nicolas Serrurier, who is always be there giving kindness supports to PhD students like me to deal with complicated administrative procedures during my staying in Montpellier, France.

This thesis is dedicated to my dear parents and brother, who always give me the confidence and strength to pursue my goals. Their unconditional support and voices filled with love always give me energy and motivation.

CONTENTS

Acknowledgement	I
Contents	III
List of Figures	VI
List of Tables	IX
Notations	X
1 Introduction	1
1.1 Thesis Context	1
1.2 CDPRs: an Overview	3
1.3 Recent Developments of Reconfigurable CDPRs	12
1.4 On the Use of Large-Dimension Reconfigurable CDPRs in Two Targeted Industrial Applications	13
1.4.1 Factory Workshop	13
1.4.2 Airplane Maintenance Workshop	21
1.5 Contributions and Content of the Thesis	27
2 Preliminaries	29
2.1 General CDPR Modeling	30
2.1.1 Kinetostatic Modeling	30
2.1.2 Dynamic Modeling	31
2.2 Cable Modeling	32
2.2.1 Cable Profile	33
2.2.2 Linearization	36
2.2.3 A Limitation of the Simplified Cable Model	37
2.2.4 Computation of the Cable Unstrained Length	39
2.3 The Tension Distribution Problem	41

2.4	Stiffness Matrix of CDPRs	43
2.4.1	Stiffness Matrix of One Cable	43
2.4.2	Stiffness Matrix of 6-DOF CDPRs	45
2.5	On the Collision Detection Problems	47
2.5.1	Interferences between Cables and Cables	48
2.5.2	Interferences between Cables and the CDPR Mobile Platform	51
2.5.3	Checking that a Given Workspace is Collision Free	54
2.5.4	Example	56
3	Extended Modeling - Application to the CoGiRo CDPR	59
3.1	The Modeling and Control of the CoGiRo CDPR	61
3.1.1	Assumptions	61
3.1.2	Using the Inverse Kinematics Solution in the CDPR Control Scheme	63
3.1.3	Modeling of Friction	64
3.2	Cable Profile with Thermal Effect	67
3.2.1	Catenary Equation with Thermal Effect	67
3.2.2	Linear Relationship between Cable Force Components	68
3.3	CDPR Extended Modeling	68
3.3.1	Cable Segment between the Drum and the Pulley	68
3.3.2	Cable Segment between the Pulley and the Cable Anchor Point	70
3.4	Solving the Inverse Kinetostatic Problem Using the Catenary Cable Model	73
3.5	Error Analysis	78
3.5.1	Impact of Thermal Effect	79
3.5.2	Impact of Cable Characteristics	80
3.5.3	Impact of the Method to Solve the CDPR Tension Distribution Problem	81
3.6	Case Study	82
3.6.1	Case 1: Neglecting the Influence of the Pulleys and of Friction	82
3.6.2	Case 2: CoGiRo with Extended CDPR Modeling	88
4	The CDPR Reconfiguration Problem	92
4.1	Introduction	93
4.1.1	Large-Dimension Reconfigurable Suspended CDPR Architecture	93
4.1.2	The General Problem of CDPR Reconfiguration	95
4.2	CDPR Reconfiguration as a Single-Objective Optimization Problem	96
4.2.1	Performance Indices	96
4.2.2	Step 1: Define Desired CDPR Performances	97
4.2.3	Step 2: Formulate Two Optimization Sub-Problems	98
4.2.4	Step 3: Determining the CDPR Reconfiguration	99

4.2.5	Case Study	101
4.2.6	Remark on the Methodology	105
4.3	CDPR Reconfiguration as a Multi-Objective Optimization Problem	107
4.3.1	Performance Indices	109
4.3.2	Scalarization of the Performance Indices	112
4.3.3	Systematic Procedure to Solve a Reconfiguration Problem	114
4.3.4	Case Study	115
5	Conclusion	121
	Publications	125
	Conferences	125
A	Complementary Modeling	127
A.1	Extended Modeling: a General Case	127
A.1.1	Cable Segment between Two Vertically Aligned Pulleys	129
A.1.2	Cable Segment between Two Horizontally Aligned Pulleys	130
A.1.3	Cable Segment between the Drum and the First Pulley	131
A.2	Tangent Point between a Line and a Circle	134

LIST OF FIGURES

1.1	The NIST Robocrane	7
1.2	The FALCON prototype	7
1.3	The DeltaBot prototype	8
1.4	The SEGESTA prototype	8
1.5	The IPAnema CDPR family	9
1.6	The ReelAx8 prototype	9
1.7	The CoGiRo prototype	10
1.8	The MARIONET crane prototype	10
1.9	The FAST project	10
1.10	Spidercam	11
1.11	Skycam	11
1.12	Handling heavy parts using cranes	13
1.13	All winches are mounted on one overhead bridge crane	15
1.14	A CDPR on two overhead bridge cranes	16
1.15	All winches can move: two pairs on overhead bridge cranes, two pairs on side rails attached to the walls	16
1.16	All winches can move: two pairs on overhead bridge cranes, two pairs on beams connecting the two bridge cranes	17
1.17	Preferred Scenario: 8-cable suspended reconfigurable CDPR, all winches are mounted on two overhead bridge cranes	17
1.18	Concept of cable-driven systems	18
1.19	Case 6-Cable CDPR: All pairs of winches can move freely on overhead bridge cranes	19
1.20	Case 8-Cable CDPR: All pairs of winches can move freely on overhead bridge cranes	19

1.21	Case 8-Cable CDPR: on each overhead bridge crane, 1 pair of winches (or cable exit points) is fixed at the middle, the other two pairs can move (within a restricted range). Additional movable beams might be used to sustain lateral forces exerted on the two cranes.	20
1.22	Using multiple CDPRs in a factory workshop	20
1.23	Conventional method of carrying workers in an airplane maintenance workshop	21
1.24	Using grid of winches to reconfigure CDPRs in 4 sections over the airplane body	23
1.25	All pairs of winches can move on fixed rails along the airplane body	23
1.26	All pairs of winches can move on reconfigurable rails (this solution is similar to factory workshop use case)	24
1.27	Fully constrained CDPRs: 4 winches can move on the rails on top of the airplane body, the other 4 winches can be switched among a grid of winches on the ground	24
1.28	Solution of using 4 CDPRs in an airplane maintenance workshop: covered areas	25
1.29	Solution of using 4 CDPRs in an airplane maintenance workshop: perspective view	25
1.30	Modified mobile platform: perspective view	26
1.31	Modified mobile platform: elongate the platform working area to reach the lower part of airplane body	26
2.1	General m -cable CDPR	30
2.2	Diagram of a sagging cable in 2D (cable local frame)	33
2.3	Sketch of a sagging cable in 3D	43
2.4	A general m -cable CDPR	48
2.5	Usual method to check interference between two cables	49
2.6	Checking interference between two cables	50
2.7	Interferences between cables and the CDPR mobile platform	52
2.8	Simplification of the mobile platform shape	52
2.9	Detecting collision between cable i and the mobile platform	53
2.10	Example of an 8-cable CDPR	56
3.1	Winch and cable transmission components of the CoGiRo prototype	60
3.2	Control scheme of the CoGiRo prototype used in the experiments	63
3.3	Measured output torque of the motor	65
3.4	Steady-state values of the friction torque	66
3.5	Cable segment AB	70
3.6	Solving the CDPR inverse kinetostatic problem using catenary cable	74
3.7	The change in the cable unstrained length at different temperatures	79

3.8	The change of cable unstrained length due to the change of the cable Young's modulus	80
3.9	The CoGiRo CDPR	81
3.10	Maximum errors of the cable unstrained length computed from different tension distribution methods	82
3.11	Accuracies of different cable models - Case 1a : following a desired trajectory . .	83
3.12	Accuracies of different cable models - Case 1b : varying payloads	84
3.13	CoGiRo control scheme: Without the influence of pulley kinematics	86
3.14	Static equilibrium poses in the workspace of CoGiRo - Case study 1	86
3.15	CoGiRo control scheme: Including the influence of pulley kinematics	88
3.16	Static equilibrium poses in the workspace of CoGiRo - Case study 2	89
4.1	Solution using large-dimension reconfigurable suspended CDPR to replace conventional cranes	94
4.2	Example of a scenario in a workshop	101
4.3	Bounds on reconfiguration parameters and desired Cartesian workspace	103
4.4	Desired trajectory	104
4.5	Results of online reconfiguration	105
4.6	Solution for the upper bounds on the reconfiguration parameters	106
4.7	CDPR Mobile platform	108
4.8	Displacements of O_p and M at the mobile platform of a CDPR	110
4.9	Using CDPRs to replace gantry nacelles in an airplane workshop	115
4.10	Reconfiguration parameters	117
4.11	Reconfiguration solutions in case $n_r = 4$	119
A.1	Drum and cable transmission components: a general case	128
A.2	Cable segment between two vertically aligned pulleys	129
A.3	Cable segment between two horizontally aligned pulleys	130
A.4	Cable segment between the drum and the first pulley	132
A.5	Tangent line from a fixed point to a circle	134

LIST OF TABLES

2.1	Collision detection computation times	57
3.1	Loss of torque due to friction in the winch	66
3.2	Measured positions of the mobile platform of CoGiRo at several static equilibrium poses - Case study 1	87
3.3	Positioning accuracy of CoGiRo at several static equilibrium poses - Case study 1	87
3.4	Measured positions of the mobile platform of CoGiRo at several static equilibrium poses - Case study 2	90
3.5	Positioning accuracy of CoGiRo at several static equilibrium poses - Case study 2	90
4.1	Results obtained by solving the different optimization problems	119

NOTATIONS

In the thesis, a vector is expressed either as a lower-case bold letter (e.g. \mathbf{f}) or as an upper-case italic letter (e.g. F). A matrix is expressed as an upper-case bold letter (e.g. \mathbf{R}).

The variables with a subscript containing the letter L (e.g. coordinate x_{Lb} or force component f_{Lbx}) indicates that these variables are expressed in the local cable frame. The variables without subscription letter L are expressed in global frame.

$CDPR$	Cable-Driven Parallel Robots
IKP	Inverse Kinetostatic Problem
$\ \mathbf{u}\ , \ \mathbf{K}\ $	The 2-norm of a vector or a matrix
$\mathbf{I}_{3 \times 3}$	Identity matrix
$\mathbf{0}_{3 \times 3}$	Null matrix
$(\mathbf{u})_{\times}$	Cross-product matrix of vector \mathbf{u}
$(x_1 \ x_2), [x_1 \ x_2]^T$	Column vectors
$[x_1 \ x_2]$	Row vectors
m	The number of cables
A_i	The base frame exit point of cable i
B_i	The anchor point of cable i , onto the mobile platform
O_p	The origin of the local frame attached to the mobile platform
\mathbf{u}_i	Unit vector that direct the cable force at the cable i anchor point
\mathbf{b}_i	Position vector of B_i expressed in mobile platform frame $\langle O_p \rangle$
C	The center of mass of the mobile platform
\mathbf{R}	Rotation matrix of the mobile platform
\mathbf{S}	Matrix that maps angular velocities onto the time derivative of Euler angle vector
$X = (P, \Phi)$	Pose vector of the mobile platform
X_c	Home pose
X_d	Desired pose
$dX = (dP, d\Phi)$	Infinitesimal displacement vector
$dP = (dx, dy, dz)$	Displacement vector in Cartesian space

$d\Phi = (d\theta_x, d\theta_y, d\theta_z)$	Displacement vector in orientation space
\mathbf{f}_e	External wrench applied by the cable on the mobile platform
dX_H	Homogeneous infinitesimal displacement vector
$d\mathbf{f}_{eH}$	Homogeneous infinitesimal wrench
m_p	Mass of the mobile platform
\mathbf{W}	CDPR wrench matrix (general case)
\mathbf{W}_x	CDPR wrench matrix (simplified cable model case)
$\mathbf{W}^+, \mathbf{W}_x^+$	Pseudo inverse matrices of wrench matrices
\mathbf{N}, \mathbf{N}_x	Null-space matrices of wrench matrices
$\boldsymbol{\tau}_b$	The vector of cable tensions at anchor points B_i
τ_a, τ_b	Cable tensions at cable end points A, B
τ_s	Cable tension at a point with cable coordinate s
τ_{\min}, τ_{\max}	Lower bound and upper bound on cable tensions
F_{B_i}, F_{A_i}	Cable force vector at end points B_i, A_i
\mathbf{a}_p	Acceleration vector of the origin O_p of the mobile platform frame
$\boldsymbol{\alpha}$	Angular acceleration vector
$\boldsymbol{\omega}$	Angular velocity vector
\mathbf{K}	Stiffness matrix of 6-DOF CDPR
\mathbf{K}_B	Stiffness matrix of one cable
\mathbf{J}	CDPR Jacobian matrix
\mathbf{K}_H	Homogeneous stiffness matrix
E	Cable Young's modulus
A_0	Cable cross-section area
w	Cable self-weight
L_0	Cable unstrained length
α_T	Thermal expansion coefficient
T_0	Reference temperature
μ_s	Static friction coefficient between pulley and cable
Γ_f	Loss torque due to frictional effect
$L_0^{(P,Q)}$	Cable unstrained length between two end points P, Q
$\mathbf{r} = (r_1, r_2, \dots)$	Vector of reconfiguration parameters
$\mathbf{r}_{\min}, \mathbf{r}_{\max}$	Lower and upper bound vectors on the reconfiguration parameters
\mathbf{C}_r	Set of reconfiguration parameters that satisfy all constraints
\mathbf{r}_{opt}	Optimal reconfiguration (planning) solution
Δ_r	Maximum step size of reconfiguration parameters being updated online

f_{Σ}

Sum of cable tensions index, wrt. a given workspace

 σ_M

Normalized upper bound on the infinitesimal displacement vector of the mobile platform

INTRODUCTION

Summary

1.1	Thesis Context	1
1.2	CDPRs: an Overview	3
1.3	Recent Developments of Reconfigurable CDPRs	12
1.4	On the Use of Large-Dimension Reconfigurable CDPRs in Two Targeted Industrial Applications	13
1.5	Contributions and Content of the Thesis	27

1.1 Thesis Context

CABLEBOT

The research leading to the results presented in this thesis is associated with the CableBOT project¹, an European Community’s Seventh Framework Programme project under grant agreement No. NMP2-SL-2011-285404.

The main objective of the CableBOT project is to develop a new generation of modular and reconfigurable CDPRs that are capable to perform many different steps in the life-cycle stages of large-scale structures.

1. <http://www.cablebot.eu>

Within CableBOT two fields of application were targeted in close cooperation to industry: Aircraft life-cycle maintenance in the aerospace industry and the construction beams post-production handling.

Several issues were addressed in the project:

- Design of reconfigurable CDPRs: Preferred implementations of reconfigurable CDPRs were proposed as solutions to the two targeted industrial applications. Powerful software tools have been developed to deal with the design and reconfigurations of CDPRs.
- CDPR simulation tools: A C++ framework has been developed allowing to create simulation scenes of CDPRs composed of elementary components such as winches, pulleys, cables and mobile platform. This software framework can be used in the design and control of CDPRs.
- CDPR control modules: Control schemes and algorithms have been developed and applied on different CDPR prototypes, providing solutions to various application scenarios.

THESIS GOAL

The main objectives of the thesis are directly related to the CableBOT project goals. We seek for possible solutions of using reconfigurable CDPR to replace conventional methods of handling large and heavy parts in a workshop.

A reconfigurable CDPR can change its geometry by adjusting the cable exit points positions or by reordering or changing the positions of the cable attachment points onto the mobile platform. Reconfigurability should enable the robot to adapt to a variety of tasks and dimensions. A reconfigurable CDPR should thus fulfil several requirements, e.g. having suitable architectures (geometries) that satisfy the following typical constraints, which represent robot capabilities:

- All poses of a given workspace can be reached.
- Workspace is singularity free.
- Adequate degrees of freedom are kept across the whole workspace.
- Cable tensions satisfy minimum and maximum values.
- Workspace is collision free (no cable interferences, no collision with objects in the workspace,...).
- Ability to balance varying reaction forces due to carried devices (e.g. robot arm) or workers.
- Desired additional constraints (load, acceleration,...) can be achieved.

To this end, we aim to develop a fundamental framework for reconfigurable CDPRS. It consists of several topics:

1. The general architecture of the studied reconfigurable CDPRS family is required. This architecture should enable the CDPRS to achieve most of the desired tasks and its implementation in the assigned environment should be feasible (e.g. in a factory workshop or in an airplane maintenance workshop).
2. Analysis tools that can aid the design and control of reconfigurable CDPRS.
3. Methods and tools to solve the CDPRS reconfiguration problem efficiently.

1.2 CDPRS: an Overview

CDPRS have been an active research topic in the past decades in favor of their appealing advantages such as light-weight, simple in design, easy to reconfigure and implement, high payload to weight ratio and relatively low cost. Compared to parallel manipulators with rigid links which are limited to work in small work cells, CDPRS use cables to position their mobile platform (end-effector) directly by controlling the length of each cable and can thus be adapted to very large workspaces. However, the use of cables can also have some peculiar drawbacks. Firstly, cables can transmit tension forces but not compression forces. Thus, all the cables driving the mobile platform should be under tension such that the tension value lies in an admissible tension range. Secondly, the nonlinear characteristics of the cables might affect the robot performance. These factors increase the difficulty of important issues such as the CDPRS kinematic and dynamic modeling, tension distribution, workspace analysis and control schemes. In other words, most of the methods related to rigid-link parallel manipulators have to be modified for CDPRS.

Possible applications of CDPRS are positioning and handling of large and heavy parts across wide workspaces such as for structure construction [1, 2], rescue operation [3, 4], rehabilitation [5, 6, 7], aerial transportation [8, 9], astronomical observation [10].

CLASSIFICATION OF CDPRS

The first general classification of CDPRS was given by Ming and Higuchi [11]. Based on the number of cables (m) and the number of degrees of freedom (n), cable-driven parallel robots were classified into two categories, namely the incompletely restrained positioning mechanisms - IRPM ($m < n + 1$), the completely restrained positioning mechanisms - CRPM ($m = n + 1$). In [12], Verhoeven introduced one more category which is the redundantly restrained positioning mechanisms - RRPM ($m > n + 1$).

In terms of force-closure (wrench-closure), CDPRs are classified into two main categories: fully constrained and under-constrained. For the first category, there exists at least one mobile pose having force-closure, for which any wrench applied on the platform can be balanced through tension forces in the cables [13]. Notable examples are the FALCON prototype [14] and the SEGESTA prototype [15]. On the contrary, for under-constrained CDPRs, the cables cannot balance any external wrench because to this end, they might have to push on the platform. Gravity is then used to keep the cables under tension. The latter case can be referred to as suspended CDPRs (all the cables are “above” the mobile platform), e.g. the NIST ROBOCRANE [16] or the CoGiRo prototype [17].

KINETOSTATIC MODELING OF CDPR

In the kinematic modeling of CDPRs, different cable models were used in previous works, including massless elastic model (straight line) [14, 18, 19, 20, 21, 22], simplified model (parabolic model) [23], and catenary model [24]. The massless elastic cable model is sufficient in many CDPR case studies. However, the effect of cable sagging due to cable mass and elasticity, especially for large-dimension CDPRs, may have great impact on the robot performance and thus should be considered in the kinematic modeling. Ottaviano presented an analysis of the effects of the cable mass and elasticity on the end-effector of a planar 2-DOF CDPR in [25]. The studies in [26, 27] specifically discuss the difference in the CDPR workspace when using the simplified or catenary cable model compared to massless elastic cable model.

Tension distribution is another important issue, especially in the case of redundant CDPRs. Several real-time capable tension distribution methods have been developed [15, 18, 19, 28, 29, 30, 31, 32, 33]. Two main approaches are applied. The first approach utilizes fast optimization tools to obtain the tension distribution in optimizing certain criteria. For example, Lim et al. in [31] use a gradient projection method to compute the solutions. Meanwhile, the authors in [29, 34] address the same problem by using minimization of the Euclidean norm of the cable tensions and p-norm of the relative cable tensions to avoid cable tension discontinuities that may be caused by linear programming. In the second approach, e.g. in [32, 33], the solutions of cable tensions are found for redundantly actuated CDPRs based on geometric considerations applied to the two-dimensional convex polytope of feasible cable tension distributions. This polytope is defined as the intersection between the set of inequality constraints on the cable tension values and the affine space of tension solutions to the mobile platform static or dynamic equilibrium. The solutions also guarantee the continuity of cable tensions in a continuous trajectory of the CDPR mobile platform.

Regarding the workspace analysis, a number of studies on the determination of CDPR workspaces have been made [1, 27, 35, 36, 37, 38]. In [39], an interval analysis based tool is developed to compute the Wrench-Feasible Workspace (WFW) of a CDPR. Several studies quantified the CDPR workspaces based on classical criteria which were used for rigid-link parallel manipulators. For example, in [40] Hay analyzed the CDPR dexterous workspace, which refers to the intersection of orientation workspaces with a range of rotation angles. The workspace "quality" of a CDPR can also be evaluated based on indices derived from its stiffness matrix (which can be used to account for the CDPR stability) [41, 42, 43].

In term of CDPR dynamics, most of previous studies consider only the dynamics of the mobile platform and the winches. Cable dynamics has rarely been addressed due to its complexity. Du et al. [44] evaluated the effect of cable vibration on the positioning accuracy of the end-effector of a large-dimension CDPR by using finite element method. In [45], Yuan et al. analyzed the elastodynamic of a 6-DOF suspended CDPR. They construct the dynamic stiffness matrix of a sagging cable and study the natural frequency of the CDPR mobile platform. They showed that the cable dynamics should be considered when it comes to perform high speed applications. In a more recent work [46], Weber made an analysis on the cable dynamics and proposed a method to reduce the vibration effect at the mobile platform of a 2-DOF CDPR.

CDPR CONTROL PROBLEM

Many control schemes used for rigid-link parallel manipulators may be adapted to cable-driven parallel robots. The most common approach is to drive the mobile platform by means of controlling the cable lengths or the required torques. A feedback control loop allows the realization of desired cable lengths corresponding to a desired position and orientation of the mobile platform, or of the motor torque corresponding to a desired CDPR dynamics. In [47], Fang et al. proposed nonlinear feedforward control laws in the joint space, taking the advantage of an optimal tension distribution. Williams et al. [48] proposed a computed torque controller using the encoder feedback for each cable length. Motion convergence using simple control laws (e.g. PD feedback controller) in the joint space was proven with a Lyapunov function and a "vector closure" analysis by Kawamura et al. [49]. Kino et al. [50] proposed a robust PD controller with an adaptive compensation for fully constrained CDPRs. In recent studies, Lamaury applied a dual-space feedforward controller [17] (which was previously successfully implemented on rigid-link parallel robots [51]). This control scheme was also implemented with a PID control law and an adaptive control law considering the use of an effective tension distribution method [32]. Similar approaches have been applied by Bruckmann et al. [15, 33].

Controlling CDPRs in the joint space sometimes face the difficulty in accomplishing accurate pose of the end-effector mainly due to the use of simplified cable models. Attempts to control CDPRs in the task space have been carried out such as with visual servoing and using real-time forward kinematic modeling. Dallej et al. [52] proposed a 3D pose visual servoing and developed a vision-based computed torque control. In a recent study, Chellal et al. [53] also proposed a vision-based position control for a 6-DOF CDPR.

Keeping all the cables under tensions during operation is another issue of CDPR control problems. The constraints set upon cable tensions make control of CDPRs a lot more challenging than their counterpart rigid-link parallel robots. Effective tension distribution methods can be used in the CDPR control schemes [15, 18, 19, 28, 29, 30, 31, 32, 33]. Taking the advantage of such methods, several control strategies were proposed to meet the conditions of positive cable tensions. Alp and Agrawal [54] described the structures of Lyapunov based controller and feedback linearizing controller that guarantee positive cable tensions. Oh and Agrawal [55, 56] proposed techniques to estimate the admissible workspace of set-point control for a cable-suspended robot under disturbances and input constraints based on a sliding mode controller. Alikhani [57] proposed a propagation algorithm in order to generate feasible set points for the end-effector motion while satisfying constraints on control inputs. In [58], Khosravi formulated a robust PID position control in task space and used a corrective term to ensure positive cable tensions.

NOTABLE CDPR PROTOTYPES AND APPLICATIONS

Since the 1980s, various CDPR prototypes have been built and studied. Early in 1989 the NIST Robocrane system for large-scale handling [16, 59, 60] is one of the first CDPR prototypes (Fig. 1.1). NIST implemented ROBOCRANE to carry on a series of application research on assembly, lifting, spraying, and building with cable robots [61, 62, 63, 64].

Later, an ultrahigh speed cable robot FALCON (Fig. 1.2), a 7-cable 6-DOF CDPR, was designed in Japan. One can say it was the first CDPR prototype for very fast pick-and-place applications [14, 49].

DeltaBot [65], a rigid-cable hybrid ultra-high-speed cable robot, was developed by Amir Khajepour at the University of Waterloo, Canada (Fig. 1.3).

SEGESTA (Fig. 1.4), another lightweight prototype, was developed at the University of Duisburg-Essen, Germany. A number of studies have been made with SEGESTA on the kinematic modeling, workspace calculation, tension distribution, and trajectory planning issues [15, 18, 28, 66, 67].



Figure 1.1: The NIST Robocrane

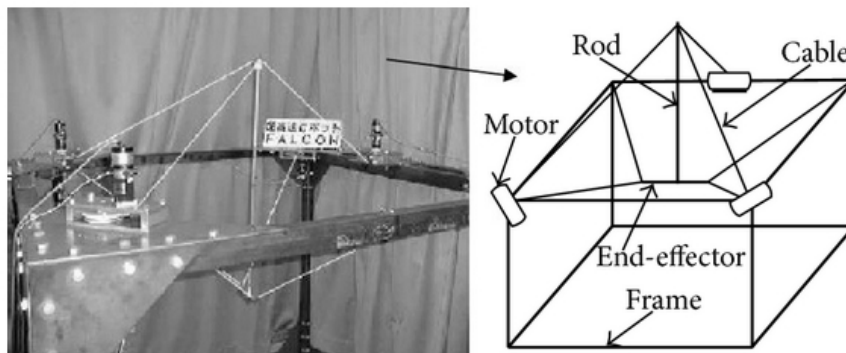


Figure 1.2: The FALCON prototype

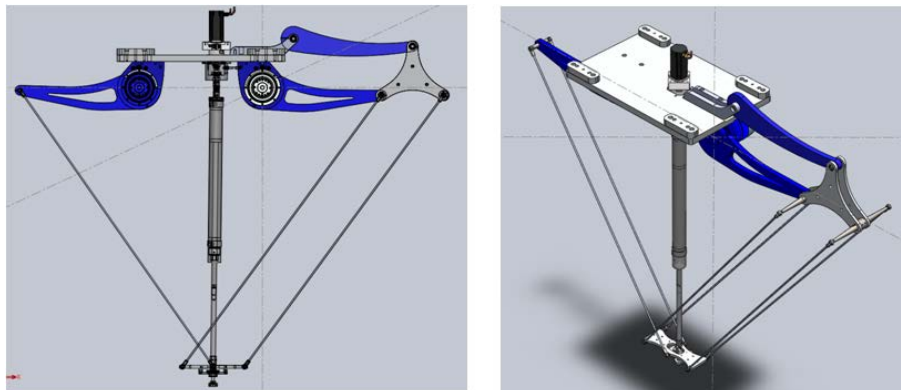


Figure 1.3: The DeltaBot prototype



Figure 1.4: The SEGESTA prototype



Figure 1.5: The IPAnema CDPR family

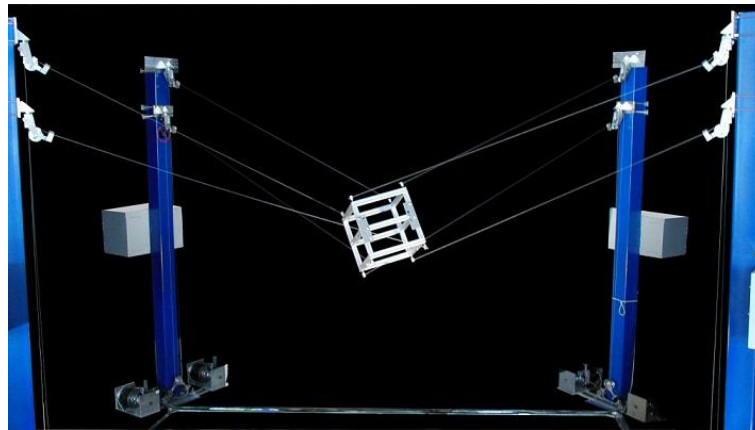


Figure 1.6: The ReelAx8 prototype

The IPAnema family of cable robots (Fig. 1.5) is developed by Fraunhofer IPA, Germany for medium to large scale inspection, handling, and assembly operations [2, 19, 30, 68].

LIRMM and Tecnalía France developed two redundantly actuated 8-cable CDPR prototypes: the small-medium workspace CDPR ReelAx8 (Fig. 1.6) and the large-dimension suspended CDPR CoGiRo (Fig. 1.7) [17, 32, 69, 70].

The CDPR prototype MARIONET crane (Fig. 1.8) for rescue and personal assistance was developed at INRIA in France [71].

The 500-meter Aperture Spherical radio Telescope (FAST), which is currently under construction in the Karst region of Guizhou Province, China [72, 73, 74] would be the world's largest cable robot. The FAST is composed of the active main reflector and the feed support system. The huge CDPR and the feed cabin constitute the feed support sys-

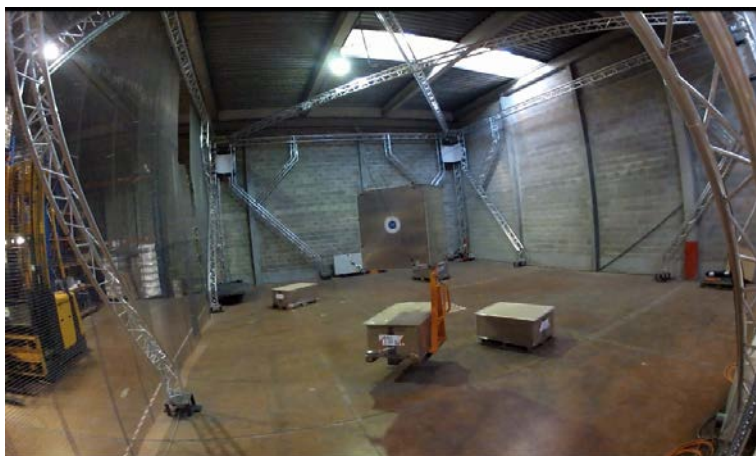


Figure 1.7: The CoGiRo prototype



Figure 1.8: The MARIONET crane prototype



Figure 1.9: The FAST project



Figure 1.10: Spidercam



Figure 1.11: Skycam

tem. The CDPR with the radius of $600m$ is driven with six steel cables, providing receivers with large workspace (Fig. 1.9).

Spidercam in Germany [75] (Fig. 1.10) and Skycam in USA [76] (Fig. 1.11) are two successful applications of CDPRS used to carry a camera over a very large area (e.g. in a soccer stadium), allowing the camera to be positioned at different angles and positions.

1.3 Recent Developments of Reconfigurable CDPRs

Most of the studies on CDPRs in the past decades have been focused on fixed configuration CDPRs where the cable exit points and attachment points are fixed at pre-defined locations. The properties of a CDPR in general can be easily changed by re-adjusting its cable layout, e.g. by adjusting the locations of the cable exit points or by changing the attachment order or positions of the cables connected to the mobile platform (or to the end-effector). For example, one can transform a fully constrained CDPR (e.g. IPAnema prototype in Fig. 1.5) into an under constrained suspended CDPR (e.g. CoGiRo prototype in Fig. 1.7) simply by moving the cable exit points to any positions where all the cables are above the mobile platform.

Recent studies [4, 77, 78, 79] deal with reconfigurable CDPRs where the geometry of the CDPRs can be reconfigured by changing its cable layout. Reconfigurability of a CDPR could greatly increase its capability (compared to fixed configuration CDPR), but at the same time, it adds redundancy and increases the complexity of the system. For the design of such CDPRs, in [77], Rosati introduced the concept of adaptive cable-driven systems. He discussed a systematic procedure to determine the design solution for planar cable-driven systems which minimizes or maximizes some local performance indices such as cable tension based criteria and dexterity of the CDPRs. Later on, Xiaobo Zhou in [78] presented an analysis framework for cooperating cable mobile robots. The proposed method to solve the reconfiguration problem is similar to that of Rosati in the sense that the solutions were derived from optimizing certain criteria. In [79], Zhou et al. proposed a generalized modeling framework for systematic design and analysis of cooperative mobile cable robots. They dealt with the redundancy resolution by optimally repositioning the mobile bases to maximize the so-called tension factor which is the ratio between minimal and maximal values of cable tensions along a given trajectory. However, all these previous studies only consider planar robot systems where important constraints such as cable interferences are not taken into account. Moreover, critical issues while using standard optimization tools to solve the redundancy of the robot system such as *the continuity of the performance indices with respect to the deciding parameters* and *the continuity and differentiability of the constraints* have not been addressed. In fact, the continuity of the tension based performance indices can be dealt with by using tension distribution methods such as the one in [32]. However, it is difficult to address the second issue since there are different types of constraints including wrench feasibility (continuous nonlinear constraints) and cable interferences (non-differentiable constraints). Furthermore, the problem becomes more complex for a highly redundant CDPR. Addressing these issues of reconfigurable CDPRs is one of our main objectives in the present thesis.

1.4 On the Use of Large-Dimension Reconfigurable CDPRs in Two Targeted Industrial Applications

Cable-driven parallel robots possess many appealing advantages. The use of cables provides great potential to CDPRs such as a wide workspace and high payload to weight ratio. We shall give a brief discussion of two possible applications for which CDPRs could replace conventional methods of handling large and heavy parts across wide workspaces. These two applications were considered in the framework of the CableBOT project.

1.4.1 Factory Workshop

Fig. 1.12 shows conventional methods to handle large and heavy parts in a workshop. In the left (Fig. 1.12a), one or multiple overhead cranes are used to manipulate the parts. Each crane offers one degree of freedom along the vertical axis and one or two degrees of freedom in lateral directions. This solution has several drawbacks including limited flexibility and reduced orientation capabilities. Most of the time when the operation requires a change of orientation of the part, there is a need of involving workers which causes safety issues. For tasks that require several degrees of freedom of the part, such traditional methods may not be sufficient. When lifting devices need more than one degree of freedom, they are complemented with other mechanisms that provide extra DOFs. As shown in Fig. 1.12b, the crane need an extra device to enable its rotational capability for some tasks that require rotational DOFs.

In those cases, using a CDPR would be much more convenient. By simply connecting



(a) Manipulating heavy part using multiple cranes (b) Crane with 10t vacuum prehension, 5 DOF

Figure 1.12: Handling heavy parts using cranes

the cables directly to the parts, the CDPR can execute the tasks that require up to 6-DOF movements.

REQUIREMENTS

In a workshop, examples of tasks are the displacement of heavy structure elements (displace structure components from one place to another within the workshop) or positioning of structure elements for assembly. Expected CDPR performances can be foreseen as follows:

- **Number of degrees of freedom required by the tasks:** For positioning tasks, the CDPR should have at least 4-DOF: translations in all directions and rotation around the vertical axis (e.g. up to $\pm 90^\circ$). For assembly tasks, six DOFs are generally required.
- **Workspace:** The robot must fit into the workshop area. Depending on the layout of a workshop, a CDPR is expected to cover a certain area or several connected sections in the workshop.
- **Required speed or cycle time:** The speed of the movements depends highly on the weight to be displaced. For light weight part, high speed motions can be used. For heavy payload (several tons), slow motion is expected. However, in both cases, the CDPR should be able to achieve a given desired performance in terms of maximum acceleration and velocity.
- **Required accuracy and stiffness:** Positioning structure elements may require a weak accuracy. However, in assembly tasks, high precision and high stiffness at the end-effector could be required. These factors could be attainable by using suitable configuration of the CDPR.
- **Requirements on reconfigurability of the CDPR:** The geometry and weight of the structures elements can change. Therefore, the CDPR has to be somehow reconfigurable, in order to fulfill the task requirements. When the CDPR uses its mobile platform to handle the part, an additional fastening device may be required to attach the part to the mobile platform. Alternatively, in the case the structure part itself becomes the mobile platform of the CDPR, a suitable strategy to attach the cables to the part is required. On the other hand, the geometry of the CDPR may need to be reconfigurable in order to fulfill different task requirements (e.g. obtaining a larger orientation range within a specific area).

PROPOSED CDPR ARCHITECTURES

It is common to use overhead bridge cranes to span all area in a workshop. As an evolution of this solution, it could be convenient to construct CDPRs using these cranes. Fig. 1.13 shows the first solution where each crane carries one CDPR. The mobile platform can be the structure part (load) itself - on which several anchor points are pre-defined to connect the cables. The winches may move freely on the overhead bridge to ensure maximum flexibility. The number of winches in this case can be varied depending on the actual need. It is to be noted that 6 winches and, hence, 6 cables may be necessary to avoid complex motions resulting from under-constraining the 6 degrees of freedom of the load. In this solution, the CDPR workspace is limited. It is not much different from a conventional crane except that it provides more rotational capability.

In a second implementation (Fig. 1.14), the CDPR is constructed by using two overhead bridge cranes. This solution should offer more flexibility in terms of workspace and in handling large structure parts.

One can imagine different approaches to positioning the cable exit points of the CDPR in order to enable its reconfigurability. Fig. 1.15 shows a possible implementation of a redundant 8-cable 6-DOF CDPR where the cable exit points can move by pairs along different directions. There are two pairs mounted on side rails attached to the wall of the workshop. This solution is not necessarily feasible because the walls may have to sustain large lateral forces. One way to overcome this problem is to add extra beams that connect the two overhead bridge cranes. The cable exit points can then move along these additional beams as

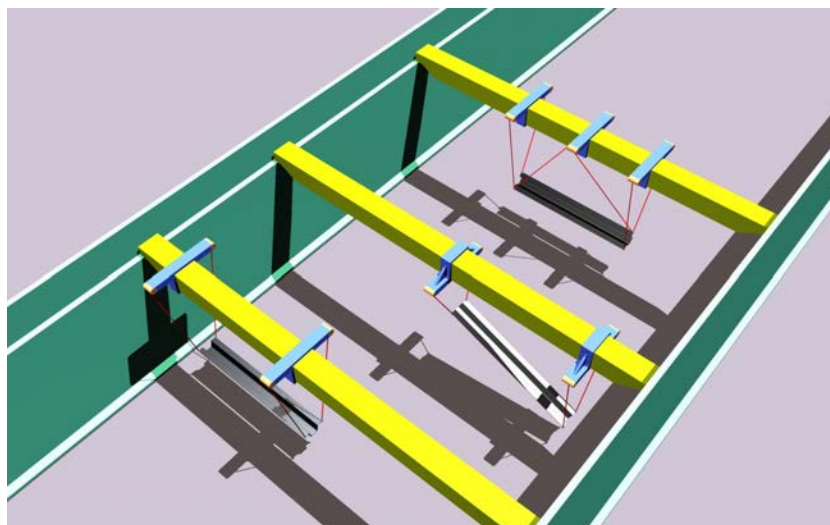


Figure 1.13: All winches are mounted on one overhead bridge crane

shown in Fig. 1.16. In this way, the lateral forces acting on the side walls of the workshop are minimized. This approach offers great reconfigurability to the CDPR. However, the workspace is still limited which is depended on the length of the extra beams. Moreover, it is not trivial to design such a system.

Fig. 1.17 shows a preferred scenario where the four pairs of cable exit points of the CDPRs are constrained to move along two overhead bridge cranes.

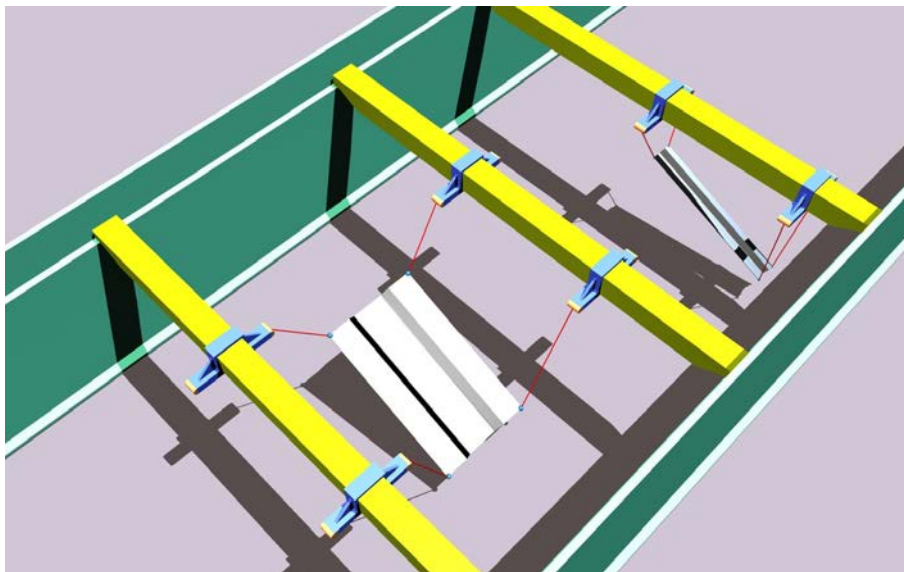


Figure 1.14: A CDPR on two overhead bridge cranes

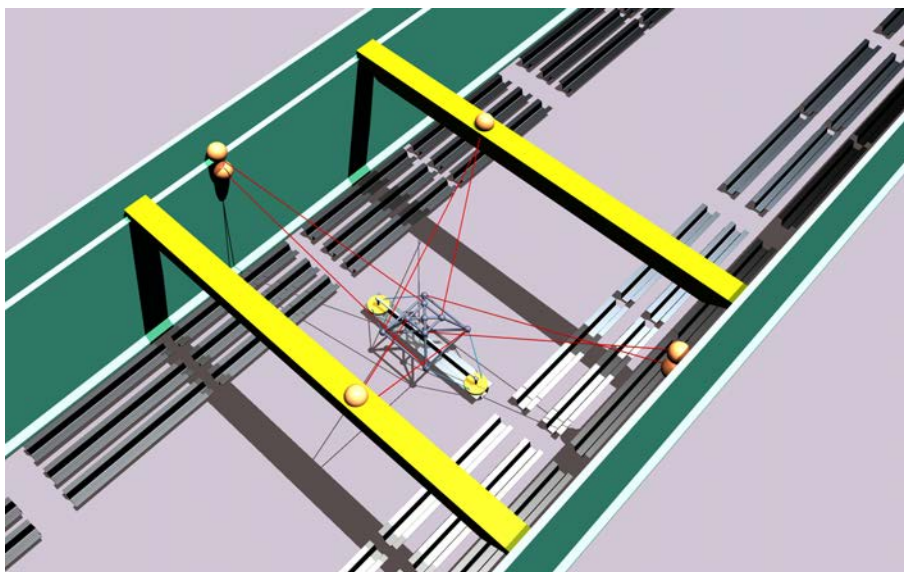


Figure 1.15: All winches can move: two pairs on overhead bridge cranes, two pairs on side rails attached to the walls

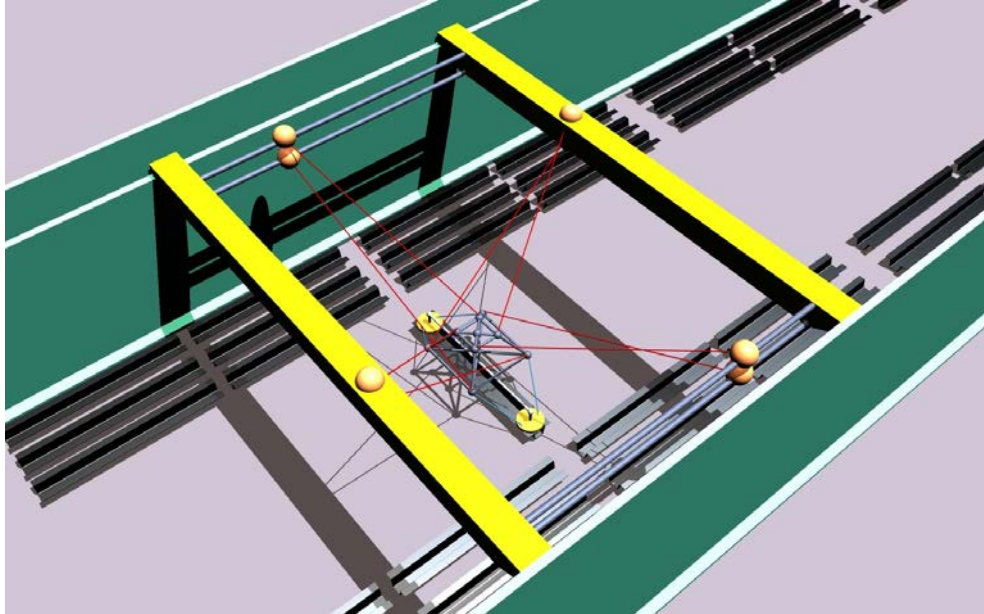


Figure 1.16: All winches can move: two pairs on overhead bridge cranes, two pairs on beams connecting the two bridge cranes

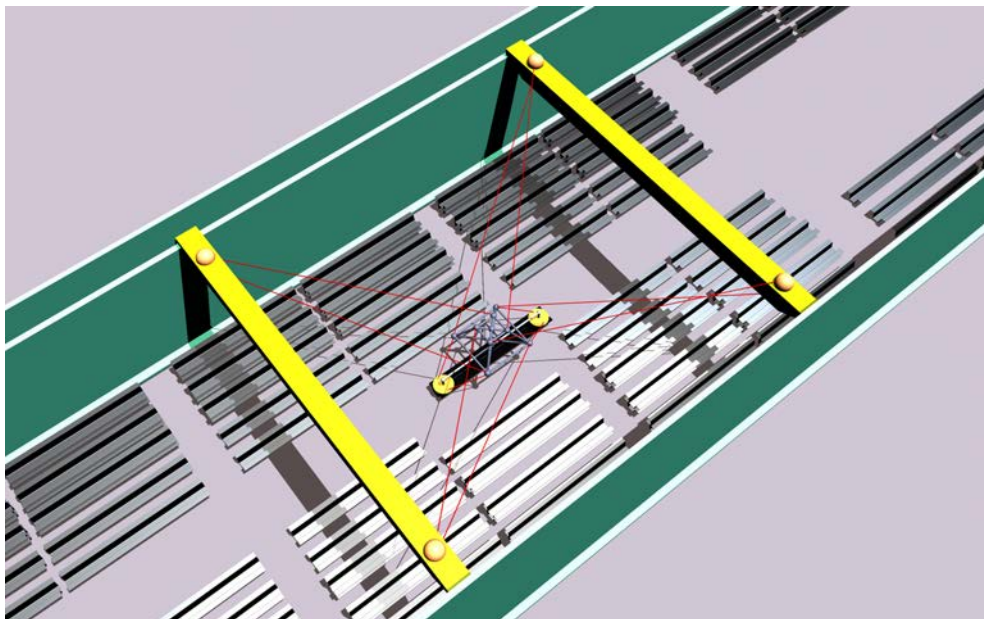


Figure 1.17: Preferred Scenario: 8-cable suspended reconfigurable CDPR, all winches are mounted on two overhead bridge cranes

PREFERRED SCENARIOS

Fig. 1.18 shows possible solutions to enable reconfigurability of a CDPR. The second case represents a more practical solution. It consists in only changing the position of the cable exit points. The winches are fixed at predefined locations on the overhead bridge crane.

The following figures Fig.1.19-1.21 detail several preferred CDPR architectures. In these solutions, the cable exit points are moving by pairs on each overhead bridge crane. To enable modularity of the system, all the cranes are similar to each other. Each of the crane can constitute a suspended CDPR. Furthermore, any two overhead bridge cranes can be used in collaboration to form a CDPR with 6 cables or 8 cables with a larger workspace and larger orientation capabilities. Fig. 1.22 shows a scenario where multiple CDPRs are used to work in different sections in a factory workshop.

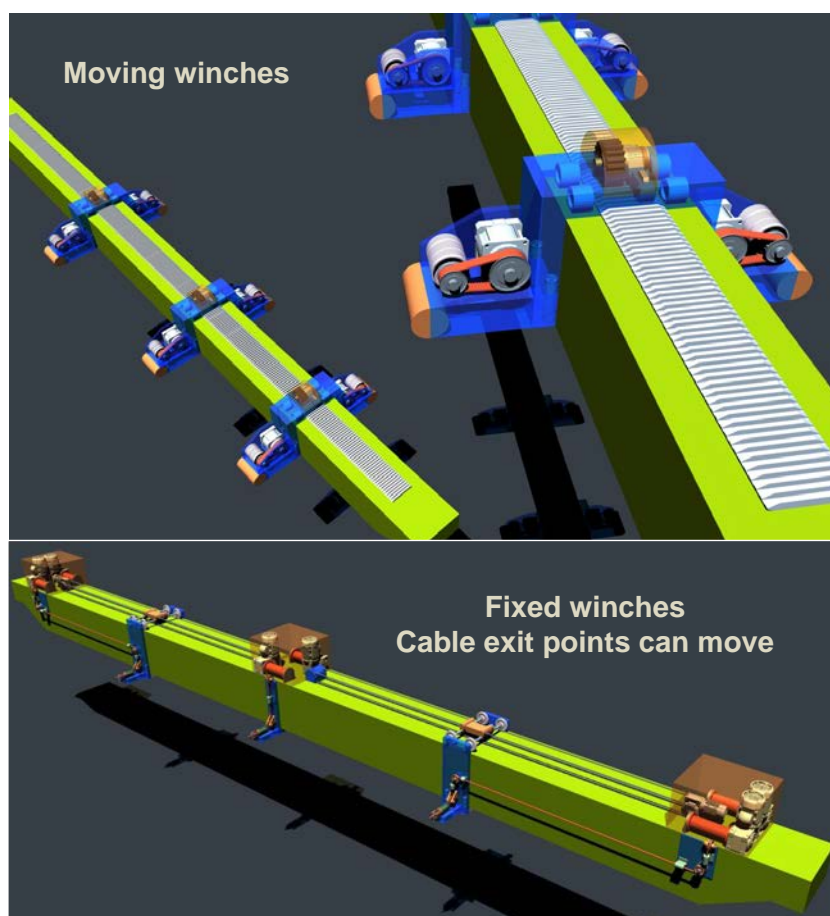


Figure 1.18: Concept of cable-driven systems

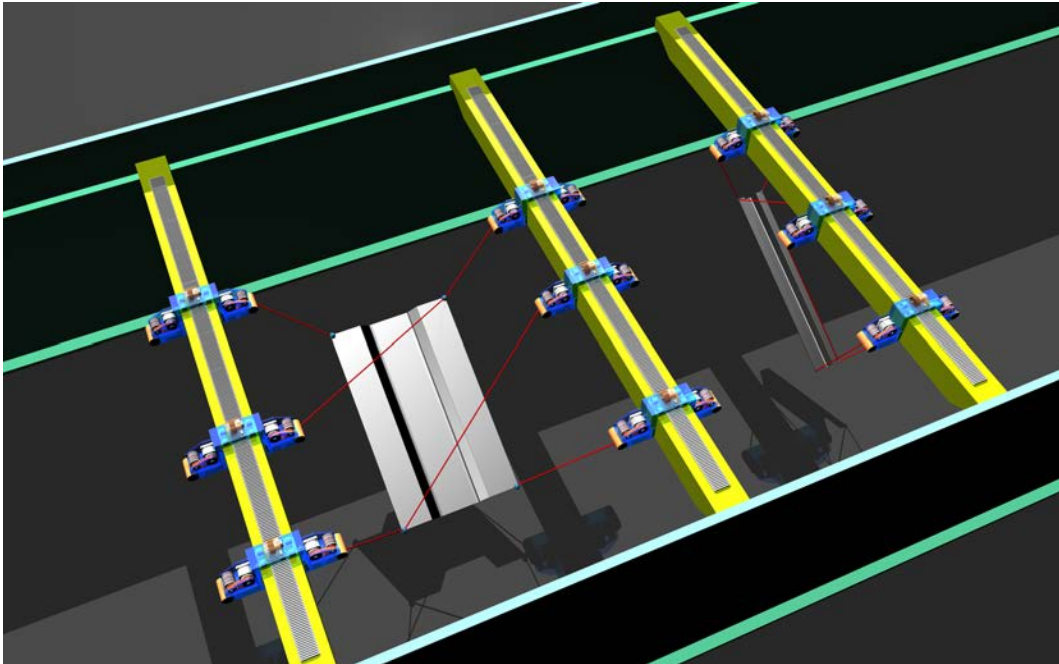


Figure 1.19: Case 6-Cable CDPR: All pairs of winches can move freely on overhead bridge cranes

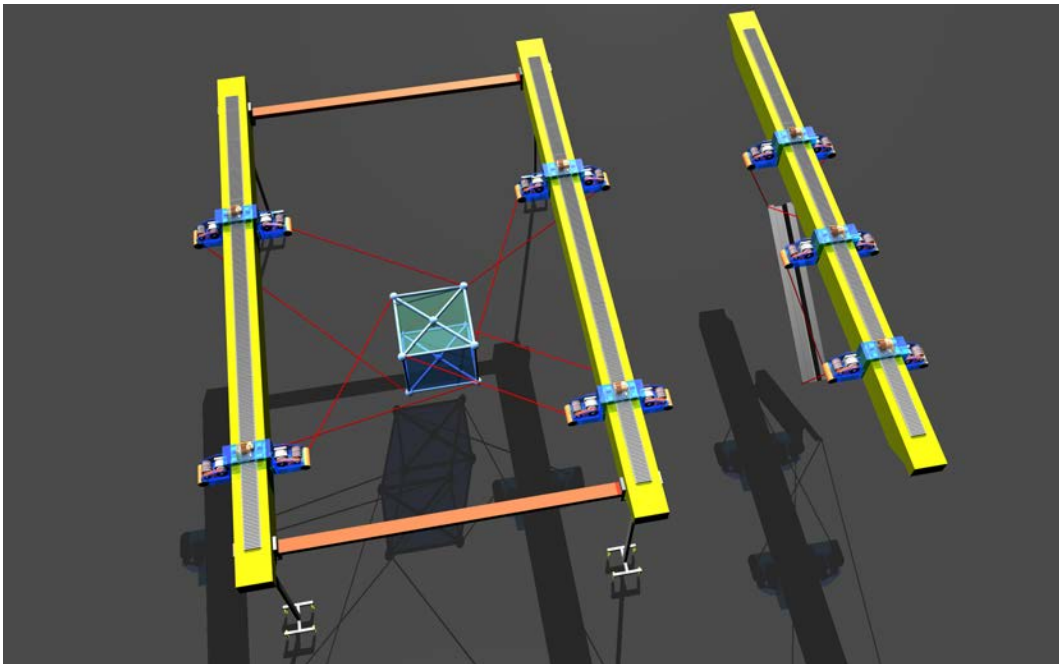


Figure 1.20: Case 8-Cable CDPR: All pairs of winches can move freely on overhead bridge cranes

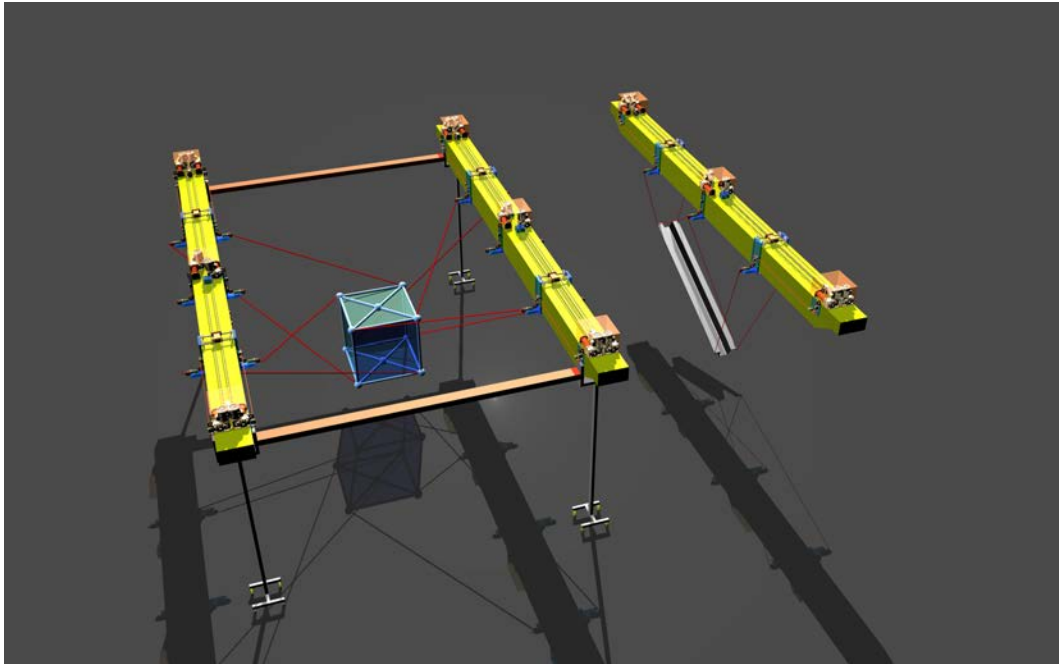


Figure 1.21: Case 8-Cable CDPR: on each overhead bridge crane, 1 pair of winches (or cable exit points) is fixed at the middle, the other two pairs can move (within a restricted range). Additional movable beams might be used to sustain lateral forces exerted on the two cranes.

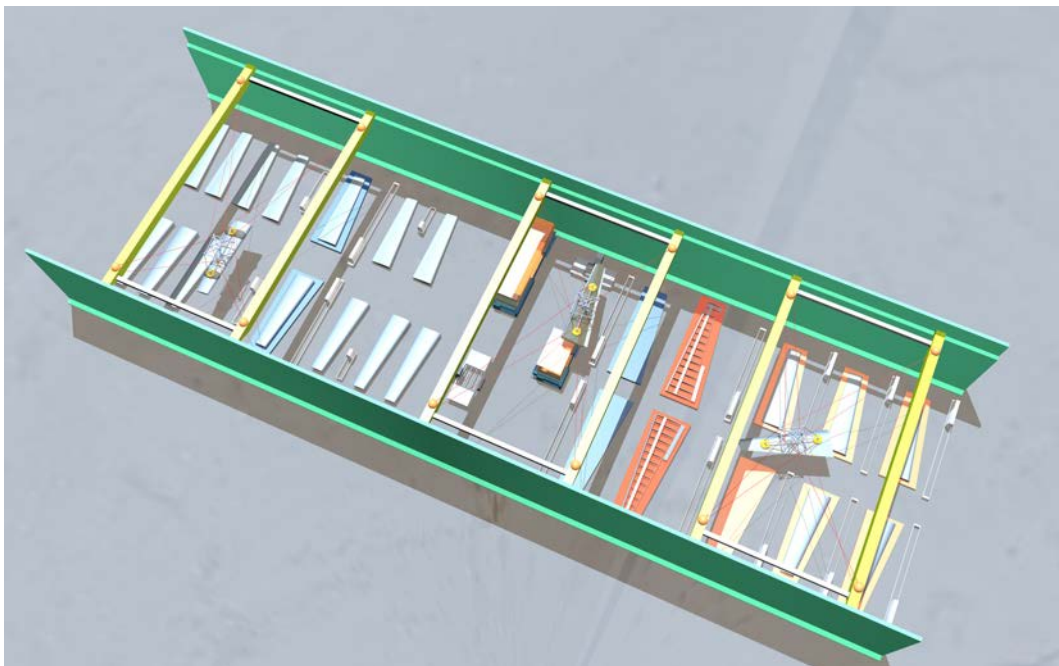


Figure 1.22: Using multiple CDPRs in a factory workshop

1.4.2 Airplane Maintenance Workshop

In the second targeted industrial application, CDPRs may be used to replace conventional methods to perform maintenance tasks in an airplane workshop. Fig. 1.23 shows the general method where several telescopic platforms are used to carry the workers across the airplane fuselage. Each telescopic platform offers 4 degrees of freedom (three translations in Cartesian space and one rotation around the vertical z-axis) which allows the task to be done quite efficiently. However, this solution has some disadvantages. Firstly, each telescopic platform weights from 9 to 11 tons which implies high costs for the building construction to sustain such heavy systems. Secondly, the workers sometimes need to work in hazardous environment where the operation requires to use chemical material like paint or stripping products. In the latter case, using CDPRs to automatically handle the tasks could be a more preferable solution.

REQUIREMENTS

To be able to replace conventional methods in an airplane maintenance workshop, there are different requirements that the CDPRs must strictly follow:

- **Number of degrees of freedom required by the tasks:** Depending on specific tasks (painting, cleaning, inspection...), the number of degrees of freedom of the mobile platform is variable. It also depends on the tools or mechanical devices embedded on the CDPR mobile platform.



Chemical paint stripping



Painting

Figure 1.23: Conventional method of carrying workers in an airplane maintenance workshop

- **Workspace:** The CDPRs are expected to reach all parts of the airplane body. Depending on the size of the airplane, several CDPRs must be used to cover different areas of the workspace simultaneously. The airplane has to be approached by the CDPRs without any shock or collision.
- **Required speed or cycle time:** In some maintenance tasks (e.g. painting), fast positioning of the mobile platform is required (e.g. velocity is greater than $0.6m/s$) in order to complete the tasks within a strictly given time limit.
- **Required accuracy and stiffness:** High accuracy is mainly required for automatic operation mode. In most use cases, it is preferable to have high stiffness at the mobile platform (e.g. carrying workers or carrying tools).
- **Requirements on reconfigurability of CDPRs:** Because of the complex shape of the airplane body, in order to reach all parts and avoid collisions, each CDPR should be able to change its cable layout (e.g. by changing the positions of the cable exit points). Suspended type CDPRs are preferable to avoid cable collisions. Reaching the upper part of the airplane body can be achieved. However, lower parts of the airplane fuselage are difficult to reach. In the latter case, suitable modifications of the mobile platform are required (e.g. by increasing the reachable range of the mobile platform or embedded tools to access the lower parts of the airplane fuselage).

PROPOSED CDPR ARCHITECTURE

Several solutions are proposed which have been inspired from the experiences of partners in the CableBOT project. In the first approach (Fig. 1.24), several CDPRs are used to cover the airplane body (at least 4 CDPRs). Possible locations to place the cable exit points of each CDPR can be set on top of the airplane body or on the ground. The geometric structure of the CDPRs can be reconfigured by switching the cables at the beginning of each task.

In a second approach, the winches can move along rails preferably positioned on the ceiling as shown in Fig. 1.25. Four CDPRs can be used to work in four separate sections according to the shape of the airplane, and to satisfy the constraint of having no cable running above the airplane due to strict requirements in some maintenance tasks (e.g. in painting tasks, the above areas of the airplane fuselage must be clean, having cables across these areas may bring dust and unwanted substances falling down on the painting surface). The main drawbacks of this solution are that the cable lengths might be quite long to span a large area and the mobile platform has to move near the boundary of the workspace. Furthermore, the building has to sustain large lateral forces exerted by the cables.

In a third scenario (Fig. 1.26), the winches of each CDPR can move freely on two overhead bridge cranes. These cranes can move along other perpendicular rails directed along the airplane main dimension (on the right-side of the figure). This solution is quite flexible since we can find optimal way to update the positions of the winches to achieve appropriate performances. On the left-side of the figure, a more complicated implementation is proposed. The directions of the rails can be oriented differently. But, in order to adapt the system to various airplanes, these rail directions have probably to be changed which makes this second solution difficult to implement and costly.

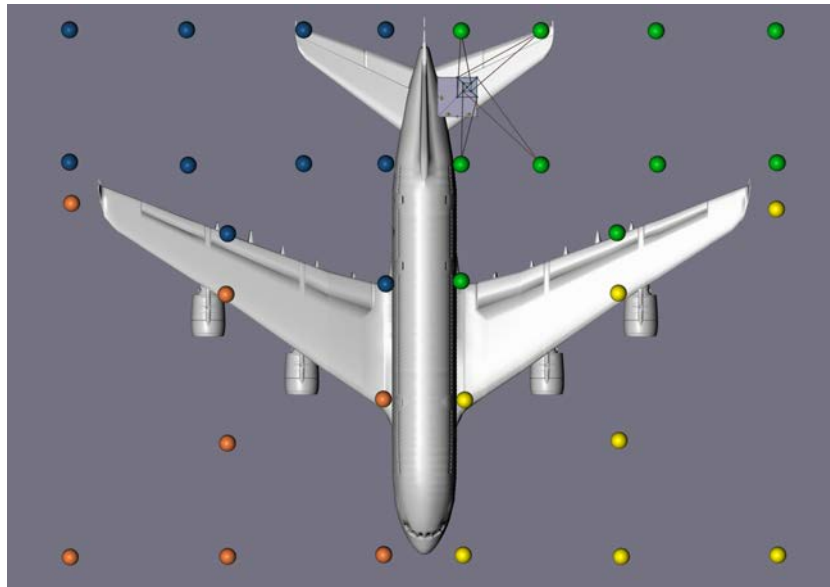


Figure 1.24: Using grid of winches to reconfigure CDPRs in 4 sections over the airplane body



Figure 1.25: All pairs of winches can move on fixed rails along the airplane body

Note that in all scenarios, it is possible to have variable implementations in order to change each CDPR property (e.g. from under constrained type into fully constrained type), thereby providing more flexible solutions. Fig. 1.27 shows a solutions where there are available winches on the ground. Each suspended CDPR can then be transformed into a fully constrained CDPR.

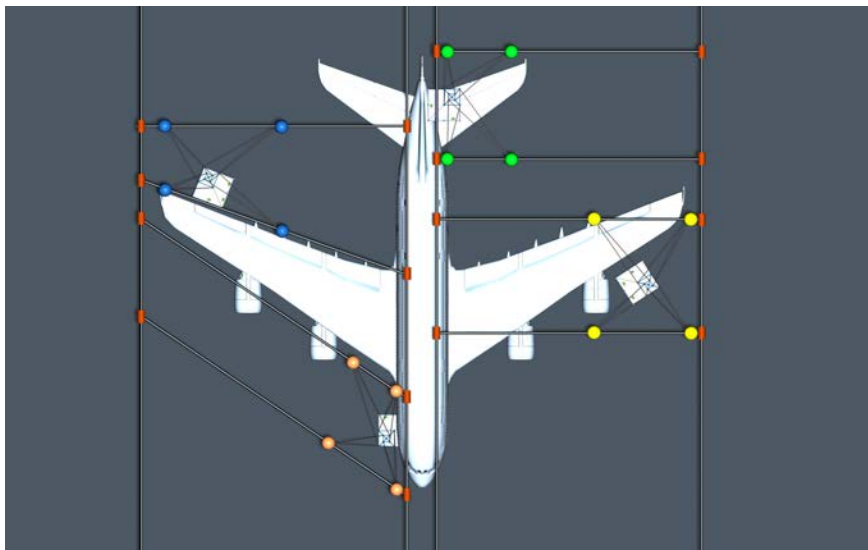


Figure 1.26: All pairs of winches can move on reconfigurable rails (this solution is similar to factory workshop use case)

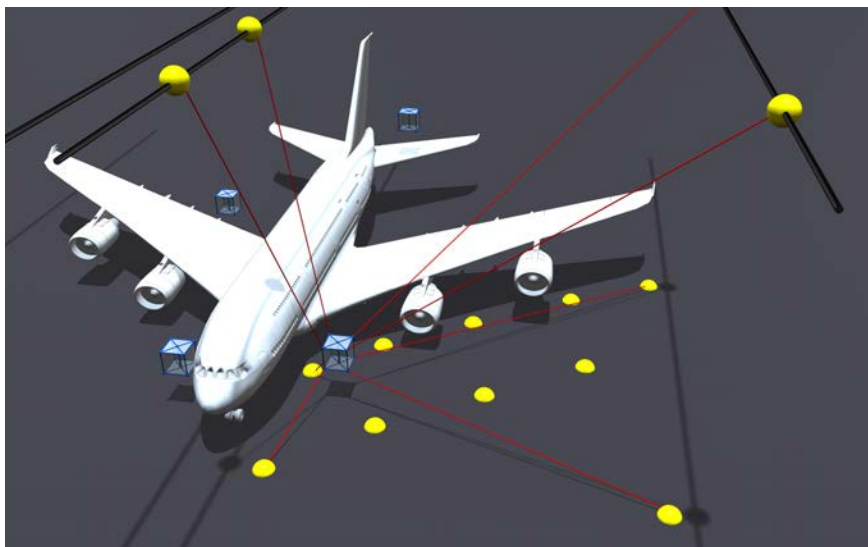


Figure 1.27: Fully constrained CDPRs: 4 winches can move on the rails on top of the airplane body, the other 4 winches can be switched among a grid of winches on the ground

PREFERRED SCENARIOS

Fig. 1.28 and 1.29 show a preferred scenario of using 4 reconfigurable CDPRS in an airplane maintenance workshop. This solution is similar to the ones proposed in factory workshop use case. The cable exit points move by pairs on the two overhead bridge cranes which can slide along parallel rails attached to the side walls of the workshop. In this setup, all four CDPRS can simultaneously perform required tasks in four given sections of the workshop.

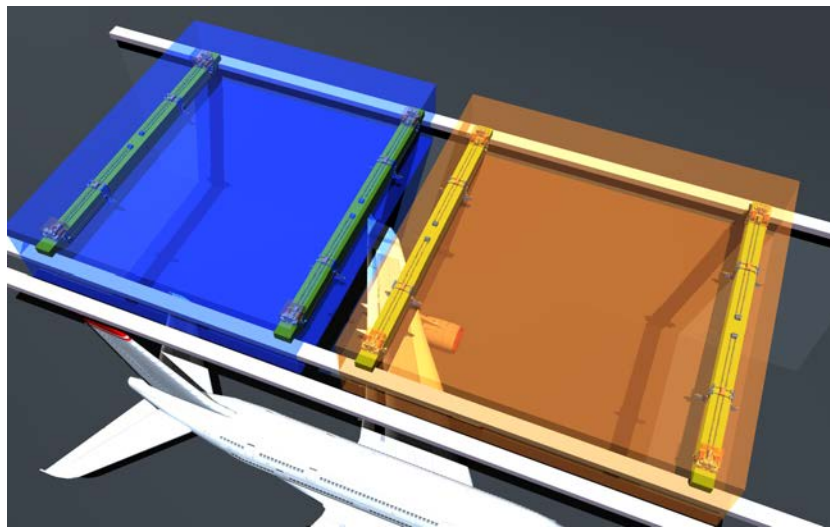


Figure 1.28: Solution of using 4 CDPRS in an airplane maintenance workshop: covered areas

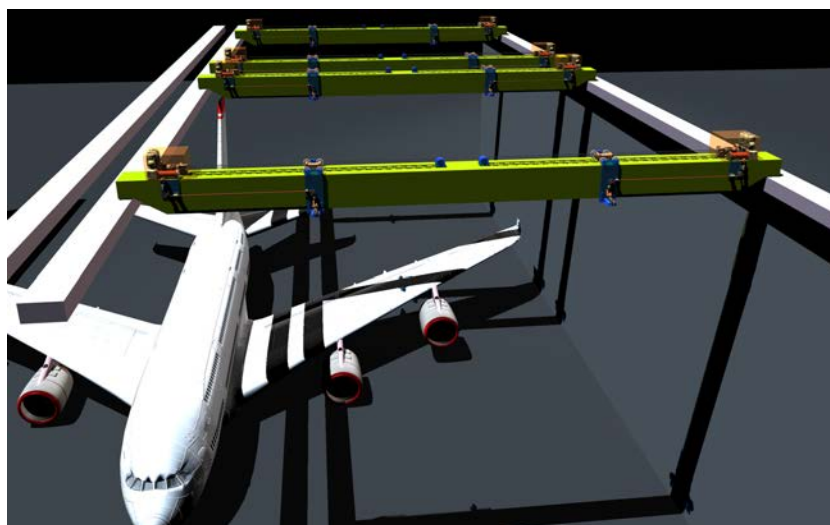


Figure 1.29: Solution of using 4 CDPRS in an airplane maintenance workshop: perspective view

To overcome the difficulty of reaching all the parts of the airplane body, suitable means are required, e.g. by adjusting the design of the mobile platform to increase its reachable range to access the lower parts of the airplane body. A possible solution (Fig. 1.30 and 1.31) is to keep the shape of the mobile platform similar to that of telescopic platforms used in conventional methods (Fig. 1.23). It is then required to find suitable locations for the cable anchor points that connect the cables to the CDPR platform in order to have a good counter-balance design that could maintain the stability of the platform taking into account the presence of workers working onboard.

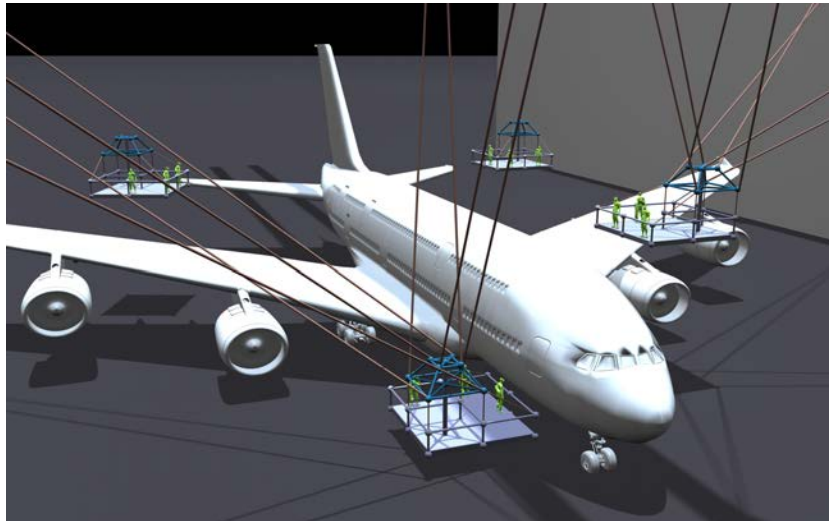


Figure 1.30: Modified mobile platform: perspective view

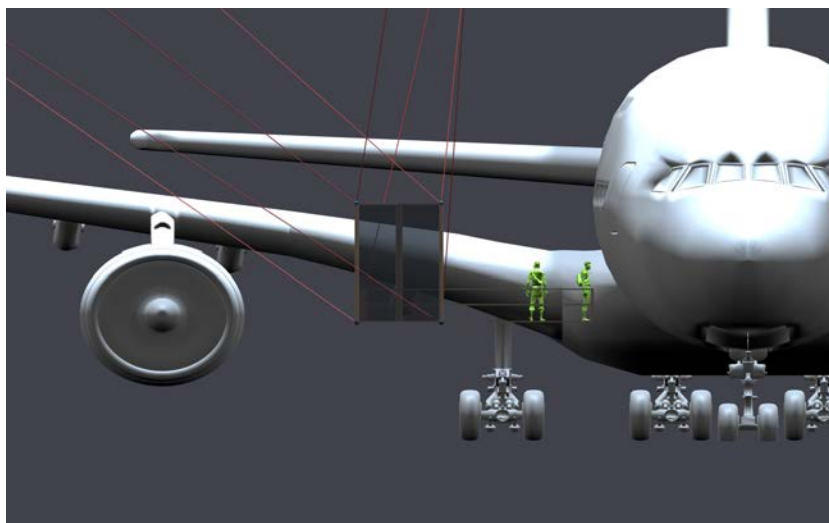


Figure 1.31: Modified mobile platform: elongate the platform working area to reach the lower part of airplane body

1.5 Contributions and Content of the Thesis

The main objective of this thesis being to develop a framework for reconfigurable CDPRs, the first step has been presented in Section 1.4 in which several general architectures of reconfigurable CDPRs were proposed (some of the solutions were inspired by the experiences from the partners in the CableBOT project). In the following chapters, I will detail my two main contributions. The first achievement is an extensive study on the CDPR modeling, including cable models suitable for large-dimension CDPRs. The second contribution consists of systematic procedures to deal with the reconfiguration (planning) problem of a family of reconfigurable CDPRs.

Chapter 2 presents the state of the art of CDPR kinematic, dynamic and elastostatic modeling. The inverse kinematics problem, the tension distribution problem and the derivation of the stiffness matrix of general 6-DOF CDPRs are addressed in detail. Several collision detection algorithms are also presented. All of these are useful for design, motion planning and control of reconfigurable CDPRs. The solutions of the inverse kinematics and tension distribution problems are used in the robot control system. In the design or planning phase, tension distribution solutions are used to verify wrench feasibility conditions guaranteeing that all cables could remain tensed while not exceeding maximum allowed cable tension values. Collision detection algorithms are needed to verify that the CDPR workspace is collision free, especially for spatial CDPRs with a large number of cables.

Chapter 3 details the extended modeling of CDPRs. The corresponding models consider most of the factors that could affect the CDPR performances such as: cable characteristics (cable mass, cable elasticity), thermal effect (the change of environment temperature), friction (between cables and pulleys, in the gear box of the winch...) and the influence of pulley kinematics. The CoGiRo prototype², an 8-cable large-dimension suspended CDPR, is used to illustrate the procedure in simulations and experiments. Our study shows that one should take into account those factors in order to improve the CDPR performance, especially its positioning accuracy.

Finally, Chapter 4 deals with the CDPR reconfiguration problem. In the scope of this thesis, we consider the reconfiguration problem as a general nonlinear optimization problem. The reconfigurability of the CDPR corresponds to the ability to adjust the positions of the cable exit points, thereby enabling the CDPR to adapt its performances. The focus of our study is on the methods to formulate the optimization problems into standard forms. It allows one to use any available (suitable) optimization software to find the optimal reconfiguration solutions. Two case studies are discussed. In the first case study,

2. <http://www.lirmm.fr/cogiro/>

the CDPR reconfiguration problem is considered as a single-objective optimization problem. A systematic procedure is proposed to solve this problem using fast optimization tools (e.g. gradient-based optimization) which enable real-time capable resolutions. It can be implemented both in offline and online CDPR operation modes. However, optimizing only one objective function to derive the CDPR reconfiguration solution may be not satisfactory enough in some cases. Thus, in the second case study, we consider the CDPR reconfiguration problem as a multi-objective optimization in which the solution is found by optimizing several performance indices. A systematic procedure is presented to formulate this problem and transform it into standard forms that could be solved with readily available optimization softwares. The proposed approach offers more reliable motion planning solutions for the CDPR while efficiently dealing with the tradeoff between several criteria.

PRELIMINARIES

Summary

2.1	General CDPR Modeling	30
2.2	Cable Modeling	32
2.3	The Tension Distribution Problem	41
2.4	Stiffness Matrix of CDPRs	43
2.5	On the Collision Detection Problems	47

This chapter is dedicated to the modeling of a general CDPR. Several aspects, fundamental to the design, motion planning and control of CDPRs, are presented. The well-known CDPR inverse kinetostatic problem (IKP) is discussed in Section 2.1. Section 2.2 presents the procedure to derive a simplified cable model which takes into account the cable mass and longitudinal elasticity. Section 2.3 briefly reminds the cable tension distribution problem of a general 6-DOF CDPR. The derivation of the stiffness matrix of a CDPR is then detailed in Section 2.4. This derivation is based on the elastic catenary cable model. Lastly, Section 2.5 discusses collision detection issues for CDPRs.

2.1 General CDPR Modeling

2.1.1 Kinetostatic Modeling

Fig. 2.1 shows a general m -cable CDPR where A_i and B_i ($i = 1, \dots, m$) are the cable i exit point and anchor point, respectively. F_{Bi} ($f_{bix}, f_{biy}, f_{biz}$) and τ_{bi} are the force and tension in cable i at anchor point B_i (x_{bi}, y_{bi}, z_{bi}). All the terms are expressed in the base frame of the robot (global frame).

The modeling of a CDPR, in general, is based on *a cable model* and *the CDPR equilibrium equations*. In [80], Irvine presents the well-known cable model known as *the elastic catenary* which takes the cable mass and elasticity into account. In [81], a cable catenary model in 3D Cartesian space is introduced. A fully 3D cable catenary model can be expressed in the following form:

$$x_{bi} = f_{1i}(L_{0i}, f_{bix}, f_{biy}, f_{biz}) \quad (2.1a)$$

$$y_{bi} = f_{2i}(L_{0i}, f_{bix}, f_{biy}, f_{biz}) \quad (2.1b)$$

$$z_{bi} = f_{3i}(L_{0i}, f_{bix}, f_{biy}, f_{biz}) \quad (2.1c)$$

where L_{0i} is the cable i unstrained length and f_{ji} are non-linear functions [81].

In the case of inverse kinematic problem, given the pose of the mobile platform then in (2.1), the coordinates of point B_i are determined. One need to find four unknown terms (which are the cable unstrained length and cable force components). The number of unknown variables is larger than the number of equations, thus it is necessary to consider the

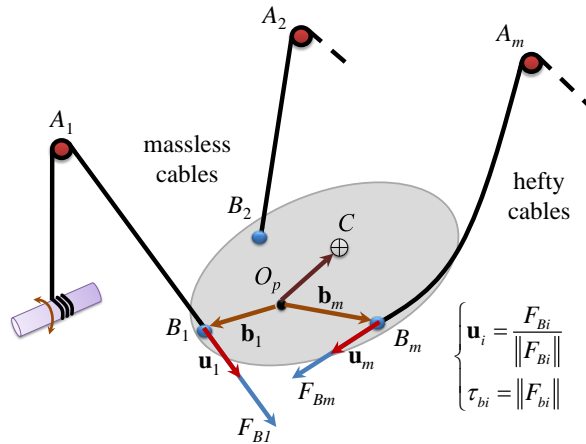


Figure 2.1: General m -cable CDPR

equilibrium equations of the mobile platform:

$$\mathbf{W}\boldsymbol{\tau}_b + \mathbf{f}_e = 0 \quad (2.2)$$

subject to:

$$\tau_{\min} \leq \tau_{bi} \leq \tau_{\max} \quad (i = \overline{1, m}) \quad (2.3)$$

and where

$$\begin{aligned} \mathbf{W} &= \begin{bmatrix} \mathbf{u}_1 & \mathbf{u}_2 & \cdots & \mathbf{u}_m \\ \mathbf{R}\mathbf{b}_1 \times \mathbf{u}_1 & \mathbf{R}\mathbf{b}_2 \times \mathbf{u}_2 & \cdots & \mathbf{R}\mathbf{b}_m \times \mathbf{u}_m \end{bmatrix} \\ \boldsymbol{\tau}_b &= \begin{bmatrix} \tau_{b1} & \tau_{b2} & \cdots & \tau_{bm} \end{bmatrix}^T \\ \mathbf{f}_e &= \begin{bmatrix} f_x & f_y & f_z & m_x & m_y & m_z \end{bmatrix}^T \end{aligned}$$

Here, \mathbf{f}_e is the wrench applied by the cables on the mobile platform, \mathbf{b}_i is the position vector of the anchor point B_i with respect to the origin of the mobile platform frame with origin O_p and \mathbf{u}_i is the unit vector directing the cable force F_{Bi} . τ_{\min} and τ_{\max} are the minimum and maximum admissible limits on the cable tensions. \mathbf{R} is the rotation matrix from the global frame to the mobile platform frame.

The condition (2.3) is to ensure the cables are always under tension ($\tau_{\min} \geq 0$) and the cable tensions are smaller than a maximum acceptable value. These conditions on the cable tensions make a CDPR different from a rigid-link parallel manipulator. The inequalities in (2.3) introduce complexity in solving the kinetostatic problems of CDPRs (inverse kinematic and tension distribution problems).

2.1.2 Dynamic Modeling

In this thesis, only the dynamics of the mobile platform is considered. Cable dynamics is neglected. The center of mass of the mobile platform is denoted C . The coordinates of C in the mobile platform frame $\langle O_p \rangle$ are $(x_c \ y_c \ z_c)$. We consider that the mobile platform moves with acceleration \mathbf{a}_p (of the origin O_p), angular velocity $\boldsymbol{\omega}$ and angular acceleration $\boldsymbol{\alpha}$. Here, the dynamics of the cables and the dynamics of the systems that drive the cable exit points, if any, are neglected.

According to Newton-Euler equations, one can write the equation of motions of the mobile platform as follows:

$$\begin{bmatrix} F \\ M_p \end{bmatrix} + \begin{bmatrix} m_p G \\ \mathbf{d} \times m_p G \end{bmatrix} + \mathbf{W}\boldsymbol{\tau}_b = 0 \quad (2.4)$$

where F and M_p are the inertia forces and moments acting on the mobile platform, and m_p is the total mass of the mobile platform. \mathbf{W} and $\boldsymbol{\tau}_b$ are defined in (2.30), $G = (0 \ 0 \ g)$ with $g = 9.81 \text{ m/s}^2$, and $\mathbf{d} = \mathbf{R} \cdot \overrightarrow{O_p C}$ is the projection of vector $\overrightarrow{O_p C}$ onto the global frame.

Because the center of mass C is distinct from O_p , we have:

$$F = m_p [\mathbf{a}_p + \boldsymbol{\alpha} \times \mathbf{d} + \boldsymbol{\omega} \times (\boldsymbol{\omega} \times \mathbf{d})] \quad (2.5)$$

$$M_p = m_p \mathbf{d} \times \mathbf{a}_p + \mathbf{I}_p \boldsymbol{\alpha} + \boldsymbol{\omega} \times (\mathbf{I}_p \boldsymbol{\omega}) \quad (2.6)$$

where \mathbf{I}_p is the moment of inertia about the reference point O_p of the mobile platform expressed in the global frame:

$$\mathbf{I}_p = \mathbf{R} \mathbf{I}_c \mathbf{R}^T + m_p [(\mathbf{d}^T \mathbf{d}) \cdot \mathbf{1}_{3 \times 3} - \mathbf{d} \mathbf{d}^T] \quad (2.7)$$

Here, \mathbf{I}_c is the polar moment of inertia (or matrix of inertia about the center of mass) of the mobile platform and $\mathbf{1}_{3 \times 3}$ is the identity matrix.

Depending on the context, either static modeling or dynamic modeling of the CDPR will be used. In fact, for control or motion planning, either (2.2) or else (2.4) will be used to compute the inverse kinematics solution (the cable unstrained lengths) and the desired cable tensions.

2.2 Cable Modeling

According to the previous section, to solve the inverse kinematics problem of a m -cable 6-DOF CDPR, there are $4m$ unknown terms ($L_{0i}, f_{bix}, f_{biy}, f_{biz}$) ($i = 1, \dots, m$) and a total of $3m + 6$ equations, including $3m$ cable equations (2.1) and the equilibrium equations (2.2) or (2.4). We need numerical methods to solve the inverse kinematics problem as well as the tension distribution problem since these two problems are non-linear and coupled together [24]. It becomes more complicated especially for the case of redundantly actuated CDPRs driven by more than 6 cables. However, such methods are usually time consuming and may be impractical in real-time control schemes. Simpler cable models are thus of interest to reduce the complexity of the problem.

Different approaches to avoid using the catenary cable model in modeling CDPRs have been proposed. In many previous studies on CDPRs, all cables have been considered massless. For robots of reasonable size and carrying light payloads massless cable models can be used, but for large-dimension robots or for robots that carry heavy payloads, the cable mass may have to be taken into account [23]. In [80], Irvine presents a parabolic cable

model. This cable model is valid if the sagging of the cable is small enough. However, the suggested validity condition is not explicitly derived. In [23], the parabolic hefty cable model is reintroduced in a simplified static analysis of large-dimension CDPRs which gives a linear relation between the cable horizontal and vertical force components. This relation helps to transform the cable tension distribution problem into one that is similar in form to the case of CDPRs with massless cables, from which one can apply advanced methods to find the cable tensions such as [18, 19, 32]. A nonlinear version of the relation between the cable horizontal and vertical force components is derived in [82] based on the catenary model. Knowing the cable tension, the cable unstrained length can be computed. In [24], Kozak gives an expression for the cable unstrained length, which takes into account the cable mass but without considering the cable elasticity. Later, an approximation of that expression is obtained by Rui Yao et al. in [83].

In this section, we shall give a discussion on the simplification of cable model as well as the determination of the cable unstrained length (solution to the inverse kinematics of a CDPR) as published in [69].

2.2.1 Cable Profile

Let us consider a steel cable that has unstrained length L_0 (m), self-weight w (N/m), elastic modulus E (Pa) and cable cross-section area A_0 (m²).

Fig. 2.2 shows the relevant coordinates and parameters of a cable lying in a vertical plane in static equilibrium. The cable is fixed between two end-points $A(x_{La}, z_{La})$ and

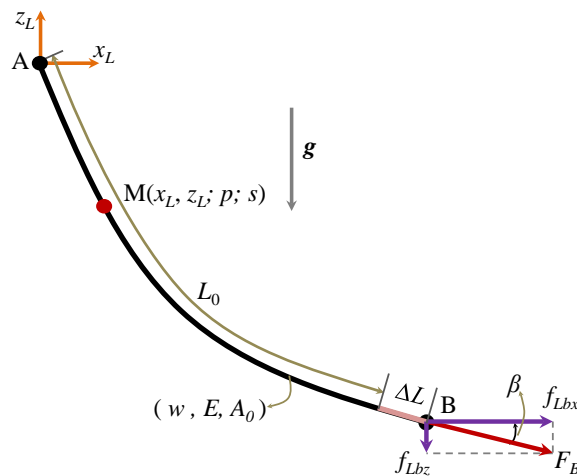


Figure 2.2: Diagram of a sagging cable in 2D (cable local frame)

$B(x_{Lb}, z_{Lb})$ ¹. All the coordinates are in the local frame attached to the vertical plane containing the cable. The term ΔL represents the strain of the cable.

A point M along the strained cable has Cartesian coordinates x_L and z_L . The variable p represents the strained length of the cable segment as measured from the end-point A of the cable to the point M . The variable s will be used to denote the unstrained length of the same cable segment. In Fig.2.2, the origin of the local frame will be placed at the end-point A . Thus, the variable s lies in the range: $0 \leq s \leq L_0$ with $M(s=0) \equiv A$ and $M(s=L_0) \equiv B$.

The well-known catenary equations can be written as follows [80]:

$$x_L(s) = x_{Lb} + \frac{f_{Lbx}(s-L_0)}{EA_0} + \frac{f_{Lbx}}{w} \ln \left[\frac{\tau_s + f_{Lbz} + w(s-L_0)}{\tau_b + f_{Lbz}} \right] \quad (2.8a)$$

$$z_L(s) = z_{Lb} + \frac{f_{Lbz}(s-L_0)}{EA_0} + \frac{w(s-L_0)^2}{2EA_0} + \frac{1}{w}(\tau_s - \tau_b) \quad (2.8b)$$

where f_{Lbx}, f_{Lbz} are the cable horizontal and vertical force components at point B and τ_s, τ_b are the tensions in the cable at point M and B , respectively:

$$\tau_s = \sqrt{f_{Lbx}^2 + [f_{Lbz} + w(s-L_0)]^2} \quad (2.9)$$

$$\tau_b = \sqrt{f_{Lbx}^2 + f_{Lbz}^2} \quad (2.10)$$

The shape of the cable must satisfy the geometric constraint:

$$\left(\frac{dx_L}{dp} \right)^2 + \left(\frac{dz_L}{dp} \right)^2 = 1 \quad (2.11)$$

which implies:

$$\frac{dp}{dx_L} = \sqrt{1 + \left(\frac{dz_L}{dx_L} \right)^2} \quad (2.12)$$

At point M , the force balance for the segment of the cable between points M and B can be written as follows:

$$\tau_s \left(\frac{dx_L}{dp} \right) = f_{Lbx} \quad (2.13a)$$

$$\tau_s \left(\frac{dz_L}{dp} \right) = f_{Lbz} + w(s-L_0) \quad (2.13b)$$

The cable tension at point M is considered to satisfy Hooke's law:

$$\tau_s = EA_0 \left(\frac{dp}{ds} - 1 \right) \quad (2.14)$$

1. the subscript L indicates the term are expressed in cable local frame

The relationship between coordinates x_L and z_L which does not depend explicitly on the variable s can be derived from (2.12), (2.13) and (2.14):

$$\frac{d^2 z_L}{dx_L^2} = \frac{w}{f_{Lbx}} \cdot \frac{EA_0}{EA_0 + \tau_s} \cdot \sqrt{1 + \left(\frac{dz_L}{dx_L}\right)^2} \quad (2.15)$$

Let us assume that $\tau_s \ll EA_0$. Then, the cable elasticity has a very little influence on the cable shape since (2.15) can be reduced to the simpler expression:

$$\frac{d^2 z_L}{dx_L^2} = \frac{w}{f_{Lbx}} \cdot \sqrt{1 + \left(\frac{dz_L}{dx_L}\right)^2} \quad (2.16)$$

The solution of (2.16) is:

$$z_L(x_L) = \frac{f_{Lbx}}{w} \cosh\left(\frac{w}{f_{Lbx}} x_L + C_1\right) + C_2 \quad (2.17)$$

which must satisfy the following boundary conditions:

$$z_L(x_{La}) = z_{La} \quad (2.18a)$$

$$z_L(x_{Lb}) = z_{Lb} \quad (2.18b)$$

As the origin of the local cable frame has been chosen at point A , $x_{La} = 0$ and $z_{La} = 0$, then:

$$C_2 = -\frac{1}{\mu} \cosh(C_1) \quad (2.19)$$

$$z_{Lb} = \frac{1}{\mu} [\cosh(\mu x_{Lb} + C_1) - \cosh(C_1)] \quad (2.20)$$

where

$$\mu = \frac{w}{f_{Lbx}} \quad (2.21)$$

The term C_1 can be found by solving (2.20)

$$C_1 = \ln\left(\frac{\sqrt{\mu^2 z_{Lb}^2 + e^{\mu x_{Lb}} + e^{-\mu x_{Lb}} - 2} + \mu z_{Lb}}{e^{\mu x_{Lb}} - 1}\right) \quad (2.22)$$

The conditions to achieve (2.22) are:

$$x_{Lb} > 0 \quad (2.23a)$$

$$f_{Lbx} > 0 \quad (2.23b)$$

(2.23a) is verified by definition of the local cable frame. (2.23b) is always true because the cable can only pull on the mobile platform. Note that (2.22) is the only solution of (2.20) because conditions (2.23a) and (2.23b) are always verified. The tangent at point B of the cable is then computed as:

$$\tan(\beta) = \left. \frac{dz_L}{dx_L} \right|_{x_L=x_{Lb}} = \frac{f_{Lbz}}{f_{Lbx}} = \sinh(\mu x_{Lb} + C_1) \quad (2.24)$$

Relationship (2.24) is similar to the one presented in [82]. Note that the simplifying assumption ($EA_0 \gg \tau_s$) and the validity conditions (2.23a) and (2.23b) are not explicit in [82].

2.2.2 Linearization

In the case of CDPRs with massless cables, several methods have been developed to solve important issues such as the tension distribution problem for 6-DOF CDPRs with a number of cables $m \geq 6$, e.g. in [18] and [32]. To take advantage of such methods, as presented in [23], in case of CDPRs with cables of non-negligible mass, one must achieve a linear relationship between the horizontal and vertical cable force components in order to transform the equilibrium equations of the mobile platform into ones similar to the case of CDPRs with massless cables. From (2.24), since $\tan(\beta)$ is a function of the cable horizontal force component f_{Lbx} , the relationship between the cable force components at end-point B is a nonlinear relationship ($f_{Lbz} = \tan(\beta) \cdot f_{Lbx}$). Hence, simplification of the term $\tan(\beta)$ needs to be performed in a proper way. To this end, one can consider the Taylor series expansion of (2.24) in term of the variable μ defined in (2.21).

In fact, choosing μ as the expansion variable is reasonable since, in the case of a CDPR with steel cables carrying heavy payloads, μ is relatively small and depends only on the cable self-weight w and the cable horizontal force component f_{Lbx} . The Taylor series expansion of $\tan(\beta)$ around the expansion point $\mu = 0$ up to order of 3 is:

$$\begin{aligned} \tan(\beta) &= -\sinh(H) + \frac{1}{2} x_{Lb} \cosh(H) \mu \\ &- \left[\frac{x_{Lb}^2 z_{Lb} \cosh(H)}{24 \sqrt{x_{Lb}^2 + z_{Lb}^2}} + \frac{1}{8} x_{Lb}^2 \sinh(H) \right] \mu^2 \\ &+ \left[\frac{1}{48} x_{Lb}^3 \cosh(H) + \frac{x_{Lb}^3 z_{Lb} \sinh(H)}{48 \sqrt{x_{Lb}^2 + z_{Lb}^2}} \right] \mu^3 + O(\mu^4) \end{aligned} \quad (2.25)$$

where

$$H = \ln \left(\frac{x_{Lb}}{\sqrt{x_{Lb}^2 + z_{Lb}^2} + z_{Lb}} \right)$$

In order to achieve a linear relationship between the cable force components f_{Lbx} and f_{Lbz} , only expansion of order 1 in (2.25) is to be considered:

$$\begin{aligned} \tan(\beta) &= -\sinh(H) + \frac{1}{2}x_{Lb}\cosh(H)\mu \\ &= \frac{z_{Lb}}{x_{Lb}} + \frac{1}{2}\sqrt{x_{Lb}^2 + z_{Lb}^2}\mu \end{aligned} \quad (2.26)$$

Finally, we obtain the linear relationship:

$$f_{Lbz} = \tan(\beta_0) \cdot f_{Lbx} + \frac{wL}{2} \quad (2.27)$$

where $\tan(\beta_0) = z_{Lb}/x_{Lb}$ and $L = \|AB\| = \sqrt{x_{Lb}^2 + z_{Lb}^2}$.

Relationship (2.27) is the same as the simplified cable model presented in [23].

In summary, we have rigorously detailed the simplifications to the elastic catenary cable modeling which lead to a linear relationship between the horizontal f_{Lbx} and vertical f_{Lbz} cable force components in (2.27). This linear relationship is the basis of the simplified static analysis introduced in [23]. The first assumption $\tau_s \ll EA_0$ was made in (2.15). If verified, it means that the cable elasticity has no real influence on the cable shape. The second assumption states that the variable μ defined in (2.21) is small enough. Depending on the context, the validity of these two assumptions may be an issue so that they should be carefully checked.

2.2.3 A Limitation of the Simplified Cable Model

In the linearization procedure presented in Section 2.2.2, if the expansion variable is chosen as $v = \mu x_b$ instead of μ , and the Taylor series expansion of $\tan(\beta)$ is performed around the expansion point $v = 0$, we obtain the same linear relationship (2.27). Hence, the accuracy of the approximation of $\tan(\beta)$ should also be justified in term of the variable v since $v > \mu$ for large-dimension CDPR (x_b can be large). Equation (2.27) is valid if v is small enough:

$$0 \leq v \leq v_{min} \quad (2.28)$$

where v_{min} is a chosen small value. This condition leads to the following constraint on the cable horizontal force component:

$$\frac{w x_{Lb}}{v_{min}} \leq f_{Lbx} \quad (2.29)$$

The validation of condition (2.29) gives an insight into the limitation of the simplified cable model. To illustrate this point, let us consider the problem which consists in determining the wrench-feasible workspace (*WFW*) [39] of a CDPR driven by m cables. *The WFW is the set of poses of the mobile platform for which, for any wrench \mathbf{f} in W_{req} , there exists a vector of cable horizontal force components \mathbf{f}_{Lbx} which is a solution to the equilibrium equations:*

$$\mathbf{W}_x \boldsymbol{\tau}_{Lbx} + \mathbf{f} = 0 \quad (2.30)$$

and verifies:

$$\tau_{min} \leq \tau_{bxi} \leq \tau_{max} \quad (i = \overline{1, m}) \quad (2.31)$$

Here, W_{req} is the required set of wrenches that the cables must apply at the reference point O_p of the mobile platform. Equation (2.30) is the modified equilibrium equations of the mobile platform obtained with the simplified static analysis presented in [23] which assumes that (2.27) is valid. For a given CDPR geometry, the wrench matrix \mathbf{W} depends only on the pose of the mobile platform. If the required set of wrenches W_{req} is also known, then the size of the *WFW* is determined by condition (2.31).

For the simplified static analysis of [23] to be valid across the *WFW*, the lower bound of (2.31) must not be smaller than:

$$\tau_{min} = \frac{w x_{Lb}}{v_{min}} \quad (2.32)$$

The size of the *WFW* depends on the admissible range $[\tau_{min}, \tau_{max}]$ of the cable horizontal force component. In fact, the upper bound on the cable forces is always determined by safety considerations. Hence, with a fixed upper bound on the cable horizontal force component ($\tau_{max} = const$), the size of the part of the *WFW* in which the simplified cable model is valid is reduced when τ_{min} increases. That makes the size of this workspace inversely proportional to x_{Lb} (and also to the cable self-weight w).

In practice, it is preferable to have a large *WFW*. For a given set of wrenches and in a large prescribed workspace, condition (2.29) may be violated in some areas. Thus, it is expected to get large errors in the approximation of the term $\tan(\beta)$. Such errors lead to a poor accuracy in solving the cable tension distribution problem with the simplified static analysis of [23], i.e., the *WFW* determination based on (2.30) is not valid. The problem is even more involved since the assumption $\tau_s \ll EA_0$ may be questioned if f_{Lbx} is large.

2.2.4 Computation of the Cable Unstrained Length

Starting from (2.14), one can derive:

$$\begin{aligned} dp &= \left(1 + \frac{\tau_s}{EA_0}\right) ds = \left(1 + \frac{f_{Lbx}}{EA_0} \cdot \frac{dp}{dx_L}\right) ds \\ \frac{dp}{dx_L} &= \left(1 + \frac{f_{Lbx}}{EA_0} \cdot \frac{dp}{dx_L}\right) \frac{ds}{dx_L} \end{aligned} \quad (2.33)$$

Substitute dp/dx from (2.12) into (2.33) to obtain:

$$\frac{ds}{dx_L} = \frac{\sqrt{1 + \left(\frac{dz_L}{dx_L}\right)^2}}{1 + \frac{f_{Lbx}}{EA_0} \sqrt{1 + \left(\frac{dz_L}{dx_L}\right)^2}} \quad (2.34)$$

If we use the solution of $z_L(x_L)$ from (2.17) and since:

$$\sqrt{1 + \left(\frac{dz_L}{dx_L}\right)^2} = \cosh(\mu x_L + C_1) \quad (2.35)$$

where C_1 is given in (2.22), then (2.34) becomes:

$$\frac{ds}{dx_L} = \frac{EA_0}{f_{Lbx}} \left(1 - \frac{1}{1+R}\right) \quad (2.36)$$

where

$$R = \frac{f_{Lbx}}{EA_0} \cosh(\mu x_L + C_1)$$

The close form solution of L_0 is given as follows:

$$\begin{aligned} L_0 &= \int_0^{L_0} ds = \int_{x_{La}=0}^{x_{Lb}} \frac{EA_0}{f_{Lbx}} \left(1 - \frac{1}{1+R}\right) dx_L \\ &= \frac{EA_0}{f_{Lbx}} \int_{x_{La}=0}^{x_{Lb}} dx_L - \frac{EA_0}{\mu f_{Lbx}} \int_{R_a}^{R_b} \frac{1}{(1+R)\sqrt{R^2 - a}} dR \\ &= \frac{EA_0}{f_{Lbx}} \left[x_{Lb} - \frac{1}{\mu} (H_a - H_b) \right] \end{aligned} \quad (2.37)$$

where

$$\begin{aligned}
 H_b &= \frac{\ln(1 + R_b) - \ln\left(a + R_b - \sqrt{1-a}\sqrt{R_b^2 - a}\right)}{\sqrt{1-a}} \\
 H_a &= \frac{\ln(1 + R_a) - \ln\left(a + R_a - \sqrt{1-a}\sqrt{R_a^2 - a}\right)}{\sqrt{1-a}} \\
 R_b &= \frac{f_{Lbx}}{EA_0} \cosh(\mu x_{Lb} + C_1) \\
 R_a &= \frac{f_{Lbx}}{EA_0} \cosh(C_1) \\
 a &= \frac{f_{Lbx}^2}{E^2 A_0^2}
 \end{aligned}$$

In order to see clearly the effect of the cable mass and elasticity on the cable unstrained length, we use Taylor series expansion to find an approximation of ds/dx_L around the expansion point $R = 0$ ($R \ll 1$ because we assume that $f_{Lbx} \ll EA_0$) as follows:

$$\frac{ds}{dx_L} = \frac{EA_0}{f_{Lbx}} \left[R - R^2 + R^3 + O(R^4) \right] \quad (2.38)$$

The cable unstrained length is thus computed as:

$$\begin{aligned}
 L_0 &= \int_0^{L_0} ds = \int_{x_{La}=0}^{x_{Lb}} \frac{EA_0}{f_{Lbx}} \left[R - R^2 + R^3 \right] dx_L \\
 &= \frac{1}{\mu} \left[\sinh(C_b) - \sinh(C_1) \right] \\
 &\quad - \frac{f_{Lbx}}{4EA_0\mu} \left[2\mu x_b - \sinh(2C_1) + \sinh(2C_b) \right] \\
 &\quad - \frac{f_{Lbx}^2}{12E^2 A_0^2 \mu} \left[9\sinh(C_1) - 9\sinh(C_b) \right. \\
 &\quad \quad \left. + \sinh(3C_1) - \sinh(3C_b) \right] \quad (2.39)
 \end{aligned}$$

with $C_b = \mu x_{Lb} + C_1$.

In (2.39), if the series expansion of ds/dx_L up to order 1 of R is only considered, the expression of L_0 is the same as the one presented in [24] where only the cable mass is taken into account (elasticity neglected). The expression of L_0 with a higher order of R takes into account both the cable mass and elasticity.

The unstrained cable length as given in (2.37) or in (2.39) is the one needed for the inverse kinematics and thus for the trajectory planning part in a control scheme of a C DPR.

2.3 The Tension Distribution Problem

Let us consider the m -cable CDPR shown in Fig. 2.1. At a given pose of the mobile platform, the coordinates of the cable exit point and anchor point of cable i are determined $A_i(x_{ai}, y_{ai}, z_{ai})$ and $B_i(x_{bi}, y_{bi}, z_{bi})$. The CDPR tension distribution problem is to find the cable forces $F_{Bi} = (f_{bix} \ f_{biy} \ f_{biz})$ at the cable anchor points $B_i (i = \overline{1, m})$. In fact F_{Bi} are found by solving the equilibrium equations of the CDPR.

In the case of CDPRs with massless cable model (e.g. massless elastic cable model), the equilibrium equations are the same as (2.2) where the unit vectors \mathbf{u}_i that direct the cable forces F_{Bi} are given as follows:

$$\mathbf{u}_i = \frac{B_i - A_i}{\|B_i - A_i\|} \quad (2.40)$$

(it means that each cable is assumed to be a straight line).

The solution for (2.2) in the case of a number of cables $m = 6$ is:

$$\boldsymbol{\tau}_b = -\mathbf{W}^{-1} \mathbf{f}_e \quad (2.41)$$

For redundantly actuated CDPRs with a number of cables $m > 6$, the solution for $\boldsymbol{\tau}$ is:

$$\boldsymbol{\tau}_b = \boldsymbol{\tau}_p + \mathbf{N} \boldsymbol{\lambda} \quad (2.42)$$

where

$$\boldsymbol{\tau}_p = -\mathbf{W}^+ \mathbf{f}_e \quad (2.43)$$

$$\mathbf{W}^+ = \text{pinv}(\mathbf{W}) \quad (\text{pseudo-inverse of } \mathbf{W})$$

$$\mathbf{N} = \text{Null}(\mathbf{W}) \quad (\text{Nullspace basis matrix of } \mathbf{W} \text{ of size } [m \times (m - 6)])$$

and $\boldsymbol{\lambda}$ is a vector of size $[(m - 6) \times 1]$.

The problem results into solving a sub-problem: “find $\boldsymbol{\lambda}$ that minimizes a performance index and satisfies $\{\boldsymbol{\tau}_{\min} - \boldsymbol{\tau}_p \leq \mathbf{N} \boldsymbol{\lambda} \leq \boldsymbol{\tau}_{\max} - \boldsymbol{\tau}_p\}$ ”. This sub-problem can be solved e.g. by methods presented in [18, 32, 33].

In the case of CDPRs with simplified cable model, because of the influence of the cable mass, the cable sags under its own weight (the cable is not a straight line). Thus, one need to reformulate the equilibrium equations (2.2) [23]. The linear relationship (2.27) in the cable local frame:

$$f_{Lbiz} = \tan(\beta_{0i}) f_{Lbix} + \frac{L_i w}{2} \quad (i = \overline{1, m}) \quad (2.44)$$

where $\tan(\beta_{0i}) = z_{Lbi}/x_{Lbi}$ and $L_i = \sqrt{x_{Lbi}^2 + z_{Lbi}^2}$, is needed to decouple the mobile platform static equilibrium equations from the cable model equations.

The force F_{Bi} could be expressed in term of f_{Lbix} :

$$F_{Bi} = [f_{bix} \ f_{biy} \ f_{biz}]^T = \mathbf{q}_i f_{Lbix} + \mathbf{f}_i \quad (2.45)$$

where

$$\mathbf{q}_i = [\cos(\gamma_i) \ \sin(\gamma_i) \ \tan(\beta_{0i})]^T \quad (2.46)$$

$$\mathbf{f}_i = \left[0 \ 0 \ \frac{L_i w}{2} \right]^T \quad (i = \overline{1, m}) \quad (2.47)$$

$$\gamma_i = \text{atan2}(y_{bi} - y_{ai}, x_{bi} - x_{ai}) \quad (2.48)$$

The equilibrium equation (2.2) could be rewritten as follows: [23]

$$\mathbf{W}_x \boldsymbol{\tau}_x + \mathbf{f}_{cab} + \mathbf{f}_e = \mathbf{0} \quad (2.49)$$

where

$$\mathbf{W}_x = \begin{bmatrix} \mathbf{q}_1 & \mathbf{q}_2 & \cdots & \mathbf{q}_m \\ \mathbf{Rb}_1 \times \mathbf{q}_1 & \mathbf{Rb}_2 \times \mathbf{q}_2 & \cdots & \mathbf{Rb}_m \times \mathbf{q}_m \end{bmatrix}$$

$$\boldsymbol{\tau}_x = \begin{bmatrix} f_{Lb1x} & f_{Lb2x} & \cdots & f_{Lbmx} \end{bmatrix}$$

$$\mathbf{f}_{cab} = \sum_{i=1}^m \begin{bmatrix} \mathbf{f}_i \\ \mathbf{Rb}_i \times \mathbf{f}_i \end{bmatrix}$$

When the wrench matrix \mathbf{W}_x is known, the solution of (2.49) in the case of a number of cables $m = 6$ is:

$$\boldsymbol{\tau}_x = -\mathbf{W}_x^{-1} (\mathbf{f}_e + \mathbf{f}_{cab}) \quad (2.50)$$

For redundantly actuated CDPRs with a number of cables $m > 6$, the solution for $\boldsymbol{\tau}_x$ is:

$$\boldsymbol{\tau}_x = \boldsymbol{\tau}_{px} + \mathbf{N}_x \boldsymbol{\lambda}_x \quad (2.51)$$

where

$$\boldsymbol{\tau}_{px} = -\mathbf{W}_x^+ (\mathbf{f}_e + \mathbf{f}_{cab})$$

$$\mathbf{W}_x^+ = \text{pinv}(\mathbf{W}_x) \quad (\text{pseudo-inverse of } \mathbf{W}_x)$$

$$\mathbf{N}_x = \text{Null}(\mathbf{W}_x) \quad (\text{Nullspace basis matrix of } \mathbf{W}_x \text{ of size } [m \times (m-6)])$$

and $\boldsymbol{\lambda}_x$ is a vector of size $[(m-6) \times 1]$.

Knowing $\boldsymbol{\tau}_x$, the force vectors F_{Bi} are obtained directly from (2.45).

2.4 Stiffness Matrix of CDPRS

2.4.1 Stiffness Matrix of One Cable

Let us consider a steel cable that has unstrained length $L_0 (m)$, self-weight $w (N/m)$, elastic modulus $E (Pa)$ and cable cross-section area $A_0 (m^2)$. Figure 2.3 shows the relevant coordinates and parameters of a cable in static equilibrium (in three dimensions). The cable is fixed between two end-points $A (x_a, y_a, z_a)$ and $B (x_b, y_b, z_b)$ (expressed in the global frame). The term ΔL represents the strain of the cable. f_{bx} , f_{by} and f_{bz} are the cable horizontal and vertical force components at point B and:

$$\tau_a = \sqrt{f_{bx}^2 + f_{by}^2 + (f_{bz} - w L_0)^2} \quad (2.52)$$

$$\tau_b = \sqrt{f_{bx}^2 + f_{by}^2 + f_{bz}^2} \quad (2.53)$$

are the tensions in the cable at points A and B , respectively.

According to the well-known elastic catenary equations [80, 81], we obtain the relation between the coordinates of points A and B :

$$x_b = x_a + \frac{f_{bx} L_0}{EA_0} - \frac{f_{bx}}{w} \ln \left[\frac{\tau_a + f_{bz} - w L_0}{\tau_b + f_{bz}} \right] \quad (2.54a)$$

$$y_b = y_a + \frac{f_{by} L_0}{EA_0} - \frac{f_{by}}{w} \ln \left[\frac{\tau_a + f_{bz} - w L_0}{\tau_b + f_{bz}} \right] \quad (2.54b)$$

$$z_b = z_a + \frac{f_{bz} L_0}{EA_0} - \frac{w L_0^2}{2EA_0} - \frac{1}{w} (\tau_a - \tau_b) \quad (2.54c)$$

If the coordinates of point A are known, then the coordinates of point B can be com-

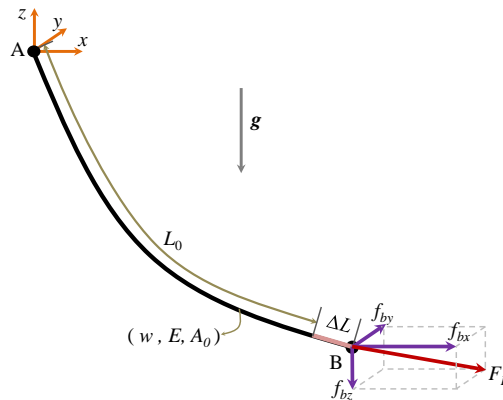


Figure 2.3: Sketch of a sagging cable in 3D

puted from the cable force components and the cable unstrained length L_0

$$B = f(f_{bx}, f_{by}, f_{bz}, L_0) \quad (2.55)$$

Differentiating both sides of (2.55) and applying the chain rule, we have:

$$\begin{aligned} dB &= \frac{\partial B}{\partial F_B} \cdot dF_B + \frac{\partial B}{\partial L_0} \cdot dL_0 \\ \Rightarrow dF_B &= \mathbf{K}_B \cdot dB - K_L \cdot dL_0 \end{aligned} \quad (2.56)$$

Here, the vector $d\mathbf{u}$ denotes an infinitesimal change in vector \mathbf{u} . F_B is the cable force at point B as shown in Figure 2.3. \mathbf{K}_B is the stiffness matrix of the cable at point B :

$$\mathbf{K}_B = \left(\frac{\partial B}{\partial F_B} \right)^{-1} \quad (2.57)$$

The vector K_L in (2.56) is

$$K_L = \left(\frac{\partial B}{\partial F_B} \right)^{-1} \cdot \left(\frac{\partial B}{\partial L_0} \right) = \mathbf{K}_B \cdot F_A \cdot \left(\frac{1}{EA_0} + \frac{1}{\tau_a} \right) \quad (2.58)$$

where $F_A = [f_{bx} \ f_{by} \ (f_{bz} - wL_0)]^T$ is the force applied by the cable at point A .

The partial derivative elements of matrices $\frac{\partial B}{\partial F_B}$ and $\frac{\partial B}{\partial L_0}$ are given as follows:

$$\begin{aligned} \frac{\partial x_b}{\partial f_{bx}} &= \frac{L_0}{EA_0} + \frac{1}{w} \ln \left(\frac{\tau_b + f_{bz}}{\tau_a + f_{bz} - wL_0} \right) + \frac{f_{bx}^2}{w} \left[\frac{1}{(\tau_b + f_{bz})\tau_b} - \frac{1}{(\tau_a + f_{bz} - wL_0)\tau_a} \right] \\ \frac{\partial x_b}{\partial f_{by}} &= \frac{f_{bx}f_{by}}{w} \left[\frac{1}{(\tau_b + f_{bz})\tau_b} - \frac{1}{(\tau_a + f_{bz} - wL_0)\tau_a} \right] \\ \frac{\partial x_b}{\partial f_{bz}} &= \frac{f_{bx}}{w} \left(\frac{1}{\tau_b} - \frac{1}{\tau_a} \right) \end{aligned}$$

$$\frac{\partial y_b}{\partial f_{bx}} = \frac{\partial x_b}{\partial f_{by}}$$

$$\begin{aligned} \frac{\partial y_b}{\partial f_{by}} &= \frac{L_0}{EA_0} + \frac{1}{w} \ln \left(\frac{\tau_b + f_{bz}}{\tau_a + f_{bz} - wL_0} \right) + \frac{f_{by}^2}{w} \left[\frac{1}{(\tau_b + f_{bz})\tau_b} - \frac{1}{(\tau_a + f_{bz} - wL_0)\tau_a} \right] \\ \frac{\partial y_b}{\partial f_{bz}} &= \frac{f_{by}}{w} \left(\frac{1}{\tau_b} - \frac{1}{\tau_a} \right) \end{aligned}$$

$$\begin{aligned}\frac{\partial z_b}{\partial f_{bx}} &= \frac{\partial x_b}{\partial f_{bz}} \\ \frac{\partial z_b}{\partial f_{by}} &= \frac{\partial y_b}{\partial f_{bz}} \\ \frac{\partial z_b}{\partial f_{bz}} &= \frac{L_0}{EA_0} + \frac{1}{w} \left[\frac{f_{bz}}{\tau_b} - \frac{f_{bz} - wL_0}{\tau_a} \right]\end{aligned}$$

$$\begin{aligned}\frac{\partial x_b}{\partial L_0} &= f_{bx} \left(\frac{1}{EA_0} + \frac{1}{\tau_a} \right) \\ \frac{\partial y_b}{\partial L_0} &= f_{by} \left(\frac{1}{EA_0} + \frac{1}{\tau_a} \right) \\ \frac{\partial z_b}{\partial L_0} &= (f_{bz} - wL_0) \left(\frac{1}{EA_0} + \frac{1}{\tau_a} \right)\end{aligned}$$

2.4.2 Stiffness Matrix of 6-DOF CDPRS

Let us consider the CDPR shown in Figure 2.1. F_{Bi} is the force applied by the mobile platform on the cable i at its end point B_i . Hence, the resultant wrench applied by the cables on the mobile platform is:

$$\mathbf{f}_c = \left[\sum_{i=1}^m -F_{Bi}, \sum_{i=1}^m -(\mathbf{Rb}_i \times F_{Bi}) \right]^T \quad (2.59)$$

Assume that an infinitesimal external wrench $d\mathbf{f}_e$ is applied on the mobile platform. Then, in static equilibrium:

$$d\mathbf{f}_e = d(-\mathbf{f}_c) = \left[\begin{array}{c} \sum_{i=1}^m dF_{Bi} \\ \sum_{i=1}^m d(\mathbf{Rb}_i \times F_{Bi}) \end{array} \right] \quad (2.60)$$

We have:

$$\begin{aligned}dF_{Bi} &= \mathbf{K}_{Bi} \cdot dB_i - K_{Li} \cdot dL_{0i} \\ &= \mathbf{K}_{Bi} \cdot d(\mathbf{Rb}_i + P) - K_{Li} \cdot dL_{0i} \\ &= \mathbf{K}_{Bi} \cdot \left(-(\mathbf{Rb}_i)_\times \cdot d\Phi + dP \right) - K_{Li} \cdot dL_{0i} \\ &= \mathbf{K}_{Bi} \cdot [\mathbf{1}_{3 \times 3}, -(\mathbf{Rb}_i)_\times] \cdot dX - K_{Li} \cdot dL_{0i}\end{aligned} \quad (2.61)$$

where $X = (x \ y \ z \ \theta_x \ \theta_y \ \theta_z)$ defines the mobile platform pose, $P = (x \ y \ z)$ is the position vector in Cartesian space of point O_p , $\theta = (\theta_x \ \theta_y \ \theta_z)$ is a vector of Euler angles,

$dP = (dx \ dy \ dz)$ is the position displacement vector, $d\Phi = \mathbf{S} \cdot d\boldsymbol{\theta}$ is the rotation displacement vector with $d\boldsymbol{\theta} = (d\theta_x \ d\theta_y \ d\theta_z)$ and $dX = (dP, d\Phi)$ is the infinitesimal displacement vector of the mobile platform. The term $(\mathbf{u})_\times$ indicates the cross product matrix of vector \mathbf{u} , $\mathbf{I}_{3 \times 3}$ is the identity matrix. The rotation matrix \mathbf{R} and the transformation matrix \mathbf{S} (which maps the time derivative of the vector of ZYX Euler angles to the mobile platform angular velocity vector) are given as follows:

$$\mathbf{R} = \begin{bmatrix} C_y C_z & C_z S_y S_x - S_z C_x & C_z S_y C_x + S_z S_x \\ C_y S_z & S_z S_y S_x + C_z C_x & S_z S_y C_x - C_z S_x \\ -S_y & C_y S_x & C_y C_x \end{bmatrix}, \quad \mathbf{S} = \begin{bmatrix} C_y C_z & -S_z & 0 \\ C_y S_z & C_z & 0 \\ -S_y & 0 & 1 \end{bmatrix} \quad (2.62)$$

with $C_x = \cos(\theta_x)$, $S_x = \sin(\theta_x)$, $C_y = \cos(\theta_y)$, ...

Moreover, we have:

$$\begin{aligned} d(\mathbf{Rb}_i \times F_{Bi}) &= d(\mathbf{Rb}_i) \times F_{Bi} + (\mathbf{Rb}_i) \times dF_{Bi} \\ &= (F_{Bi})_\times^T \cdot (\mathbf{Rb}_i)_\times^T \cdot d\Phi + (\mathbf{Rb}_i) \times dF_{Bi} \\ &= [(\mathbf{Rb}_i)_\times \cdot \mathbf{K}_{Bi}, \quad \mathbf{H}_i - (\mathbf{Rb}_i)_\times \cdot \mathbf{K}_{Bi} \cdot (\mathbf{Rb}_i)_\times] \cdot dX \\ &\quad - (\mathbf{Rb}_i)_\times \cdot K_{Li} \cdot dL_{0i} \end{aligned} \quad (2.63)$$

Here, the matrix \mathbf{H}_i is defined as:

$$\mathbf{H}_i = (F_{Bi})_\times^T \cdot (\mathbf{Rb}_i)_\times^T \quad (2.64)$$

Finally, from (2.60), (2.61), (2.63) we obtain:

$$d\mathbf{f}_e = \mathbf{K} \cdot dX - \mathbf{K}_L \cdot dL_0 \quad (2.65)$$

where

$$\mathbf{K} = \begin{bmatrix} \sum_{i=1}^m \mathbf{K}_{Bi} & -\sum_{i=1}^m \mathbf{K}_{Bi} \cdot (\mathbf{Rb}_i)_\times \\ \sum_{i=1}^m (\mathbf{Rb}_i)_\times \cdot \mathbf{K}_{Bi} & \sum_{i=1}^m \mathbf{H}_i - \sum_{i=1}^m (\mathbf{Rb}_i)_\times \cdot \mathbf{K}_{Bi} \cdot (\mathbf{Rb}_i)_\times \end{bmatrix} \quad (2.66)$$

and

$$\mathbf{K}_L = \begin{bmatrix} K_{L1} & K_{L2} & \dots & K_{Lm} \\ (\mathbf{Rb}_1)_\times \cdot K_{L1} & (\mathbf{Rb}_2)_\times \cdot K_{L2} & \dots & (\mathbf{Rb}_m)_\times \cdot K_{Lm} \end{bmatrix} \quad (2.67)$$

where K_{Li} ($i = \overline{1, m}$) is given in (2.58).

If when the infinitesimal wrench $d\mathbf{f}_e$ is applied on the mobile platform all the cable unstrained lengths are assumed to be unchanged ($dL_0 = \mathbf{0}$), then we obtain \mathbf{K} as the stiffness matrix of the CDPR at the mobile platform.

Note that, as an additional merit of (2.65), at the equilibrium state ($d\mathbf{f}_e = \mathbf{0}$), we also obtain the Jacobian matrix of the CDPR:

$$\mathbf{J} = \mathbf{K}^{-1} \cdot \mathbf{K}_L \quad (2.68)$$

2.5 On the Collision Detection Problems

For CDPRs, collisions happen in several cases:

- Interferences between cables and cables
- Interferences between cables and the mobile platform
- Interferences between the mobile platform and its surrounding environment
- Interferences between cables and their surrounding environment

Efficient methods to detect such collisions become necessary, especially for spatial CDPR having a large number of cables (e.g. $m \geq 6$) such as the NIST robot crane [16], the Marionet CDPR [4, 71] and the CoGiRo prototype [32]. These methods could be used in two main situations:

- Design/motion planning: required to check the capability of CDPR (e.g. compute the bounds on the orientation and Cartesian spaces within which there is no cable interference).
- Control: required to guarantee safety issues in operating CDPR in real-time.

In most situations, the latter case can be avoided if all the safety constraints are dealt with from checking the capability of CDPR over a desired workspace. In this section, we mainly discuss the verification of collision free conditions for a CDPR in the design or offline planning phases.

In fact, the cable interference problem has not been extensively addressed. Studies on this topic can be listed as [84, 85, 86, 87, 88, 89, 90].

About the collisions between cables or between the CDPR mobile platform with its surrounding environment, one can use AABB or OORB tree methods [91]. These methods are fast and effective for large and complex shape objects (triangulations of the mobile platform and obstacles may consist of a lot of vertices). One can also find an efficient method in [90] to deal with these two collision detection problems.

For CDPRs with light-weight cables, the cables can be considered as straight lines. For CDPRs using hefty cables, the mobile platform weight is expectedly large, the cable sag-

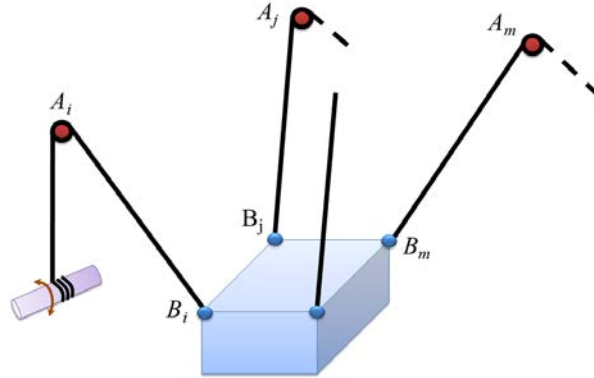


Figure 2.4: A general m -cable CDPR

ging effects may not really affect the algorithms, thus it may also be sufficient enough to consider the cables as straight lines. In either cases, the interferences between cables and cables can be treated as interferences between straight line segments. The interferences between cables and the CDPR mobile platform can be considered as collisions between straight line segments and triangles (the latter triangulating the surface of the CDPR mobile platform). Usual methods [91] can be applied to detect such interferences. However, these methods are only suited for real-time situations and are not satisfactory enough to verify the cable interference free conditions for a prescribed Cartesian workspace and a given set of orientation ranges. In [85], Merlet discussed algorithms to detect interferences between cables and cables as well as between cables and the mobile platform. However, the proposed methods were only applied to constant platform orientation cases and did not apply for a range of orientations. In [89], Perreault presented an analysis of the cable interference-free workspace of CDPR. The analysis was also mainly applied to the cases of CDPR with constant orientation.

In this section, we discuss some algorithms that could improve the efficiency of the verification of collision free operation with respect to given CDPR Cartesian workspace and orientation workspace. These algorithms concern only the interferences between cables and cables, and cables and the CDPR mobile platform.

2.5.1 Interferences between Cables and Cables

Let us consider a m -cable CDPR as shown in Fig. 2.4. We will consider the interference between two cables A_iB_i and A_jB_j ($i \neq j$).

Fig. 2.5 illustrates a general method to detect the collision between two cables. In the first case (Fig. 2.5a), the two cables i and j are not colliding since the distance between

the two cables d_{ij} is greater than a given small value ϵ (this value can be chosen as the cable diameter). In the second case (Fig. 2.5b) when the cable i moves toward the cable j , according to the collision condition $d_{ij} < \epsilon$, the two cables collide. Note that, in this state, the cable j is “behind” the plane $(A_i B_i B_j)$. In this case, one can say that the two cables are going to collide but a real collision has not yet happened. In the third case (Fig. 2.5c), the same collision condition is valid. However, the cable j is “in front of” the plane $(A_i B_i B_j)$. In this case, a real collision between the two cables i and j has occurred. This algorithm can be formalized as follows [84, 87, 89]:

A real collision between the two cables i and j will occur if the two following conditions are met

- i)* the distance between the two cables is very small: $d_{ij} < \epsilon$
- ii)* the position of the cable j (or the cable exit point A_j) with respect to the plane $(A_i B_i B_j)$ changes sign (e.g. switch from “behind” position to “in front of” position)

It is enough to use this algorithm for real-time collision detection where the positions of cable exit point A_i and cable anchor point B_i are updated online in each sample time (while the mobile platform is following a trajectory). The computation of d_{ij} can be found in [91].

However, in the design phase, where the collision free conditions need to be verified with respect to a range of orientations and a volume of Cartesian space, this usual method may not be really effective.

In fact, to check the cable interferences, it could be enough to consider the second condition (*ii*) (in the usual algorithm) while neglecting the first condition (*i*) ($d_{ij} < \epsilon$). The two cables i and j can be far away (the distance d_{ij} can be large) but their relative positions will tell us whether or not there was a collision when the mobile platform “moved” from an arbitrary pose X_p to another pose X_q in the CDPR workspace.

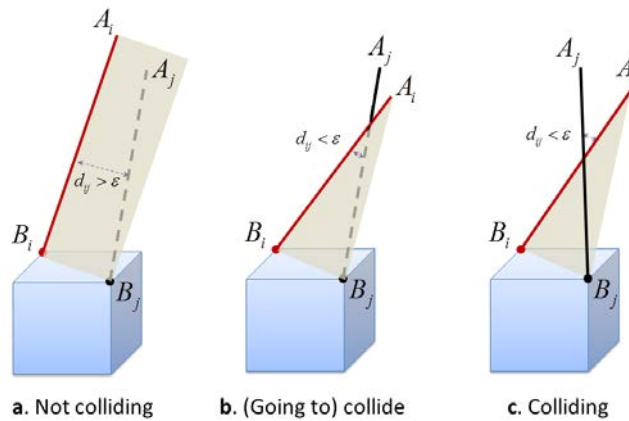


Figure 2.5: Usual method to check interference between two cables

Fig. 2.6 illustrates the method proposed to detect the interference between the two cables i and j . Suppose that the CDPR mobile platform moves from an initial pose X_p to an arbitrary pose X_q where a rotation and/or a translation occur. In the first case (Fig. 2.6a), when the mobile platform “moves” from pose X_p to pose X_q , the cable j is always “behind” the plane $(A_i B_i B_j)$. There should be no collision between the two cables i and j . In the second case (Fig. 2.6b), the position of cable j with respect to the plane $(A_i B_i B_j)$ changed sign so that a collision probably occurred between the two cables.

The collision detection algorithm between the two cables consists of the following steps:

- **Step 1.** At pose X_p , compute the position of $A_j B_j$ with respect to plane $(A_i B_i B_j)$ and store it in the variable $s_{ij}(X_p)$:

$$\begin{cases} s_{ij}(X_p) = 1, & \text{if } A_j B_j \text{ is “in front of” the plane } (A_i B_i B_j) \\ s_{ij}(X_p) = 0, & \text{if } A_j B_j \text{ lies on the plane } (A_i B_i B_j) \\ s_{ij}(X_p) = -1, & \text{if } A_j B_j \text{ is “behind” the plane } (A_i B_i B_j) \end{cases} \quad (2.69)$$

with

$$s_{ij} = \text{sign} \left(\left(\overrightarrow{A_i B_i} \times \overrightarrow{A_i B_j} \right)^T \cdot \overrightarrow{A_i A_j} \right) \quad (2.70)$$

Here, the two cable exit points A_i and A_j must not be coincident: $A_i \neq A_j$.

- **Step 2.** At pose X_q , compute the projection image $A'_j B_j$ of cable $A_j B_j$ onto the plane $(A_i B_i B_j)$:

$$A'_j = A_j - t * \mathbf{n} \quad (2.71)$$

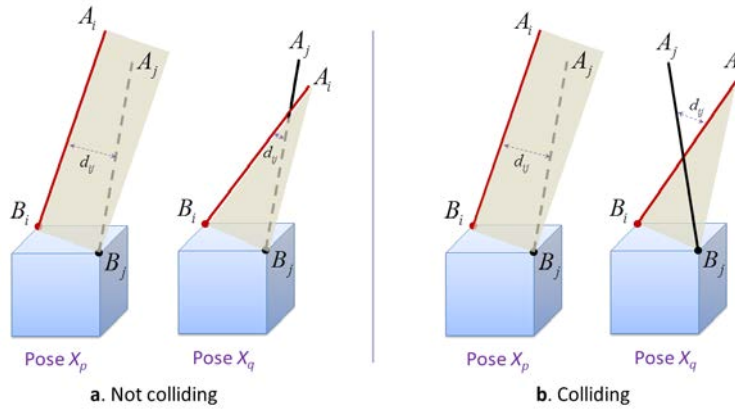


Figure 2.6: Checking interference between two cables

with

$$\mathbf{n} = \overrightarrow{A_i B_i} \times \overrightarrow{A_i B_j}$$

$$t = \frac{\mathbf{n}^T \cdot \overrightarrow{A_i A_j}}{\mathbf{n}^T \mathbf{n}}$$

- **Step 3.** At pose X_q , compute the position of $A_j B_j$ with respect to plane $(A_i B_i B_j)$ and store it in the variable $s_{ij}(X_q)$ by using (2.70).

If $s_{ij}(X_q) == s_{ij}(X_p)$, then no collision should have occurred.

If $s_{ij}(X_q) \neq s_{ij}(X_p)$ and $A'_j B_j$ is not intersecting $A_i B_i$, then no collision should have occurred.

If $s_{ij}(X_q) \neq s_{ij}(X_p)$ and $A'_j B_j$ is intersecting $A_i B_i$, then we consider that a collision between the two cables i and j occurred.

In this algorithm, for a m -cable CDPR, step 1 requires to compute s_{ij} in (2.70) N_{cc} times:

$$N_{cc} = \frac{m \cdot (m - 1)}{2} \quad (2.72)$$

The algorithm stops if there exists any i, j for which a collision occurs (thus, the times of performing steps 2 and 3 is $N_{2,3} \leq N_{cc}$).

This algorithm considers that given the two arbitrary poses X_p and X_q , if a collision is detected, then there exists no collision free trajectory that allows the CDPR mobile platform to move from pose X_p to pose X_q (regardless of any trajectory planning method).

2.5.2 Interferences between Cables and the CDPR Mobile Platform

METHOD 1

Suppose that the CDPR mobile platform is triangulated into N_{Δ} triangles. The first approach to detect the interferences between cables and the CDPR mobile platform is quite straightforward using the method to detect collision between line segments and triangles [91].

At pose X_p , for each cable i , we check for the interferences between cable i and all the triangles that do not belong to the planes which contain the cable end point B_i . If there is a collision then we stop the checking process and give out a warning.

Fig. 2.7 shows an example of the collision between cables i and the mobile platform.

The computational time in this case depends on the number of vertices of the mobile platform as well as the number of cables. This method is time consuming and not really

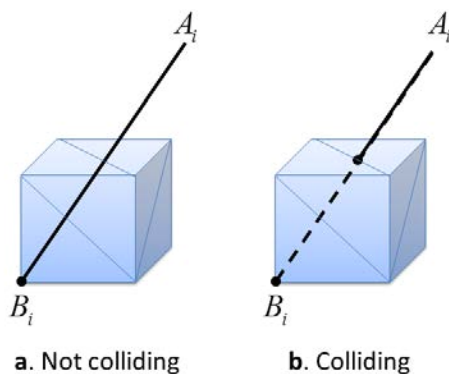


Figure 2.7: Interferences between cables and the CDPR mobile platform

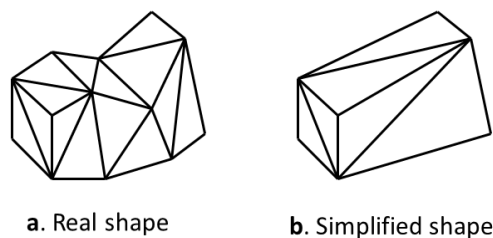


Figure 2.8: Simplification of the mobile platform shape

effective if the mobile platform has a complex shape (triangulated with a large number of triangles $N_{\Delta} \gg 1$). To avoid excessive computational time, we can approximate the mobile platform shape by a simple convex shape whose number of triangles is reduced considerably, e.g. in Fig. 2.8 (the simplified shape should enclose the CDPR mobile platform).

METHOD 2

Although the first method to detect the interferences between cables and the mobile platform is simple, the issue of computational time may remain if the mobile platform has a complex shape and the simplification procedure cannot significantly reduce the number of its vertices.

We propose a heuristic method which consists in checking *whether or not the cable $A_i B_i$ belongs to the subspace (convex cone) spanned by its nearest edges*. Fig. 2.9 shows an illustrating example of this approach.

The algorithm is given in the following steps:

- **Step 1.** Perform a simplification of the mobile platform to transform it into a simpler

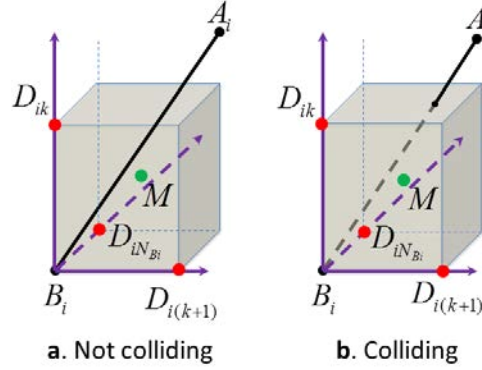


Figure 2.9: Detecting collision between cable i and the mobile platform

convex shape while keeping important vertices. This simplified convex shape should enclose the CDPR mobile platform.

- **Step 2.** Determine the nearest neighbor vertices D_{ik} ($k = \overline{1, N_{Bi}}$) of anchor points B_i in such a way that the convex cone spanned by the vectors $(\overrightarrow{B_i D_{i1}}, \overrightarrow{B_i D_{i2}}, \dots, \overrightarrow{B_i D_{iN_{Bi}}})$ includes the CDPR mobile platform. N_{Bi} should be the minimum number of such nearest neighbor vertices of B_i .
- **Step 3.** Compute the positions (or the signs) of an arbitrary point M lying within the mobile platform shape with respect to the planes $(B_i D_{ik} D_{i(k+1)})$ and store them into vector S_{Bi} of size $[N_{Bi} \times 1]$:

$$S_{Bi}(k) = \text{sign} \left(\left(\overrightarrow{B_i D_{ik}} \times \overrightarrow{B_i D_{i(k+1)}} \right)^T \cdot \overrightarrow{D_{ik} M} \right) \quad (2.73)$$

For instance, the point M can be chosen as the origin of the local frame attached to the mobile platform or as the platform center of mass. Note that all the cases where $S_{Bi}(k) = 0$ in (2.73) are considered invalid (the point M must lie strictly inside the mobile platform shape).

- **Step 4.** At an arbitrary pose X_p , compute the signs S_{Ai} of the cable exit point A_i with respect to the N_{Bi} planes $(B_i D_{ik} D_{i(k+1)})$ (vector S_{Ai} is of size $[N_{Bi} \times 1]$):

$$S_{Ai}(k) = \text{sign} \left(\left(\overrightarrow{B_i D_{ik}} \times \overrightarrow{B_i D_{i(k+1)}} \right)^T \cdot \overrightarrow{D_{ik} A_i} \right) \quad (2.74)$$

If $\exists i$ and $\exists k$ ($i = \overline{1, m}$, $k = \overline{1, N_{Bi}}$) such that $S_{Ai}(k) = 0$, then the cable $A_i B_i$ is considered to be colliding with the mobile platform.

If $S_{Ai} \equiv S_{Bi}$, then the cable $A_i B_i$ is considered to be colliding with the mobile platform.

If $S_{Ai} \neq S_{Bi}$ and $S_{Ai}(k) \neq 0$ ($\forall k$), then there is no collision.

Note that the steps 1-3 could only be done at the initial step of a sequence of execution of the algorithm (for instance during an optimization of along a trajectory of the mobile

platform). Then, step 4 will be used to check the interferences between the cables and the mobile platform for each considered robot configuration.

This approach utilizes the fact that the positions of a point lying within the mobile platform with respect to the planes $(B_i D_{ik} D_{i(k+1)})$ never change. One only need to evaluate (2.74) N_{cp} times to check the collision, where:

$$N_{cp} = \sum_{i=1}^m N_{Bi} \quad (2.75)$$

This method is fast and reliable. However, there are still a few limitations to this approach. The algorithm only works under the condition that the mobile platform has a convex shape. In case the mobile platform shape is concave, a pre-process (Step 1) is needed to convert it into a convex object (with a number of vertices as small as possible) in order to apply the algorithm. Currently, we are not aware of an efficient (fast) method of selecting the right number of the nearest neighbor vertices D_{ik} of anchor point B_i . One still has to manually select the vertices D_{ik} . The process of simplifying the mobile platform shape to reduce its complexity can be done with available CAD softwares e.g. [92].

2.5.3 Checking that a Given Workspace is Collision Free

Let us consider an application where one want to verify the cable interferences of a CDPR with respect to a given Cartesian workspace and platform orientation range. The CDPR workspace is given as follows:

$$\begin{aligned} x_{\min} &\leq x \leq x_{\max} \\ y_{\min} &\leq y \leq y_{\max} \\ z_{\min} &\leq z \leq z_{\max} \\ \theta_{x\min} &\leq \theta_x \leq \theta_{x\max} \\ \theta_{y\min} &\leq \theta_y \leq \theta_{y\max} \\ \theta_{z\min} &\leq \theta_z \leq \theta_{z\max} \end{aligned}$$

where $X = (x \ y \ z, \theta_x \ \theta_y \ \theta_z)$ denotes the mobile platform pose. Assume that the Cartesian workspace is discretized into a finite set of N_p points and the orientation workspace is discretized into a finite set of N_q points (these points can be chosen as extreme points which lie on the workspace boundaries). Let us take an arbitrary pose X_c of the given workspace where we assume that there is no cable interference:

$$X_c = (x_c \ y_c \ z_c, \theta_{xc} \ \theta_{yc} \ \theta_{zc}) \quad (2.76)$$

The verification of the absence of collisions in the assigned workspace is illustrated in the following pseudocode:

```

Compute  $s_{ij}(X_c)$  in (2.70);
Simplify the CDPR mobile platform shape (if it is necessary);
Determine the  $N_{B_i}$  nearest neighbor vertices  $D_{ik}$  of  $B_i$ ;
Compute  $S_{B_i}(X_c)$  in (2.73);
 $OK = 1$ ; (there is no collision)
for  $k = 1 : N_p$ 
  for  $l = 1 : N_q$ 
     $X = (x_k \ y_k \ z_k, \theta_{xl} \ \theta_{yl} \ \theta_{zl})$ ;
     $OK =$  Check the interferences between cables and cables;
    if ( $OK == 0$ ) break;
     $OK =$  Check the interferences between cables and the mobile platform;
    if ( $OK == 0$ ) break;
  end;
end;

```

In short, we perform the verification process at each discrete points in Cartesian space and orientation space. The reference (initial) state of the mobile platform is computed at the pose X_c . In the step checking the interferences between cables and cables, the initial pose is always X_c , and the destination pose is X . This means that when the mobile platform "moves" from pose X_c to pose X , the checking process stops if there is any interference detected. In the step checking the interferences between the cables and the mobile platform, the second approach is used. There is no collision if the returned value of the checking variable is $OK = 1$.

In this way, the collision free condition of the CDPR with respect to a given workspace is verified in the sense that, when $OK = 1$ is returned, there should always exist one collision free path starting from the home pose X_c to any pose (among the considered discrete set of poses) in the workspace. When $OK = 0$ is returned, there very probably exists no collision free trajectory that allows the mobile platform to move freely within the given workspace (regardless of any path planning method).

Currently, this approach has only been validated on examples. One can select just one home pose X_c to check whether or not a prescribed workspace is collision free (X_c can be chosen as the center pose of the given workspace). To increase the reliability, we can apply

the algorithm to a set of N_c home poses X_c and with large numbers of discrete poses (N_p and N_q are large) but the computational time is proportional to $N_c \times N_p \times N_q$.

2.5.4 Example

Let us consider the 8-cable CDPDR shown in Fig. 2.10. The mobile platform is a cube with 8 vertices. In this example, we show the computation time for each function call to check the collisions between cables and cables, and between cables and the CDPDR mobile platform (using method 1 and method 2) while assuming that the mobile platform moves from the home pose X_c to the destination pose X_d . The home pose is $X_c = (0 \ 0 \ 0, 0 \ 0 \ 0)$ (m, rad). The destination pose is varied. The results are given in Table 2.1. We use MATLAB to run the simulation on a PC with CPU core i7-2620M 2.7GHz.

In the case of checking the collision between cables and cables, the number of cables is $m = 8$. The computation time is quite large. The maximum computation time for checking the collision is around $t_{cc} \approx 4.65$ ms.

In the case of checking the collision between the cables and the CDPDR mobile platform using the first method, the mobile platform surface is triangulated into 12 triangles. For each cable, one need to verify potential collision with a maximum of 6 triangles. The maximum number of calls of the primitive test used to detect the collision between a line segment and a triangle is $6 \times m = 48$. The maximum computation time is around $t_{cp1} \approx 5.3$ ms.

On the other hand, in the second method, the mobile platform has a convex shape. For

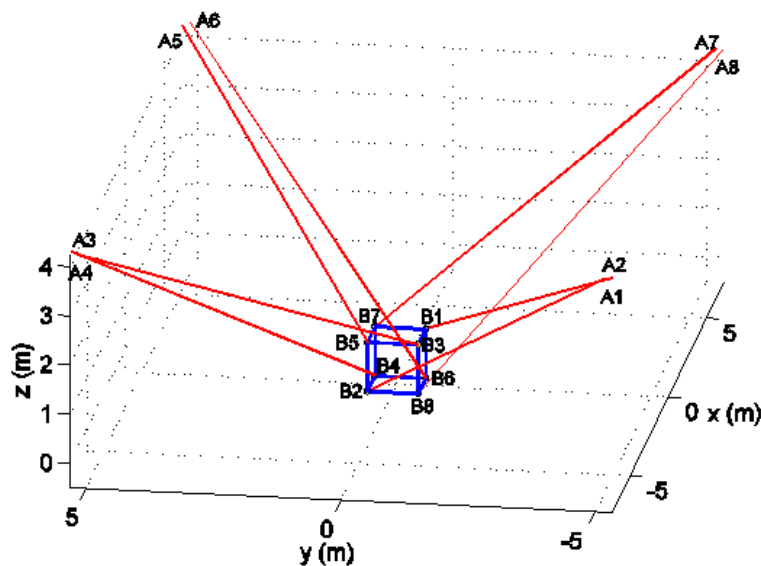


Figure 2.10: Example of an 8-cable CDPDR

Table 2.1: Collision detection computation times

Destination pose $X_d (m, rad)$	Cables-Cables (ms)	Cables-Platform (method 1) (ms)	Cables-Platform (method 2) (ms)
(0 0 0, 0 0 $-\pi/4$)	4.63 (no collision)	4.61 (collision)	0.74 (collision)
(2 0 1, $\pi/3 -\pi/3$ 0)	4.57 (collision)	4.79 (collision)	0.92 (collision)
(0 0 0, 0 $-\pi/3 -\pi/4$)	4.54 (collision)	4.50 (collision)	0.39 (collision)
(0 0 1, 0 0 $\pi/4$)	4.65 (no collision)	5.28 (no collision)	1.47 (no collision)
(0 2 0, 0 0 0)	4.61 (no collision)	5.30 (no collision)	1.46 (no collision)
(0 0 2, $\pi/4$ 0 0)	4.63 (no collision)	5.27 (no collision)	1.44 (no collision)

each vertex B_i , there are a minimum of 3 neighboring vertices. The computation time in this case is significantly reduced compared to the first method. The maximum computation time is around $t_{cp2} \approx 1.47 ms$

Assume that one want to verify the CDPR capability over a given workspace where the Cartesian workspace is discretized into $N_p = 20$ points and the orientation workspace is discretized into the minimum number $N_q = 8$ points (taking only the extreme values of each angle into account). The number of considered home poses is $N_c = 10$ points. If we choose to use the second method to check the collision between the cables and the CDPR mobile platform, the maximum computation time to verify the collision free collision condition for the given workspace is around:

$$t_{\max} = N_c \times N_p \times N_q \times (t_{cc} + t_{cp2}) = 10 \times 20 \times 8 \times (4.65 + 1.47) ms = 9.792 s$$

Currently, it is up to the user to choose appropriate values of N_c , N_p and N_q , considering the trade off between reliability of the result and computation time. It is worth noting that, by using parallel computing (taking the advantages of both powerful CPU and GPU), one can also greatly reduce the computation times of the presented methods.

In summary, several algorithms to detect the cable interferences of a CDPR have been discussed. The presented heuristic approaches improve the usual methods of detecting cable collisions in term of efficiency. Two types of cable interferences have been considered: collisions between cables and cables as well as collisions between cables and the CDPR mobile platform. The application of these tools was illustrated by an example of checking the collision free condition of a CDPR with respect to given Cartesian workspace and orientation workspace. The proposed approach offers the user a fast method to check collisions.

As a perspective, it may be possible to prove the presented algorithms with respect to certain family types of CDPR under some geometric constraints.

Conclusion

In this chapter, several preliminary tools to deal with the CDPR modeling were presented. The inverse kinematics problem, tension distribution problems, stiffness of CDPRs as well as collision detection tools were discussed. These tools are useful to motion control of CDPRs (cable model, inverse kinematics, tension distribution) and to determine CDPR reconfigurations (CDPR modeling, tension distribution, CDPR stiffness, collision detection).

EXTENDED MODELING - APPLICATION TO THE CoGiRo CDPR

Summary

3.1	The Modeling and Control of the CoGiRo CDPR	61
3.2	Cable Profile with Thermal Effect	67
3.3	CDPR Extended Modeling	68
3.4	Solving the Inverse Kinetostatic Problem Using the Catenary Cable Model	73
3.5	Error Analysis	78
3.6	Case Study	82

Despite having many advantages over rigid-link manipulators, there are challenging issues in using CDPRs. One significant drawback of CDPRs is their low positioning accuracy. Firstly, because cables are used to position the end-effector, CDPRs are much more compliant than rigid link manipulators. Secondly, the nonlinear nature of the cable behavior makes it difficult to effectively solve important problems of CDPRs such as the inverse kinematic and tension distribution problems. Thus, different simplified cable models may have to be used in order to reduce the complexity of these problems.

In many previous studies, only a part of the cable (the cable segment $A_i B_i$) is considered in the modeling of a CDPR. The influences of pulleys as well as other factors such as friction and cable dynamics are neglected or compensated by a constant value added to the cable unstrained length (which is then used in the CDPR control scheme). These

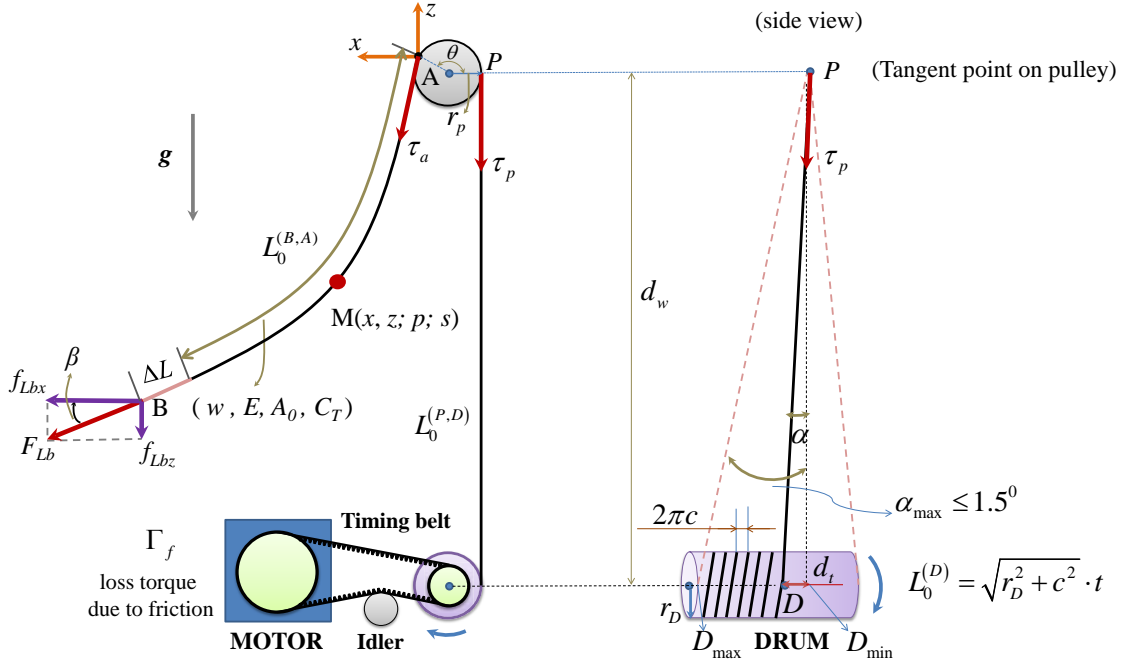


Figure 3.1: Winch and cable transmission components of the CoGiRo prototype

simplifications might have a great impact on the CDP performance. In [68, 93], A. Pott and V. Schmidt addressed the influence of pulley kinematics on CDPs. However, only the massless elastic cable model was used.

Nevertheless, there is always a tradeoff between the computation time and performance when a simplified cable model is used, e.g., when a simplification is made to the elastic catenary cable model [80, 81]. In this chapter, the main goal is to find a cable model that could improve substantially the CDP positioning accuracy, taking into account most of the factors that could affect the CDP performance such as thermal effect on the cable, friction (between the cable and the pulleys/drums, in the winch), cable mass and cable elasticity.

This chapter is thus dedicated to the extended modeling of CDPs. In Section 3.1, an extended model taking into account the influence of pulleys and friction is presented. Only a static analysis is considered (we neglected cable dynamics). This model corresponds in fact to the current implementation of the CoGiRo prototype which consists of 8 cables and 8 routing pulleys (Fig. 3.1). The control scheme of the CoGiRo robot is also presented and we explain how the IKP solution is used and how to compensate the loss of torque due to the friction in the winches. Then, we present in Section 3.2 equations describing the cable profile taking into account thermal effect, cable mass and cable elasticity. Section 3.3 details the extended modeling including the computation of the cable unstrained length

with respect to each part of the cable based on the catenary cable equations. An analysis of the error sensitivity of the cable length is given afterward in Section 3.5 which compares the differences in cable unstrained length between massless cable model, simplified cable model and the elastic catenary cable model. Two case studies are given in section 3.6. In the first case study, the positioning accuracies obtained by using different cable models are compared, in simulation and experiment on the CoGiRo robot (the influence of pulley kinematics is neglected). In the second case study, an experiment with the CoGiRo prototype is presented, in which we show the impact of the extended modeling (taking into account the pulley kinematics and friction in the winch) on the CDPR positioning accuracy.

3.1 The Modeling and Control of the CoGiRo CDPR

3.1.1 Assumptions

Several segments of a cable of a CDPR connect the cable exit point to the drum, the cable passing through one or several pulleys. The elongation of the cable along those segments should be taken into account. Fig. 3.1 shows the cable-driven system of each winch of the CoGiRo prototype [17].

In order to fully describe the behavior of the cable one should consider all the effects that cause the cable deformation such as friction contact (between cable and pulley, in the winch and in the motor), environment temperature, deformation of the base frame of the whole robot system. However, in practice, it is difficult to include all these factors in the modeling. Thus, to reduce the complexity of the corresponding extended CDPR model, we make the following assumptions:

- The friction between the cables and the pulleys are neglected. This assumption is usually valid when the number of transmission pulleys is small (e.g. 1 or 2 pulleys for each cable) and the pulley is well lubricated. If there is a large number of pulleys in each cable routing system, pulley friction should be taken into account.
- There are no deformation of the cable segments that mount on the pulley and on the drum of the winch.
- The deformations of the CDPR supporting frame are neglected. This assumption is not always valid, especially for CDPRs with light weight supporting frame. In practice, it is possible to have a bulky design of the supporting frame so that the deformation is minimized. In the case of the CoGiRo prototype, the deformation of the supporting frame does have a certain impact on the position of the upper pulleys from

which the cable extends toward the mobile platform. However, the impact is small and negligible (the measured error on the pulley position lies within 1 – 1.5 *mm* while carrying a weight of 200kg with large movements of the mobile platform across the workspace).

Let us denote $L_0^{(P,Q)}$ the cable unstrained length between any two points P and Q . For the CoGiRo prototype, the total cable unstrained length (from the drum to the cable anchor point B) is computed as follows:

$$L_T = O(L_0) + L_0^{(D,P)} + L_0^{(P,A)} + L_0^{(A,B)} \quad (3.1)$$

where $O(L_0)$ is the cable deformation due to undetermined uncertainties. $L_0^{(D,P)}$ is the cable unstrained length between the drum and the pulley. $L_0^{(P,A)}$ is the cable unstrained length of the cable segment that mount on the pulley. $L_0^{(A,B)}$ is the cable unstrained length of the cable segment between the pulley and the cable anchor point B .

Assume that L_D is the cable unstrained length that mount on the drum, then:

$$L_T + L_D = L_{total} = const \quad (3.2)$$

where L_{total} is the total length of each cable (and should be constant).

By our assumption, we have:

$$O(L_0) = 0 \quad (3.3)$$

$$L_0^{(P,A)} = \widehat{PA} = r_p \theta \quad (3.4)$$

where r_p is the radius of the pulleys and θ is the angle of the arc \widehat{PA} .

The cable tensions τ_p and τ_a at points P and A satisfy the following relation (if static friction is considered) [94]:

$$\tau_a = e^{\mu_s \theta} \tau_p \quad (3.5)$$

where μ_s is the static friction coefficient between the cable and the pulley surface (when $\mu_s \theta < 0$, $\tau_p > \tau_a$, the winch is pulling the cable and vice versa). According to our assumption for CoGiRo, $\mu_s = 0$ which means that the cable tension is the same on both sides of the pulley ($\tau_a = \tau_p$).

The cable unstrained length from the drum to the cable anchor point B is thus computed as follows:

$$L_T = r_p \theta + L_0^{(D,P)} + L_0^{(A,B)} \quad (3.6)$$

Suitable cable models are then needed to compute the two terms $L_0^{(D,P)}$ and $L_0^{(A,B)}$.

where r_q is a ratio to convert a cable length into a motor angular displacement (r_q depends on the drum radius and on the gear or belt transmission ratio).

Through the PID controller (Fig. 3.2), the required torques are created for the motors to reach the desired position q_d . The total desired motor torque including the compensations from the feed-forward terms is given as follows:

$$\Gamma_d = \Gamma_{qd} + \Gamma_{ff} \quad (3.8)$$

where Γ_{qd} is the total desired torque created from the joint space and a compensation from the moment caused by the mobile platform dynamics, in other words, it is the torque that balances the mobile platform at the desired pose. Γ_{ff} is the desired torque that compensate for the loss of torque due to friction in the winch and due to the inertia of the motor and drum.

3.1.3 Modeling of Friction

In practice, if the pulleys are well lubricated, the friction between the cable and pulley can be neglected. However, the friction in the winch and in the motor must be considered. It is important to note that in the winches of CoGiRo, a timing belt is used to transfer the drive torque. With proper pre-tension (by using the idler pulley), the timing belt provides a no-slip operation which minimizes uncertain frictional effect due to slippage.

In the control scheme, the loss of torque due to friction (Γ_f) and the inertia moment of the rotor and drum is compensated by using a feed-forward term:

$$\Gamma_{ff} = I_\Sigma \ddot{q} + \Gamma_f \quad (3.9)$$

where I_Σ is the total inertia of the rotor and drum "seen" at the motor shaft.

When the rotor rotates at constant speed, the angular acceleration is $\ddot{q} = 0$, which gives $\Gamma_{ff} = \Gamma_f$. To determine the friction torque Γ_f , we use the following expression (which is adapted from friction force equation in [95, 96]):

$$\Gamma_f = \left[\Gamma_c + (\Gamma_s - \Gamma_c) e^{-\left(\frac{|\dot{q}|}{\dot{q}_s}\right)^\delta} \right] \text{sign}(\dot{q}) + C_v \dot{q} \quad (3.10)$$

where Γ_c is the *Coulomb friction torque*, Γ_s is the *static friction torque*, \dot{q} is the angular speed of the rotor, \dot{q}_s is the so-called *Stribeck velocity* (which indicates the velocity range in which the Stribeck effect is effective) and C_v is the viscous friction coefficient. The exponent δ is a tuning parameter.

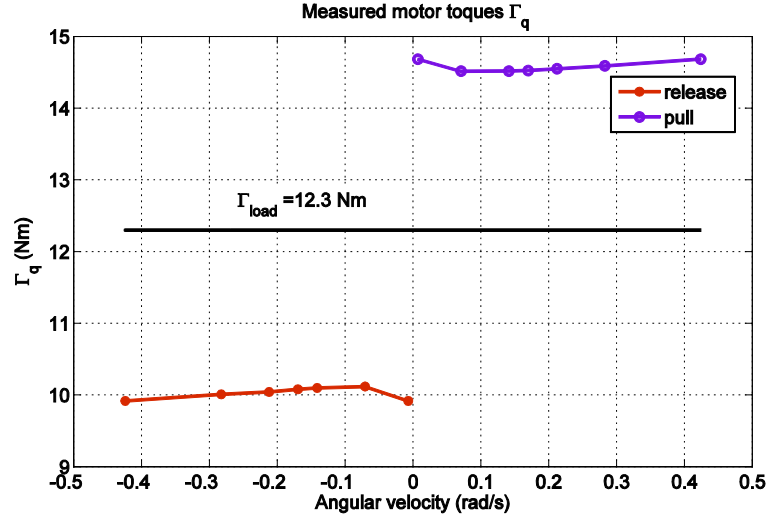


Figure 3.3: Measured output torque of the motor

In fact, in [96], Bender indicates that (3.10) is the steady-state value of the friction torque at constant velocity. Please refer to [96] for more details of the full friction model (namely *the Generalized Maxwell-Slip Model*).

The five unknown parameters in (3.10) are found by solving a least-square optimization problem which minimizes the means square of the friction torque errors:

$$\text{minimize } \frac{1}{N} \sum_{i=1}^N [\Gamma_f(i) - \Gamma_{fm}(i)]^2 \quad (3.11)$$

where N is the number of the data samples and Γ_{fm} is the measured friction torque.

To measure the loss of torque due to friction, we performed a test with one winch of the CoGiRo prototype and measured the torque output of the motor Γ_q during a simple pulling (positive direction) and releasing (negative direction) of a payload (56kg) at different constant speeds of the motor. The results show that there is a substantial difference in the torques required for pulling and for releasing (Fig. 3.3).

In the steady state (the motor rotates at constant velocity), the measured motor torque (Γ_q) accounts for balancing the payload (Γ_{load}) and the friction in the winch (Γ_{fm}):

$$\Gamma_q = \Gamma_{load} + \Gamma_{fm} \quad (3.12)$$

The term Γ_{load} can be computed from the payload and the torque transmission ratio r_t :

$$\Gamma_{load} = \frac{\Gamma_D}{r_t} = \frac{m_{load} g r_D}{r_t} \quad (3.13)$$

Table 3.1: Loss of torque due to friction in the winch

Speed \dot{q} (rad/s)	$\Gamma_{fm}(release)$ (Nm)	Speed \dot{q} (rad/s)	$\Gamma_{fm}(pull)$ (Nm)
-0.00707	-2.3829	+0.00707	+2.3829
-0.0707	-2.1816	+0.0707	+2.2128
-0.1414	-2.2034	+0.1414	+2.2143
-0.1697	-2.2203	+0.1697	+2.2224
-0.2121	-2.2582	+0.2121	+2.2466
-0.2828	-2.2917	+0.2828	+2.2917
-0.4214	-2.3822	+0.4214	+2.3819

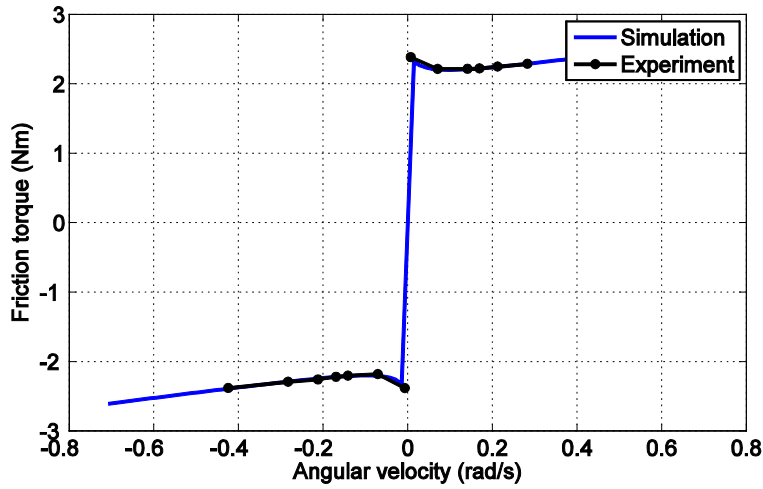


Figure 3.4: Steady-state values of the friction torque

where $m_{load} = 56(kg)$, $g = 9.81(m/s^2)$, $r_t = 3$ and $r_D = 0.0675(m)$ is the radius of the drum. Thus we can compute $\Gamma_{fm} = \Gamma_q - \Gamma_{load}$. Table 3.1 shows the resultant loss of torque due to friction in the winch.

In the optimization problem (3.11), we selected three decision parameters (Γ_s , Γ_c , C_v). The value range of \dot{q}_s can be guessed easily from the experiment curve. The parameter δ can be tuned. At each value of δ , a set of solution is found. The procedure is repeated until a good approximation of the experimental curve is obtained. In the experiments made on the CoGiRo robot, the values are found as follows: $\dot{q}_s = 0.025(rad/s)$, $\delta = 0.5$, $\Gamma_c = 2.0459(Nm)$, $\Gamma_s = 2.6062(Nm)$, $C_v = 0.7879(Nms/rad)$. Fig. 3.4 shows the experiment results and approximation curve.

Let us note that during our experiments to determine the friction effects, we performed a test where we measured the absolute positioning accuracy of the mobile platform at a static equilibrium pose in two cases: with and without friction compensation (the total carried weight is $195kg$). The results showed that there is a difference of up to $3 - 4mm$

in the positioning accuracy between the two cases. This means the friction in the winch should be taken into account in the CDPR control system.

3.2 Cable Profile with Thermal Effect

Assume that the cable segment AB has unstrained length L_0 (m), self-weight w (N/m), elastic modulus E (Pa) and cable cross-section area A_0 (m^2). Fig. 3.1 shows the relevant coordinates and parameters of AB lying in a vertical plane in static equilibrium. *The origin of the local frame is placed at the end-point A* (this point is important).

3.2.1 Catenary Equation with Thermal Effect

Assume that the thermal effect on the cable length linearly depends on the uniform temperature change. Then, the cable tension at a point M on the cable is considered to satisfy Hooke's law [97]:

$$\tau_s = EA_0 \left(\frac{dp}{ds} - C_T \right) \quad (3.14)$$

where $C_T = 1 + \alpha_T (T - T_0)$, where α_T is the thermal expansion coefficient, T is the temperature of the environment at the current state and T_0 is the reference temperature. We choose $T_0 = 25$ ($^{\circ}C$) and $\alpha_T = 1e - 5$ ($^{\circ}C^{-1}$) (standard value for steel material lies in a range of $(10 - 13)e - 6$ ($^{\circ}C^{-1}$)¹).

Note that with $C_T = 1$, relation (3.14) becomes (2.14) in Section 2.2.1 (thermal effect is neglected).

The catenary cable equations [80] with thermal effect are:

$$x_L(s) = x_{Lb} + \frac{f_{Lbx}(s - L_0)}{EA_0} + \frac{C_T f_{Lbx}}{w} \ln \left[\frac{\tau_s + f_{Lbz} + w(s - L_0)}{\tau_b + f_{Lbz}} \right] \quad (3.15a)$$

$$z_L(s) = z_{Lb} + \frac{f_{Lbz}(s - L_0)}{EA_0} + \frac{w(s - L_0)^2}{2EA_0} + \frac{C_T}{w} (\tau_s - \tau_b) \quad (3.15b)$$

From (3.15), one can easily derive the cable unstrained length between any two points P, Q for massless elastic cable ($w = 0$) as follows:

$$L_0^{(P,Q)} = \frac{\|P - Q\|}{C_T + \frac{\tau_b}{EA_0}} \quad (3.16)$$

1. http://www.engineeringtoolbox.com/linear-expansion-coefficients-d_95.html

When the cable mass is considered ($w \neq 0$) simplified cable model is used to compute $L_0^{(P,Q)}$.

3.2.2 Linear Relationship between Cable Force Components

Following a procedure similar to the one presented in Section 2.2, the tangent at point B of the cable can be found:

$$\tan(\beta) = \frac{f_{Lbz}}{f_{Lbx}} = \sinh(\mu_T x_{Lb} + C_1) \quad (3.17)$$

where

$$\mu_T = \frac{w}{C_T f_{Lbx}} \quad (3.18)$$

$$C_1 = \ln \left(\frac{\sqrt{\mu_T^2 z_{Lb}^2 + e^{\mu_T x_{Lb}} + e^{-\mu_T x_{Lb}} - 2} + \mu_T z_{Lb}}{e^{\mu_T x_{Lb}} - 1} \right) \quad (3.19)$$

Using Taylor series expansion around the expansion point $v_T = \mu_T x_{Lb} = 0$, one can obtain a linear relationship between the vertical and horizontal cable force components at the cable end point B :

$$f_{Lbz} = \tan(\beta_0) \cdot f_{Lbx} + \frac{wL}{2C_T} \quad (3.20)$$

where $\tan(\beta_0) = z_{Lb}/x_{Lb}$ and $L = \|AB\| = \sqrt{x_{Lb}^2 + z_{Lb}^2}$.

Relation (3.20) is necessary in order to solve the tension distribution problem of the CDPR. It is valid if the two following conditions are verified:

$$\tau_s \ll EA_0 \quad (3.21)$$

$$0 \leq v_T \ll 1 \quad (3.22)$$

3.3 CDPR Extended Modeling

3.3.1 Cable Segment between the Drum and the Pulley

Let us consider the cable segment between the drum and the pulley as shown in Fig. 3.1. α is the tilt angle of the cable with respect to the vertical axis, α_{\max} is the maximum tilt

angle of the cable and, by design of the winch, it is less than a small angle ($\alpha_{\max} \leq 1.5^\circ$). c is the step of the helix of the part of the cable wound on the drum and t (rad) is the total rotation angle of the helix. r_D is the radius of the drum. D is the tangent point between the cable and the drum. D_{\min} and D_{\max} are the tangent points between the cable and the drum when the cable are at a vertical position ($\alpha = 0$) and at the most tilt angle position ($\alpha = \alpha_{\max}$), respectively.

The part of the cable wound on the drum can be consider as a helix with radius r_D and pitch $2\pi c$. Its total length is computed as:

$$L_0^{(D)} = \sqrt{r_D^2 + c^2} \cdot t \quad (3.23)$$

If the elastic cable model is used, then the cable unstrained length of the cable segment PD can be computed as follows:

$$L_0^{(D,P)} = \frac{\sqrt{d_w^2 + d_t^2}}{C_T + \frac{\tau_p}{EA_0}} \quad (3.24)$$

where d_w is the vertical distance between the tangent point on the pulley and the drum center point, and d_t is the distance from the cable tangent point on the drum to the vertical axis position (see Fig. 3.1):

$$d_t = c \cdot |t_0 - t| \quad (3.25)$$

where t_0 is the total angle of the helix when the cable reaches a vertical position.

For CoGiRo, in most cases, because the angle between the cable and the vertical axis is small $\alpha \leq \alpha_{\max} = 1.5^\circ$, we have $d_t \ll d_w$. Thus, to reduce the complexity of the computation, we assume that $PD \approx d_w = 5.15(m)$, i.e., the cable segment between the pulley and drum is in vertical position. The cable unstrained length between the pulley and the drum can be computed as:

$$L_0^{(D,P)} = \frac{d_w}{C_T + \frac{\tau_p}{EA_0}} \quad (3.26)$$

The difference in cable unstrained length of the segment PD when the cable is in the vertical position and in the most tilt angle position is:

$$\Delta_D = \frac{PD_{\max} - PD_{\min}}{C_T + \frac{\tau_p}{EA_0}} = \frac{d_w [1/\cos(\alpha_{\max}) - 1]}{C_T + \frac{\tau_p}{EA_0}} \approx \frac{1.76(mm)}{C_T + \frac{\tau_p}{EA_0}} \quad (3.27)$$

Δ_D is the maximum error in computing the cable unstrained length while assuming the cable is in vertical position.

3.3.2 Cable Segment between the Pulley and the Cable Anchor Point

Fig. 3.5 shows the cable segment AB . $F_{La}(f_{Lax}, f_{Laz})$ and $F_{Lb}(f_{Lbx}, f_{Lbz})$ are the cable forces at points $A(x_{La}, z_{La})$ and $B(x_{Lb}, z_{Lb})$ (expressed in the cable local frame). In this case, we only know the location of a fixed point of the pulley (normally the tangent point P is fixed). The position of the cable exit point A depends on the angle θ_a . The relation (2.27) now becomes (all the terms are expressed in the frame attached to the pulley tangent point P) [98]:

$$\begin{aligned} f_{Lbz} &= \frac{\langle A \rangle z_{Lb}}{\langle A \rangle x_{Lb}} \cdot f_{Lbx} + \frac{wL}{2C_T} \\ &= \frac{\langle P \rangle z_{Lb} - \langle P \rangle z_{La}}{\langle P \rangle x_{Lb} - \langle P \rangle x_{La}} \cdot f_{Lbx} + \frac{wL}{2C_T} \\ &= \frac{\langle P \rangle z_{Lb} - r_p \sin(\theta_a)}{\langle P \rangle x_{Lb} - r_p [1 + \cos(\theta_a)]} \cdot f_{Lbx} + \frac{wL}{2C_T} \end{aligned} \quad (3.28)$$

where

$$\begin{aligned} \theta_a &= -\text{atan2}(f_{Lax}, f_{Laz}) \\ &= -\text{atan2}(f_{Lbx}, f_{Lbz} - wL_0^{(A,B)}) \\ &(\theta_a > 0, f_{Lax} > 0, f_{Laz} < 0) \end{aligned} \quad (3.29)$$

Because the angle θ_a is a function of the cable force components in (3.29), Eq. (3.28) does not establish a linear relationship between the cable force components. Consequently,

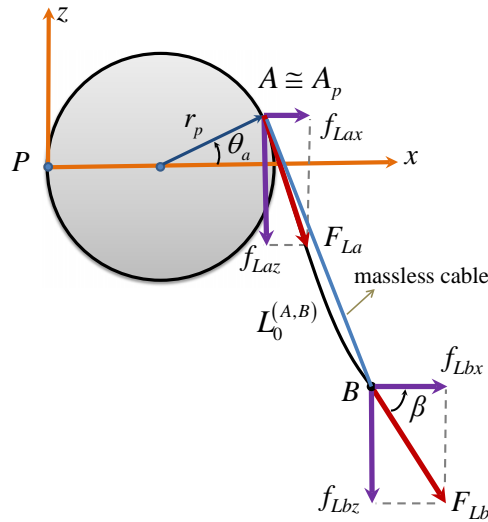


Figure 3.5: Cable segment AB

we cannot use the method presented in Section 2.2 to find $L_0^{(A,B)}$. In order to use a linear relationship similar to (3.20), the position of the cable exit point A must be independent from f_{Lbz} and f_{Lbx} . We propose to select a point $A_p(x_{Lap}, z_{Lap})$ instead of A in a way such that the line A_pB is tangent to the pulley at point A_p . In other words, A_p is the position of A when the cable is a straight line segment (massless cable model).

The coordinates of the point A_p depend only on the coordinates of the cable anchor point B . In the pulley frame $\langle P \rangle$:

$$\langle P \rangle z_{Lap} = \frac{z_{Lb} r_p^2 + r_p |x_{Lb} - r_p| \sqrt{z_{Lb}^2 + (x_{Lb} - r_p)^2} - r_p^2}{z_{Lb}^2 + (x_{Lb} - r_p)^2} \quad (3.30a)$$

$$\langle P \rangle x_{Lap} = r_p + \sqrt{r_p^2 - z_{Lap}^2} \quad (3.30b)$$

Note that in this case, the z-coordinate of point A_p is always positive (the determination of A_p is detailed in Appendix A.2).

The coordinates of A_p in the global frame are computed as follows:

$$A_p = P + [\langle P \rangle x_{Lap} \cos(\gamma), \langle P \rangle x_{Lap} \sin(\gamma), \langle P \rangle z_{Lap}]^T \quad (3.31)$$

where

$$\gamma = \text{atan2}(y_b - y_p, x_b - x_p) \quad (3.32)$$

being given the coordinates of point $P(x_p, y_p, z_p)$ and point $B(x_b, y_b, z_b)$ in the global frame.

When the massless elastic cable model is used, the cable unstrained length $L_0^{(A_p, B)}$ is computed from (3.16):

$$L_0^{(A_p, B)} = \frac{\|A_p - B\|}{C_T + \frac{\tau_p}{EA_0}} \quad (3.33)$$

We can now compute the total cable unstrained length from the winch to the point B :

$$L_T = \frac{d_w + \|A_p - B\|}{C_T + \frac{\tau_p}{EA_0}} + r_p (\pi - \theta_{ap}) \quad (3.34)$$

where

$$\theta_{ap} = \text{asin}\left(\frac{\langle P \rangle z_{Lap}}{r_p}\right) \quad (3.35)$$

When the simplified cable model is used, we need (3.20) to find the cable force components first, then, the cable unstrained length $L_0^{(A_p, B)}$ is computed as follows:

$$\begin{aligned}
L_0^{(A_p, B)} &= \int_0^{L_0} ds = \int_{x_{Lap}=0}^{x_{Lb}} \frac{EA_0}{f_{Lbx}} \left(1 - \frac{1}{1+R}\right) dx_L \\
&= \frac{EA_0}{f_{Lbx}} \int_{x_{Lap}=0}^{x_{Lb}} dx_L - \frac{EA_0}{\mu_T f_{Lbx}} \int_{R_a}^{R_b} \frac{1}{(1+R)\sqrt{R^2-a}} dR \\
&= \frac{EA_0}{f_{Lbx}} \left[x_{Lb} - \frac{1}{\mu_T} (H_a - H_b) \right] \tag{3.36}
\end{aligned}$$

where

$$\begin{aligned}
R &= \frac{f_{Lbx}}{C_T EA_0} \cosh(\mu_T x_L + C_1) \\
H_b &= \frac{\ln(1+R_b) - \ln\left(a + R_b - \sqrt{1-a}\sqrt{R_b^2-a}\right)}{\sqrt{1-a}} \\
H_a &= \frac{\ln(1+R_a) - \ln\left(a + R_a - \sqrt{1-a}\sqrt{R_a^2-a}\right)}{\sqrt{1-a}} \\
R_b &= \frac{f_{Lbx}}{C_T EA_0} \cosh(\mu_T x_{Lb} + C_1) \\
R_a &= \frac{f_{Lbx}}{C_T EA_0} \cosh(C_1) \\
a &= \frac{f_{Lbx}^2}{C_T^2 E^2 A_0^2}
\end{aligned}$$

It is important to note that in (3.19) and (3.36), x_{Lb} and z_{Lb} are the coordinates of point B expressed in the local frame $\langle A_p \rangle$. In other words, we have

$$x_{Lb} = \langle A_p \rangle x_{Lb} = \langle P \rangle x_{Lb} - \langle P \rangle x_{Lap} \tag{3.37a}$$

$$z_{Lb} = \langle A_p \rangle z_{Lb} = \langle P \rangle z_{Lb} - \langle P \rangle z_{Lap} \tag{3.37b}$$

In our experience, to implement (3.36) (in C/C++,...) one should be careful with numerical issues (e.g. round off errors). We suggest to use double precision floating point numbers (*double*) to prevent such issues (instead of using single precision numbers, e.g. *float*).

The cable unstrained length from the winch to the cable anchor point B can now be computed as follows:

$$L_T = \frac{d_w}{C_T + \frac{\tau_p}{EA_0}} + r_p (\pi - \theta_{ap}) + \frac{EA_0}{f_{Lbx}} \left[x_{Lb} - \frac{1}{\mu_T} (H_a - H_b) \right] \quad (3.38)$$

3.4 Solving the Inverse Kinetostatic Problem Using the Catenary Cable Model

Let us consider again the general inverse kinetostatic problem (IKP) of Section 2.2. As mentioned before, from (2.1) and (2.2), we have $3m + 6$ equations to find $4m$ unknown variables. When the number of cables is $m \leq 6$, if it exists, the solution should be unique. In the case of redundantly actuated CDPR with $m > 6$, there are an infinite number of solutions. It is necessary to compute a solution of the CDPR IKP problem using the elastic catenary cable model in order to validate the solutions obtained with the massless elastic cable model and the simplified cable model (and also to determine the initial state of the CDPR in the control system).

In the following, we propose an iterative method to compute the cable unstrained lengths and force components using the elastic catenary cable model. The method considers only the cable segments between the pulleys and the cable anchor points (segments $A_i B_i$) taking into account the influence of the pulleys. For the other part of the cable, one can use (3.26) to compute the unstrained length of the segment from the pulley to the drum.

Let us consider a pose of the mobile platform $X = [x \ y \ z \ \theta_x \ \theta_y \ \theta_z]^T$, the cable parameters (w, E, A_0) , the thermal constant C_T , the coordinates of A_i and B_i and the wrench vector \mathbf{f}_e . Define two vectors:

$$H_i = [f_{bix} \ f_{biy} \ f_{biz} \ L_{0i}]^T \quad (3.39)$$

$$V_i = [x_{bi} \ y_{bi} \ z_{bi} \ \tau_{bi}]^T \quad (3.40)$$

with $\tau_{bi} = \sqrt{f_{bix}^2 + f_{biy}^2 + f_{biz}^2}$

The catenary cable equations in three dimensions including the thermal effect can be

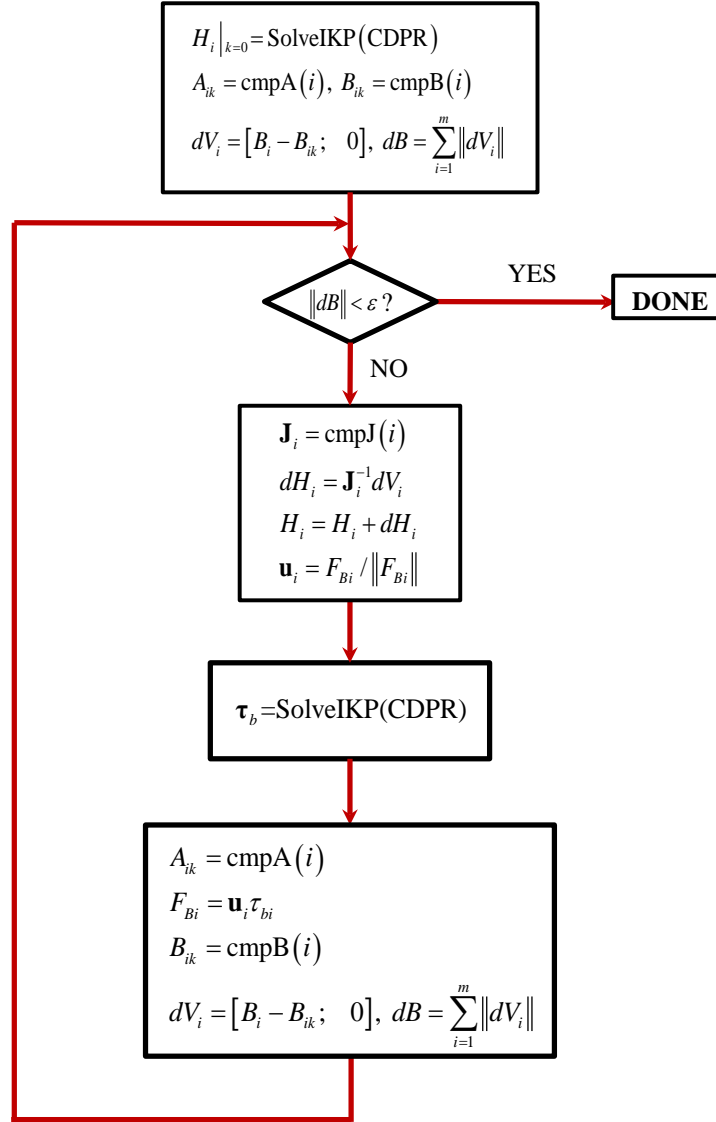


Figure 3.6: Solving the CDP inverse kinetostatic problem using catenary cable

formulated as follows:

$$x_{bi} = x_{ai} + \frac{f_{bix} L_{0i}}{EA_0} - \frac{C_T f_{bix}}{w} \ln \left[\frac{\tau_{ai} + f_{biz} - w L_{0i}}{\tau_{bi} + f_{biz}} \right] \quad (3.41a)$$

$$y_{bi} = y_{ai} + \frac{f_{biy} L_{0i}}{EA_0} - \frac{C_T f_{biy}}{w} \ln \left[\frac{\tau_{ai} + f_{biz} - w L_{0i}}{\tau_{bi} + f_{biz}} \right] \quad (3.41b)$$

$$z_{bi} = z_{ai} + \frac{f_{biz} L_{0i}}{EA_0} - \frac{w L_{0i}^2}{2EA_0} - \frac{C_T}{w} (\tau_{ai} - \tau_{bi}) \quad (3.41c)$$

An algorithm to compute the cable unstrained length $L_0^{(A_i, B_i)}$ and the cable force F_{B_i} will now be described (Fig. 3.6).

BEGIN Algorithm

Step 1: Compute an initial estimation of the solution by solving the IKP problem with massless elastic cable model or simplified cable model:

$$H_i(k=0) = \text{SolveIKP}(\text{CDPR})$$

Update all necessary terms:

$$\begin{aligned} A_{ik} &= \text{cmpA}(i) \\ B_{ik} &= \text{cmpB}(i) \\ dV_i &= [B_i - B_{ik}; 0] \\ dB &= \sum_{i=1}^m \|dV_i\| \end{aligned}$$

where $\text{cmpA}(i)$ and $\text{cmpB}(i)$ denote the functions to compute the new coordinates of the cable exit points A_i and the anchor points B_i .

Step 2: If $dB < \varepsilon$ then stop, else move to **Step 3**

Step 3: Update the vector H_i and unit vector \mathbf{u}_i (that directs cable force vector F_{Bi}) for each cable:

$$\begin{aligned} \mathbf{J}_i &= \text{cmpJ}(i) \\ dH_i &= \mathbf{J}_i^{-1} dV_i \\ H_i &= H_i + dH_i \\ \mathbf{u}_i &= \frac{F_{Bi}}{\|F_{Bi}\|} \end{aligned}$$

where $\text{cmpJ}(i)$ denotes the function to compute the jacobian matrix \mathbf{J}_i . The components of \mathbf{J}_i are defined after the algorithm description.

Step 4: Solve the tension distribution problem via (2.2), take redundancy into account if necessary (e.g. using the method presented in [32]):

$$\boldsymbol{\tau}_b = \text{SolveIKP}(\text{CDPR})$$

Step 5: Re-update the cable forces with the new tension values, A_{ik} , B_{ik} and dB , then

come back to **Step 2**:

$$\begin{aligned}
A_{ik} &= \text{cmpA}(i) \\
F_{Bi} &= \mathbf{u}_i \tau_{bi} \\
B_{ik} &= \text{cmpB}(i) \\
dV_i &= [B_i - B_{ik}; 0] \\
dB &= \sum_{i=1}^m \|dV_i\|
\end{aligned}$$

END Algorithm

In each iteration, the coordinates of the anchor points B_i are updated using (3.41). The routine to update the coordinates of the cable exit points A_i is given as follows:

$$\theta_{ai} = \text{atan2}\left(\sqrt{f_{bix}^2 + f_{biy}^2}, |f_{biz} - wL_{0i}|\right) \quad (3.42)$$

$$x_{Lai} = r_p [1 + \cos(\theta_{ai})] \quad (3.43)$$

$$z_{Lai} = r_p \sin(\theta_{ai}) \quad (3.44)$$

$$A_{ik} = P_i + [x_{Lai} \cos(\gamma_i), x_{Lai} \sin(\gamma_i), z_{Lai}]^T \quad (3.45)$$

where

$$\gamma_i = \text{atan2}(y_{bi} - y_{pi}, x_{bi} - x_{pi}) \quad (3.46)$$

In the algorithm given above, the Jacobian matrix \mathbf{J}_i is computed as follows:

$$\mathbf{J}_i = \frac{\partial V_i}{\partial H_i} = \begin{bmatrix} \frac{\partial x_{bi}}{\partial f_{bix}} & \frac{\partial x_{bi}}{\partial f_{biy}} & \frac{\partial x_{bi}}{\partial f_{biz}} & \frac{\partial x_{bi}}{\partial L_{0i}} \\ \frac{\partial y_{bi}}{\partial f_{bix}} & \frac{\partial y_{bi}}{\partial f_{biy}} & \frac{\partial y_{bi}}{\partial f_{biz}} & \frac{\partial y_{bi}}{\partial L_{0i}} \\ \frac{\partial z_{bi}}{\partial f_{bix}} & \frac{\partial z_{bi}}{\partial f_{biy}} & \frac{\partial z_{bi}}{\partial f_{biz}} & \frac{\partial z_{bi}}{\partial L_{0i}} \\ \frac{\partial \tau_{bi}}{\partial f_{bix}} & \frac{\partial \tau_{bi}}{\partial f_{biy}} & \frac{\partial \tau_{bi}}{\partial f_{biz}} & \frac{\partial \tau_{bi}}{\partial L_{0i}} \end{bmatrix} \quad (3.47)$$

where

$$\begin{aligned}
\frac{\partial x_{bi}}{\partial f_{bix}} &= \frac{L_{0i}}{EA_0} + \frac{C_T}{w} \ln\left(\frac{\tau_{bi} + f_{biz}}{\tau_{ai} + f_{biz} - wL_{0i}}\right) \\
&+ \frac{C_T f_{bix}^2}{w} \left[\frac{1}{(\tau_{bi} + f_{biz}) \tau_{bi}} - \frac{1}{(\tau_{ai} + f_{biz} - wL_{0i}) \tau_{ai}} \right] \\
\frac{\partial x_{bi}}{\partial f_{biy}} &= \frac{C_T f_{bix} f_{biy}}{w} \left[\frac{1}{(\tau_{bi} + f_{biz}) \tau_{bi}} - \frac{1}{(\tau_{ai} + f_{biz} - wL_{0i}) \tau_{ai}} \right] \\
\frac{\partial x_{bi}}{\partial f_{biz}} &= \frac{C_T f_{bix}}{w} \left(\frac{1}{\tau_{bi}} - \frac{1}{\tau_{ai}} \right)
\end{aligned}$$

$$\begin{aligned}\frac{\partial y_{bi}}{\partial f_{bix}} &= \frac{\partial x_{bi}}{\partial f_{biy}} \\ \frac{\partial y_{bi}}{\partial f_{biy}} &= \frac{L_{0i}}{EA_0} + \frac{C_T}{w} \ln\left(\frac{\tau_{bi} + f_{biz}}{\tau_{ai} + f_{biz} - wL_{0i}}\right) \\ &+ \frac{C_T f_{biy}^2}{w} \left[\frac{1}{(\tau_{bi} + f_{biz})\tau_{bi}} - \frac{1}{(\tau_{ai} + f_{biz} - wL_{0i})\tau_{ai}} \right] \\ \frac{\partial y_{bi}}{\partial f_{biz}} &= \frac{C_T f_{biy}}{w} \left(\frac{1}{\tau_{bi}} - \frac{1}{\tau_{ai}} \right)\end{aligned}$$

$$\begin{aligned}\frac{\partial z_{bi}}{\partial f_{bix}} &= \frac{\partial x_{bi}}{\partial f_{biz}} \\ \frac{\partial z_{bi}}{\partial f_{biy}} &= \frac{\partial y_{bi}}{\partial f_{biz}} \\ \frac{\partial z_{bi}}{\partial f_{biz}} &= \frac{L_{0i}}{EA_0} + \frac{C_T}{w} \left[\frac{f_{biz}}{\tau_{bi}} - \frac{f_{biz} - wL_{0i}}{\tau_{ai}} \right]\end{aligned}$$

$$\begin{aligned}\frac{\partial x_{bi}}{\partial L_{0i}} &= f_{bix} \left(\frac{1}{EA_0} + \frac{C_T}{\tau_{ai}} \right) \\ \frac{\partial y_{bi}}{\partial L_{0i}} &= f_{biy} \left(\frac{1}{EA_0} + \frac{C_T}{\tau_{ai}} \right) \\ \frac{\partial z_{bi}}{\partial L_{0i}} &= (f_{biz} - wL_{0i}) \left(\frac{1}{EA_0} + \frac{C_T}{\tau_{ai}} \right)\end{aligned}$$

$$\begin{aligned}\frac{\partial \tau_{bi}}{\partial f_{bix}} &= \frac{f_{bix}}{\tau_{bi}} \\ \frac{\partial \tau_{bi}}{\partial f_{biy}} &= \frac{f_{biy}}{\tau_{bi}} \\ \frac{\partial \tau_{bi}}{\partial f_{biz}} &= \frac{f_{biz}}{\tau_{bi}} \\ \frac{\partial \tau_{bi}}{\partial L_{0i}} &= 0\end{aligned}$$

In (2.1) or (3.41), there are only 3 equations but 4 unknown variables in vector H_i . In usual iterative methods, a $[3 \times 4]$ jacobian matrix is formed by taking the derivative $\partial B_i / \partial H_i$. One then need to compute the pseudo inverse of this rectangular matrix, which in our experience leads to poor convergence. By introducing the vector V_i , a squared full-rank Jacobian matrix is formulated in (3.47). The last term τ_{bi} in vector V_i plays the role of a virtual term (we only know the coordinates of the end-points B_i). When updating the

error vector dV_i , the last element of this vector is set to $d\tau_{bi} = 0$ since it always ensures a true statement (at the convergence solution, we have $dV_i = \mathbf{0}$). These changes greatly increase the convergence rate of the algorithm. In fact, in our experience, this algorithm often converges within 5 or 6 iterations with the precision $\epsilon = 1e - 10$.

It is important to note that this algorithm greatly depends on the method used to solve the tension distribution problem of the CDPR. Indeed, each tension distribution solving method computes a local solution of the IKP problem. For example, we use the principle solution τ_p (pseudo-inverse solution) from (2.43) with the massless elastic cable model as the initial starting point for H_0 . The algorithm used in this case should guarantee that the solution obtained with the catenary cable model is the local minimum around the initial guess H_0 . Even with the simplified cable model if we use the same pseudo-inverse solution as the initial guess for the cable tensions, the algorithm gives the same convergence solution obtained with the elastic catenary cable model.

Let us note that in the control system of a CDPR, it is better to avoid using different methods to solve the tension distribution problem. For example, we use method 1 (pseudo-inverse solution) and method 2 (e.g. method presented in [32]) to solve the tension distribution problem in real-time control. At some poses one can find feasible solutions (for cable tensions) by using method 1 but fail to find feasible solutions with method 2. Thus, both methods are used in the control system in order to increase the probability of obtaining a feasible solution (for the cable tensions). However, because two different methods generate two different solutions, it may lead to discontinuities along a trajectory followed by the CDPR mobile platform. In most cases, a sudden discontinuity could be harmful for the CDPR. Therefore, it is preferable to implement only one method to solve the IKP problem in order to obtain consistent solutions.

3.5 Error Analysis

In this section, several tests are presented to analyze the impact of thermal effect, cable Young's modulus and tension distribution method on the cable unstrained length. We perform these tests in simulation for the CoGiRo prototype. In all the tests, the total weight of the mobile platform is 195 kg. Steel cables are used. The characteristics of the cables are given as follows:

- Cable Young's modulus: $E = 35e + 9 (Pa)$
- Cable cross-section area: $A_0 = 8.2051e - 06 (m^2)$
- Cable self-weight: $w = 0.6278 (N/m)$

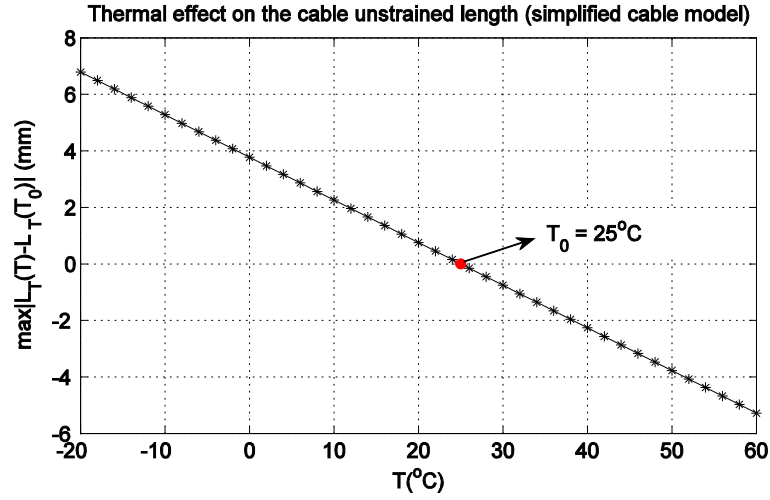


Figure 3.7: The change in the cable unstrained length at different temperatures

We compute the error in the cable unstrained length L_T between its value under the effect of a certain factor and its value in a reference state.

3.5.1 Impact of Thermal Effect

In order to see the impact of the temperature, we compute the change in the cable unstrained length from the winch to the anchor point B of a cable of the CoGiRo prototype at various temperatures. Fig. 3.7 shows the difference in the cable unstrained length L_T at difference temperatures compared to its value at the reference temperature ($T_0 = 25^\circ C$): $dL(T) = L_T(T) - L_T(T_0)$.

We use the simplified cable model (taking into account the pulley kinematics) and the method in [32] to solve the tension distribution problem. The solution is computed at the home pose $X_0 = (0 \ 0 \ 0, \ 0 \ 0 \ 0)$ ($m, \ rad$) and at different values of $dT = T - T_0$. The cable unstrained length at the reference temperature ($T_0 = 25^\circ C$) is $L_T(T_0) = 15.15 \ m$.

It can be seen that, there is a substantial change in the cable unstrained length with respect to a large change of temperature. For example, at $0^\circ C$ ($dT = -25^\circ C$), there is a difference of $4 - 5 \ mm$ in the cable unstrained length. In other words, the thermal effect should be considered if the CDPR is working in an environment with large changes of temperature.

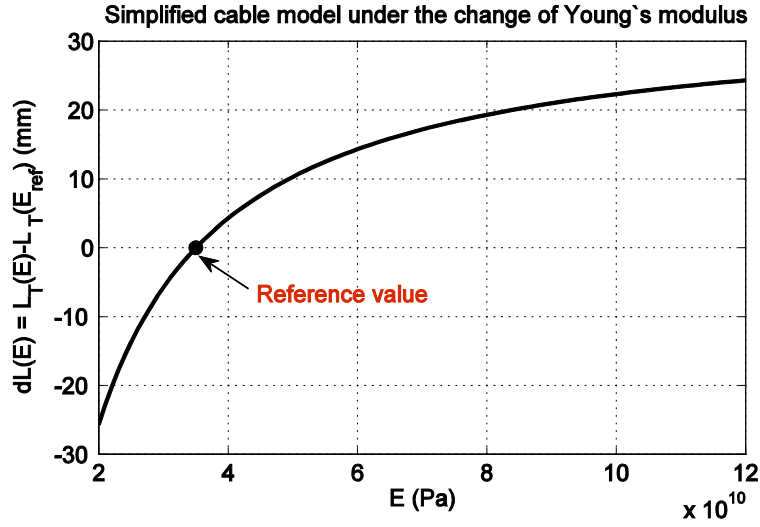


Figure 3.8: The change of cable unstrained length due to the change of the cable Young's modulus

3.5.2 Impact of Cable Characteristics

Among the three given cable parameters, the cable self-weight can be identified accurately. However it is not easy to justify the cable Young's modulus and the cable cross-section area. These factors indeed play important roles in deriving the CDP IKP solution. In this test, we keep the value of the cable cross-section area and change the value of the cable Young's modulus to see its effect on the cable unstrained length.

We compute the change in the cable unstrained length with respect to difference values of E , in a manner similar to Section 3.5.1. The temperature remains constant $dT = 0^\circ C$. The mobile platform is at the home position X_0 . We compute $dL(E) = L_T(E) - L_T(E_{ref})$.

Fig. 3.8 shows the change in L_T at different values of E compared to the reference value $E_{ref} = 3.5e + 10 (Pa)$, using the simplified cable model (taking into account the pulley kinematics). The change of the cable unstrained length is quite sensitive to the change of the cable Young's modulus. Only 10% in difference in E_{ref} could results in a difference of 4 – 5 mm in the cable unstrained length.

In practice, the term E (and also A_0) is in fact not a constant value, due to various uncertainties (e.g. cable rotation, increased temperature at contact point with pulley or drum, etc...). It can be assumed that the values of E lies within a range (E_{min}, E_{max}). From a characteristic curve such as the one shown in Fig. 3.8, one can estimate the error in the cable unstrained length L_T due to a change of E . In order to have good solutions for the CDP IKP problem, it is important to identify the range of possible values of E accurately.

3.5.3 Impact of the Method to Solve the CDPR Tension Distribution Problem

So far, to our best knowledge, there is no study that addresses the issue of using different tension distribution methods in solving the CDPR IKP problem. It is an issue since the obtained cable tensions directly affect the IKP solution.

In this section, we will compare the results of solving the IKP problem using two different methods to solve the CDPR tension distribution. The first method consists in using the pseudo-inverse solution $\boldsymbol{\tau}_p$. The second method is the one presented in [32] (we call this method as the “barycentric method”). The massless elastic cable model and the simplified cable model are considered, taking into account the pulley kinematics. The cable unstrained length L_T obtained with each of these two cable models is compared to the value of L_T obtained with the catenary cable model.

We compute the maximum difference in the cable unstrained length L_T of each cable model and the one obtained with the catenary cable model (2.8) (among the 8 cables) across a prescribed workspace (discretized into a finite number of equilibrium poses - Fig. 3.9):

$$dL_{\max} = \max |L_T(\text{model}) - L_T(\text{catenary})| \quad (3.48)$$

The results are shown in Fig. 3.10. In the case of the pseudo-inverse solution (“pinv method”), significant differences in the values of L_T are obtained when using the simplified cable model compared to the massless elastic cable model. When a “better” tension

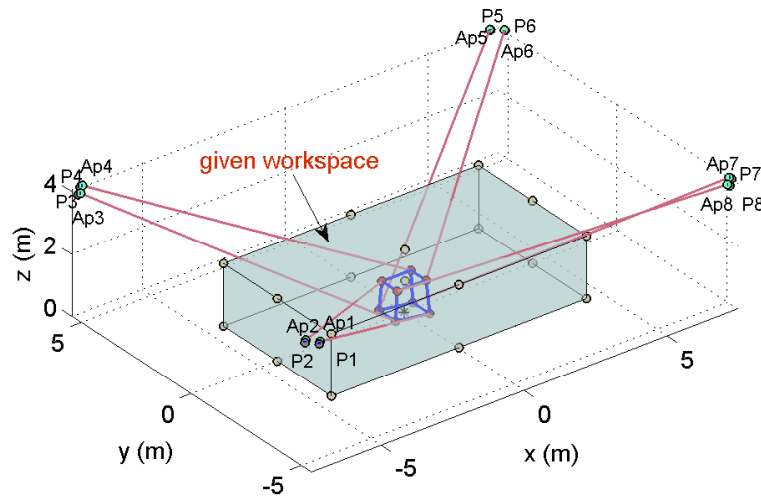


Figure 3.9: The CoGiRo CDPR

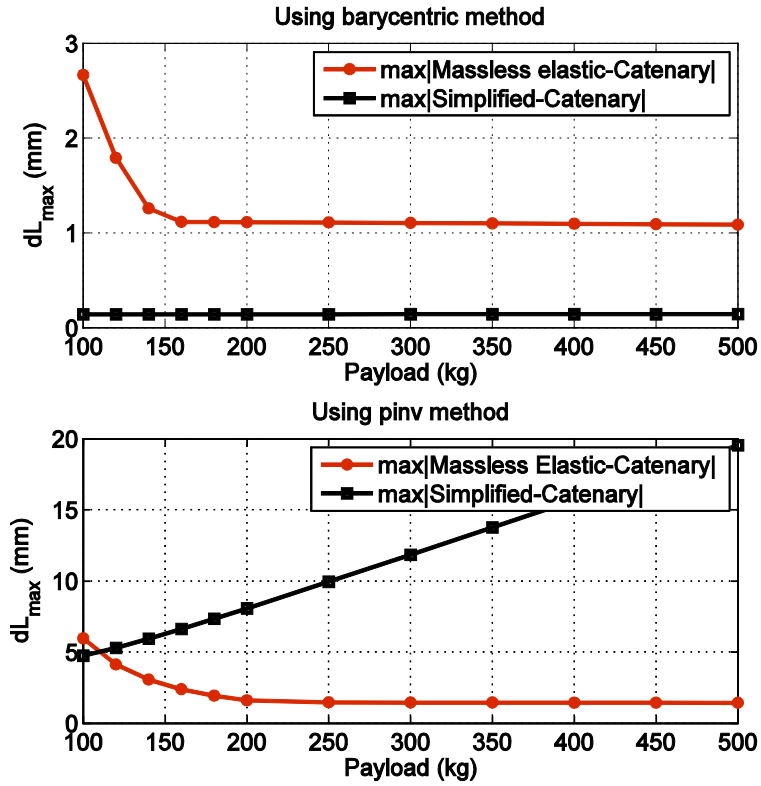


Figure 3.10: Maximum errors of the cable unstrained length computed from different tension distribution methods

distribution method is used (in this case, the “barycentric method”), the best results are obtained when using the simplified cable model.

This example shows that when using the simplified cable model, a suitable tension distribution method should be used.

3.6 Case Study

3.6.1 Case 1: Neglecting the Influence of the Pulleys and of Friction

The validation of the simplified cable model with the cable length expression (2.39) was performed in simulation and experimentally on the CoGiRo prototype [69]. The characteristics of the steel cables driving the mobile platform were chosen as:

- $E = 35e9$ (Pa)
- $A_0 = 8.2051e-06$ (m^2)
- $w = 0.62784$ (N/m)

SIMULATION

The reference point O_p of the mobile platform of the robot follows a prescribed trajectory in the Cartesian space $X_t = (x_t \ y_t \ z_t)$ with constant orientation $\alpha_{x,y,z} = (0 \ 0 \ 0)$ (X-Y-Z Euler angle convention). The total mass of the mobile platform and the payload is $m_p = 500 \text{ kg}$. X_t is the position of O_p at time t . Smoothed trapezoidal velocity method [99] is used to generate the desired trajectory. The robot is simulated using the massless cable model ($L_{0iMassless} = \|A_i B_i\|$), the elastic cable model (where only elasticity and not mass is considered) and the simplified hefty cable model with different expressions of cable unstrained length corresponding to Taylor series expansion of L_0 up to order 1 and 2 of R in (2.39). The cable unstrained lengths of the elastic cable model are computed as follows:

$$L_{0iElastic} = \frac{L_{0iMassless}}{1 + \frac{\tau_i}{EA_0}} \quad (i = \overline{1, m}) \quad (3.49)$$

where τ_i is the cable tension of the i -th cable obtained in the case of the massless cable model.

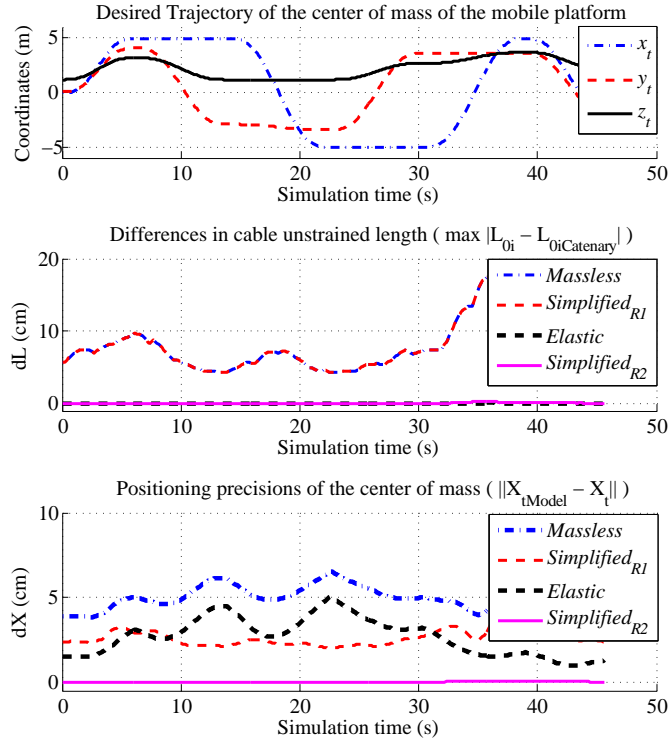


Figure 3.11: Accuracies of different cable models - Case 1a : following a desired trajectory

Different criteria are used to evaluate the results:

$$dL = \max_{1 \leq i \leq m} |L_{0i} - L_{0iCatenary}| \quad (3.50)$$

$$dX_{Model} = \|X_{tModel} - X_t\| \quad (3.51)$$

where L_{0i} is the unstrained length of the i -th cable in the cases of the massless (no elastic), massless elastic and simplified hefty cable models. $L_{0iCatenary}$ is the unstrained length of the i -th cable in case of the elastic catenary cable model. X_{tModel} is the simulated position of O_p at time t obtained for the CDP with a given cable model.

The variable v (introduced in Section 2.2.3) is computed in case of the simplified hefty cable models to illustrate the discussion of Section IV:

$$v_{\max} = \max_{1 \leq i \leq m} \frac{w x_{Lbi}}{f_{Lbxi}} \quad (3.52)$$

To check the assumption $\tau_s \ll EA_0$, we compute also the ratio

$$\eta_{\max} = \max_{1 \leq i \leq m} \frac{\tau_i}{EA_0} \quad (3.53)$$

The method presented in [32] is used to solve the tension distribution problem in case of the massless cable model and the simplified static analysis [23]. The results are then

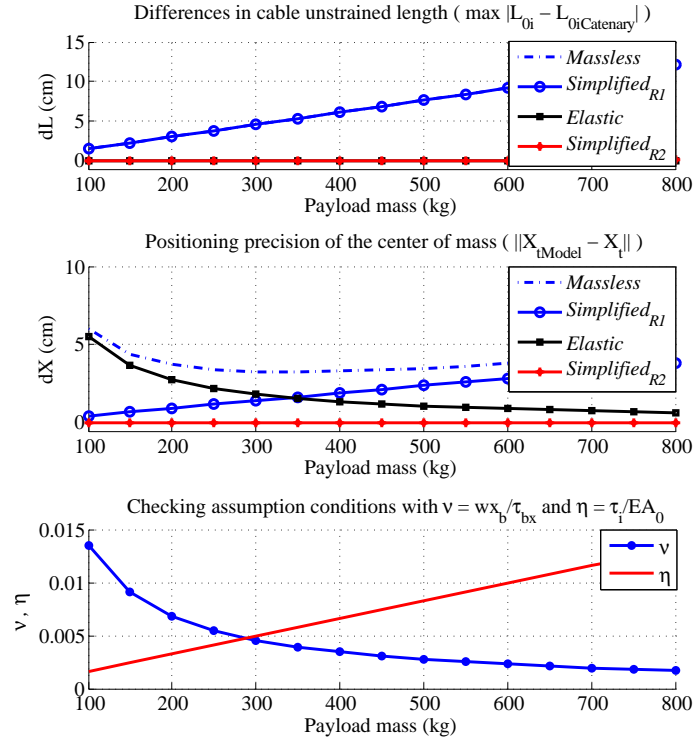


Figure 3.12: Accuracies of different cable models - Case 1b: varying payloads

compared to the one obtained by means of the elastic catenary cable model which is considered to be the reference.

Figure 3.11 shows that the hefty cable models lead to improve the results of the inverse kinematics solving (unstrained cable length computation) in comparison to the massless cable model. The massless (no elastic) cable model and simplified hefty cable model which has expression of L_{0i} with order 1 of R in (2.39) (*Simplified_{R1}* in Fig. 3.11) have a similar accuracy. The simplified cable model which uses the expression of L_{0i} with order 2 of R in (2.39) (considering both cable mass and cable elasticity, *Simplified_{R2}* in Fig. 3.11) gives the best accuracy. Note that, in term of solving the inverse kinematics, the massless elastic cable model and *Simplified_{R2}* give similar results. It means that the elasticity has a large impact on the cable lengths. This is reasonable for the steel cables with the given characteristics (the term EA_0 is relatively small).

In the second test, the reference point of the mobile platform of the robot is fixed at $O_p = (0 \ 0 \ 0)$ in the Cartesian space. The total mass of the mobile platform and the payload is varied in the range $100 \leq m_p \leq 800 \text{ kg}$. Figure 3.12 shows that the cable model *Simplified_{R2}* gives the best results. The impact of elasticity becomes more visible when the payload increases.

Now, let us consider the two assumptions suggested in Section 2.2.3 for the simplified cable models to be valid. The evolutions of the two variables v_{\max} and η_{\max} in Fig. 3.12 reveal a tradeoff of the simplified models. When the payload is small, η_{\max} is small, thus the first assumption $\tau_s \ll EA_0$ is valid but v_{\max} is large, hence the second assumption $v \ll 1$ is violated and vice versa. According to this example, it can be seen that the validity of a simplified cable model is a difficult issue when solving kinetostatic problem of CDPRs.

EXPERIMENT on CoGiRo

In our tests, the sagging of the cables is only considered between the points A_i and B_i (Fig. 3.13). The cable segments from points A_i to the winch drums are vertical (no sagging) and assumed unstressed (the elongations are compensated by adding some offsets to the cable lengths). The total mass of the mobile platform in our tests is $m_p = 210 \text{ kg}$. The position of the reference point O_p of the mobile platform is measured by a laser tracker. The tension distribution problem is solved by using the method in [32] based on the static analysis of [23].

The control scheme of CoGiRo is shown in Fig. 3.13 [17]. We used (2.39) to compute the desired cable unstrained lengths.

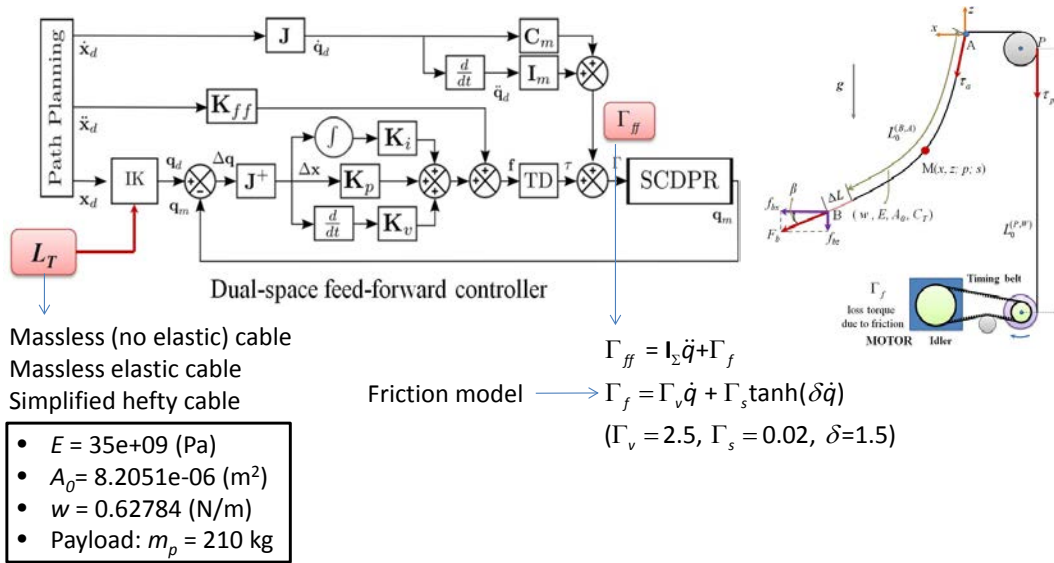


Figure 3.13: CoGiRo control scheme: Without the influence of pulley kinematics

The robot positioning accuracy is evaluated at several static equilibrium poses inside its workspace. Figure 3.14 shows the positions of these points (top view). The criteria (3.51), (3.52) and (3.53) are used to verify the results. In Tab. 3.2, X_L, X_E, X_{R1}, X_{R2} are the measured positions of the center of mass of the mobile platform in case of the massless, elastic, *Simplified_{R1}* and *Simplified_{R2}* cable models, respectively.

Table 3.3 shows that the cable model *Simplified_{R2}* gives the best results. The massless elastic cable model has accuracies quite close to *Simplified_{R2}*. The massless (no elastic) cable model and *Simplified_{R1}* provide similar results with a lower accuracy. This is reason-

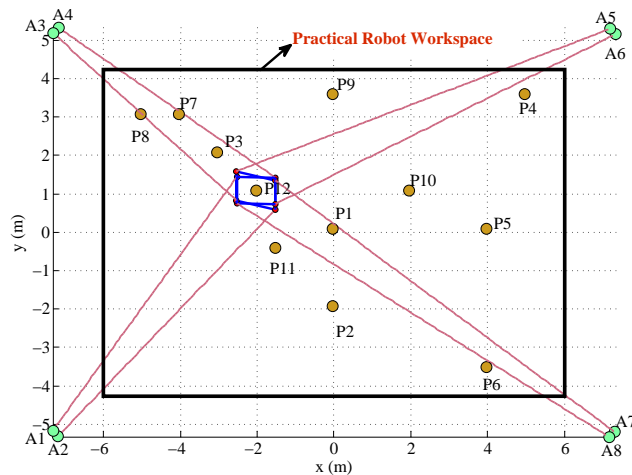


Figure 3.14: Static equilibrium poses in the workspace of CoGiRo - Case study 1

Table 3.2: Measured positions of the mobile platform of CoGiRo at several static equilibrium poses - Case study 1

Static poses (x_c, y_c, z_c) (m)	X_L (x_c, y_c, z_c) (m)	X_{R1} (x_c, y_c, z_c) (m)	X_E (x_c, y_c, z_c) (m)	X_{R2} (x_c, y_c, z_c) (m)
$P_1(0.0, 0.0, 1.0)$	(-0.001, 0.000, 0.881)	(-0.001, 0.000, 0.882)	(-0.001, -0.002, 0.979)	(-0.000, -0.002, 0.997)
$P_2(0.0, -2.0, 1.3)$	(0.001, -1.991, 1.161)	(0.001, -1.990, 1.161)	(-0.002, -1.993, 1.275)	(-0.001, -1.993, 1.294)
$P_3(-3.0, 2.0, 0.2)$	(-2.997, 1.993, 0.142)	(-2.998, 1.994, 0.143)	(-2.989, 1.990, 0.194)	(-2.988, 1.988, 0.203)
$P_4(5.0, 3.5, 0.5)$	(4.999, 3.493, 0.444)	(4.999, 3.489, 0.448)	(4.987, 3.490, 0.478)	(4.987, 3.492, 0.483)
$P_5(4.0, 0.0, 0.7)$	(3.999, 0.003, 0.610)	(4.001, 0.001, 0.616)	(3.988, 0.003, 0.672)	(3.988, 0.005, 0.679)
$P_6(4.0, -3.6, 1.0)$	(4.006, -3.594, 0.907)	(4.007, -3.598, 0.911)	(3.987, -3.595, 0.960)	(3.987, -3.591, 0.964)
$P_7(-4.0, 3.0, 0.8)$	(-4.006, -2.990, 0.732)	(-4.003, -2.995, 0.727)	(-3.993, -2.990, 0.771)	(-3.993, -2.989, 0.775)
$P_8(-5.0, 3.0, 1.1)$	(-4.996, 2.995, 1.044)	(-4.994, 2.994, 1.046)	(-4.984, 2.988, 1.081)	(-4.985, 2.987, 1.083)
$P_9(0.0, 3.5, 0.9)$	(-0.004, 3.481, 0.816)	(-0.003, 3.481, 0.824)	(-0.001, 3.490, 0.902)	(-0.002, 3.490, 0.904)
$P_{10}(2.0, 1.0, 1.0)$	(1.999, 0.995, 0.896)	(1.997, 0.994, 0.900)	(1.989, 0.995, 0.976)	(1.992, 0.993, 0.983)
$P_{11}(-1.5, -0.5, 0.8)$	(-1.499, -0.503, 0.705)	(-1.499, -0.502, -0.706)	(-1.495, -0.502, 0.778)	(-1.495, -0.505, 0.782)
$P_{12}(-2.0, 1.0, 0.6)$	(-2.003, 0.989, 0.518)	(-2.002, 0.990, 0.521)	(-1.997, 0.990, 0.583)	(-1.996, 0.987, 0.585)

Table 3.3: Positioning accuracy of CoGiRo at several static equilibrium poses - Case study 1

Static poses (x_c, y_c, z_c) (m)	dX_L (cm)	dX_{R1} (cm)	dX_E (cm)	dX_{R2} (cm)	v_{\max}	η_{\max}
$P_1(0.0, 0.0, 1.0)$	11.89	11.83	2.08	0.32	0.004	0.006
$P_2(0.0, -2.0, 1.3)$	13.91	13.90	2.61	0.93	0.006	0.008
$P_3(-3.0, 2.0, 0.2)$	5.86	5.76	1.66	1.72	0.013	0.005
$P_4(5.0, 3.5, 0.5)$	5.65	5.28	2.71	2.33	0.020	0.005
$P_5(4.0, 0.0, 0.7)$	9.05	8.38	3.03	2.49	0.011	0.005
$P_6(4.0, -3.6, 1.0)$	9.37	8.98	4.25	3.96	0.015	0.007
$P_7(-4.0, 3.0, 0.8)$	6.85	7.35	3.12	2.85	0.013	0.006
$P_8(-5.0, 3.0, 1.1)$	5.63	5.48	2.73	2.65	0.013	0.006
$P_9(0.0, 3.5, 0.9)$	8.61	7.82	1.01	1.08	0.018	0.008
$P_{10}(2.0, 1.0, 1.0)$	10.40	10.07	2.70	2.05	0.007	0.007
$P_{11}(-1.5, -0.5, 0.8)$	9.55	9.43	2.21	1.91	0.007	0.005
$P_{12}(-2.0, 1.0, 0.6)$	8.25	7.95	1.98	2.01	0.008	0.005

able since we obtained similar results in simulation for the inverse kinematics (Fig. 3.11, "Differences in cable unstrained length"). In the case of the considered CDPR (CoGiRo prototype), these experimental results confirm the strong impact of the cable elasticity on the robot accuracy (dX_E in Tab. 3.3), notably when compared to the cable mass alone (dX_{R1}). It remains that the best results are obtained by considering both cable mass and elasticity (dX_{R2}).

In Tab. 3.3, at equilibrium points that are close to the center of the practical workspace (v_{\max} is small), the position accuracy is good (e.g. at points P_1 and P_2). As it could be expected, the accuracy of the robot reduces when the mobile platform is positioned near the workspace boundary (e.g. at points $P_4 - P_8$). Indeed, the value of the variable v_{\max} increases when P_c approaches the workspace boundary (when x_c and y_c are large) which creates expected errors in solving the inverse kinematic problem. In addition, the variable η_{\max} has relatively large values, which reduces the accuracy of the simplified cable models.

This fact confirms our analysis of the limitation of the simplified cable model in Section 2.2.3.

3.6.2 Case 2: CoGiRo with Extended CDPR Modeling

To illustrate the impact of the extended CDPR modeling (Section 3.3), we performed some experiments with the CoGiRo prototype taking into account the influence of pulleys and of friction. The simplified cable model with the cable length expression (3.36) and the massless elastic cable model are compared. To see the impact of different methods in solving the tension distribution problem, the pseudo-inverse solution and the barycentric method [32] were used. The characteristics of the steel cables driving the mobile platform are:

- $E = 100e9$ (Pa)
- $A_0 = 8.2051e-06$ (m^2)
- $w = 0.62784$ (N/m)

The control scheme of CoGiRo in this case is shown in Fig. 3.15.

In this experiment, we revised our estimation of the cable Young's modulus as $E = 100e9$ (Pa) (which is much larger than the value used in the previous experiment). Note also that, as shown in Fig. 3.15, the friction model is not the same as the one used in the first experiment (without influence of pulley kinematics). It is replaced by a better model obtained from the identification procedure in Section 3.1.3.

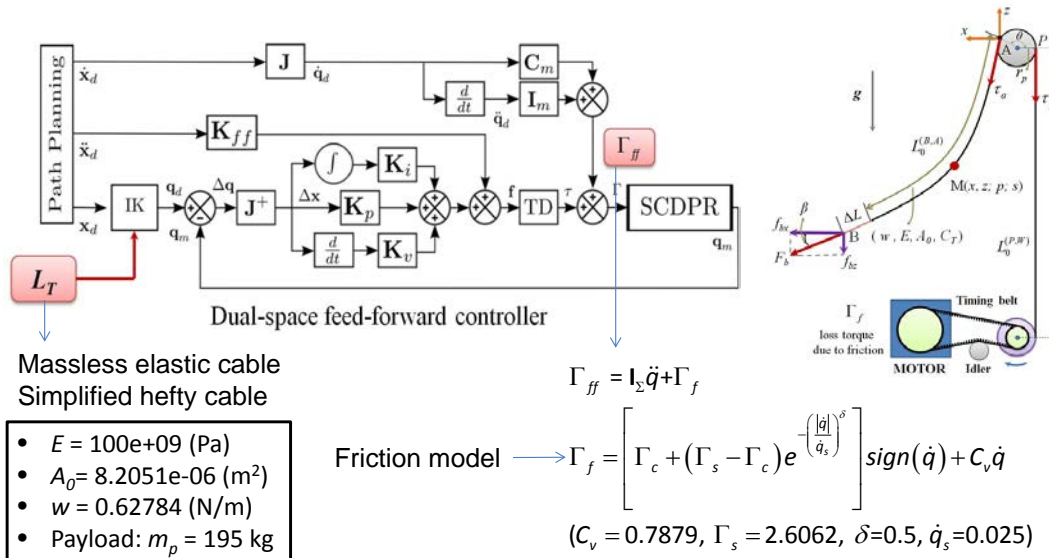


Figure 3.15: CoGiRo control scheme: Including the influence of pulley kinematics

The robot positioning accuracy is evaluated at several static equilibrium poses inside its workspace $X_d = (P_d, \Phi_d)$ (m, rad). Figure 3.16 shows the positions of these points (top view). In Tab. 3.4, $X_E(pin v)$, $X_S(pin v)$, $X_E(bary)$, $X_S(bary)$ are the measured positions and orientations of the mobile platform in case of the massless elastic cable model and the simplified hefty cable model with the solutions to the tension distribution problem obtained using the pseudo-inverse ('pinv') and the barycentric method ('bary'). At several poses, we purposely set some "non-zero" orientation of the mobile platform.

We compute the positioning accuracy in the Cartesian space and the orientation space to validate the performances of the two cable models. The results are shown in Tab. 3.5.

We however only looked at the positioning accuracy in the Cartesian space. The performances of the CDPR in the case of using the barycentric method is better than those obtained when using the pseudo-inverse to solve the tension distribution. The simplified cable model ($dP_S(bary)$) performs slightly better than the massless elastic cable model ($dP_E(bary)$). These results reflect our analysis in Section 3.5.

If we compare the results in this experiment with the one obtained in the first case study (which neglects the influence of pulleys and friction), one can see that the maximum positioning errors are smaller. In the first case study, maximum errors lie within the range of 3 – 4cm for the simplified cable models and 3 – 4.25cm for the massless elastic cable model (Tab. 3.3), whereas in the second case study, the maximum errors lie within the range of 1 – 2cm for the simplified cable model and 1.5 – 2.5cm for the massless elastic cable model (Tab. 3.5). These numbers show a significant improvement.

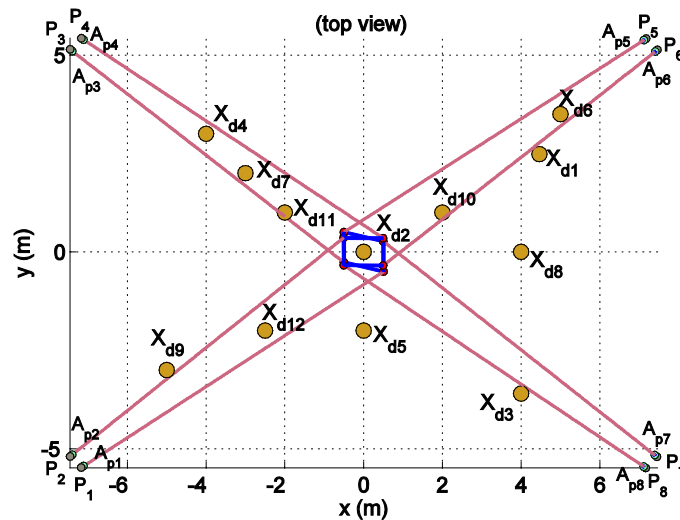


Figure 3.16: Static equilibrium poses in the workspace of CoGiRo - Case study 2

Table 3.4: Measured positions of the mobile platform of CoGiRo at several static equilibrium poses - Case study 2

Testing poses $P_d(x_c, y_c, z_c) (m)$ $\Phi_d(\theta_x, \theta_y, \theta_z) (rad)$	$X_E(\text{pinv})$ $(x_c, y_c, z_c) (m)$ $(\theta_x, \theta_y, \theta_z) (rad)$	$X_S(\text{pinv})$ $(x_c, y_c, z_c) (m)$ $(\theta_x, \theta_y, \theta_z) (rad)$	$X_E(\text{bary})$ $P_d(x_c, y_c, z_c) (m)$ $(\theta_x, \theta_y, \theta_z) (rad)$	$X_S(\text{bary})$ $(x_c, y_c, z_c) (m)$ $(\theta_x, \theta_y, \theta_z) (rad)$
$P_{d1}(4.463, 2.485, 0)$ $\Phi_{d1}(0, -0.1745, -0.785)$	(4.4480, 2.4855, -0.0047) (-0.0036, -0.1764, -0.7821)	(4.4476, 2.4867, -0.0063) (-0.0029, -0.1759, -0.7821)	(4.4465, 2.4870, -0.0057) (-0.0027, -0.1753, -0.7814)	(4.4512, 2.4897, -0.0059) (-0.0043, -0.1765, -0.7854)
$P_{d2}(0, 0, 1.3)$ $\Phi_{d2}(0, -0.1745, 0)$	(-0.0045, 0.00182, 1.2822) (0.0007, -0.1712, -0.0018)	(-0.0053, 0.0024, 1.28) (0.0013, -0.1707, -0.0017)	(-0.0044, 0.0013, 1.2856) (0.0006, -0.1703, -0.0019)	(-0.0043, 0.0031, 1.2868) (0.0009, -0.1698, -0.0020)
$P_{d3}(4, -3.6, 1)$ $\Phi_{d3}(0, 0, 0)$	(3.9945, -3.589, 0.9810) (0.0033, -0.0009, 0.0003)	(3.9940, -3.5893, 0.9796) (0.0036, -0.0003, 0.0006)	(3.9940, -3.5882, 0.9808) (0.0031, 0.0005, 0.0011)	(3.9944, -3.5887, 0.9844) (0.0027, 0.0004, 0.0006)
$P_{d4}(-4, 3, 0.8)$ $\Phi_{d4}(0, 0, 0)$	(-4.0035, 2.9956, 0.7866) (-0.0017, 0.0040, -0.0027)	(-4.0034, 2.9957, 0.7867) (-0.0018, 0.004, -0.0026)	(-4.0026, 2.9949, 0.7854) (-0.0017, 0.0038, -0.003)	(-3.9979, 2.9957, 0.7836) (-0.0053, 0.0012, -0.0025)
$P_{d5}(0, -2, 1.3)$ $\Phi_{d5}(-0.1745, 0, -0.5236)$	(-0.0054, -1.9939, 1.2816) (-0.1738, -0.0006, -0.5236)	(-0.0089, -1.9936, 1.2786) (-0.1707, 0.0017, -0.5236)	(-0.0059, -1.9922, 1.2769) (-0.1713, -0.0021, -0.5223)	(-0.0083, -1.9905, 1.2823) (-0.1693, 0.0036, -0.5229)
$P_{d6}(5, 3.5, 0.5)$ $\Phi_{d6}(0.0873, 0.0873, 0)$	(4.9907, 3.4973, 0.4897) (0.082, 0.0841, -0.0015)	(4.9910, 3.4977, 0.4900) (0.0816, 0.0843, -0.0013)	(4.9900, 3.4999, 0.4897) (0.0840, 0.0811, -0.0017)	(4.9955, 3.4995, 0.4908) (0.0814, 0.0802, -0.0026)
$P_{d7}(-3, 2, 0.2)$ $\Phi_{d7}(0, 0, -0.6981)$	(-3.0079, 1.9978, 0.1906) (-0.0009, 0.0015, -0.7007)	(-3.0078, 1.9979, 0.1908) (-0.0010, 0.0015, -0.7007)	(-3.0065, 1.9980, 0.1963) (-0.0014, -0.0011, -0.6986)	(-3.0019, 1.9981, 0.1936) (-0.0033, -0.0001, -0.6988)
$P_{d8}(4, 0, 0.7)$ $\Phi_{d8}(0, 0, 0)$	(3.9935, 0.0008, 0.6837) (-0.0019, -0.0004, -0.0020)	(3.9937, 0.0008, 0.6842) (-0.0018, -0.0002, -0.0019)	(3.9933, 0.0027, 0.6863) (-0.0010, -0.0034, -0.0018)	(3.9980, 0.0010, 0.6863) (-0.0047, -0.0033, -0.0018)
$P_{d9}(-5, -3, 1.1)$ $\Phi_{d9}(-0.0873, 0, -0.3491)$	(-5.0072, -2.9940, 1.0809) (-0.08473, 0.0037, -0.3531)	(-5.0075, -2.9941, 1.0810) (-0.0850, 0.0039, -0.3533)	(-5.0059, -2.9928, 1.0825) (-0.0838, 0.0034, -0.3527)	(-5.0014, -2.9939, 1.0811) (-0.0854, 0.0028, -0.3503)
$P_{d10}(2, 1, -1)$ $\Phi_{d10}(0, 0, 0)$	(1.9938, 1.0027, -1.0051) (-0.0024, 0.0005, -0.0005)	(1.9938, 1.0028, -1.0052) (-0.0021, 0.0006, -0.0005)	(1.9933, 1.0016, -1.0043) (-0.0017, 0.0002, -0.0014)	(1.9966, 1.0017, -1.0043) (-0.0048, -0.0002, 0.0019)
$P_{d11}(-2, 1, 0)$ $\Phi_{d11}(0, 0, -0.8727)$	(-2.0090, 1.0044, -0.0069) (0.0001, 0.00002, -0.8752)	(-2.0091, 1.0044, -0.0068) (0.0003, -0.0002, -0.8753)	(-2.007, 1.0033, -0.0029) (-0.0007, -0.0010, -0.8772)	(-2.0051, 1.0027, -0.0059) (-0.0028, 0.0003, -0.8719)
$P_{d12}(-2.5, -2, 0.8)$ $\Phi_{d12}(0, -0.0873, -0.3491)$	(-2.5063, -1.9915, -0.8076) (0.0023, -0.087, -0.3478)	(-2.5064, -1.9916, -0.8079) (0.0026, -0.087, -0.3479)	(-2.5051, -1.9913, -0.8037) (0.0027, -0.0871, -0.3523)	(-2.5049, -1.9917, -0.8043) (0.0005, -0.0837, -0.3477)

Table 3.5: Positioning accuracy of CoGiRo at several static equilibrium poses - Case study 2

$P_d(x_c, y_c, z_c) (m)$ $\Phi_d(\theta_x, \theta_y, \theta_z) (rad)$	$dP_E(\text{pinv}) (mm)$ $d\Phi_E(\text{pinv}) (mrad)$	$dP_S(\text{pinv}) (mm)$ $d\Phi_S(\text{pinv}) (mrad)$	$dP_E(\text{bary}) (mm)$ $d\Phi_E(\text{bary}) (mrad)$	$dP_S(\text{bary}) (mm)$ $d\Phi_S(\text{bary}) (mrad)$
$P_{d1}(4.463, 2.485, 0)$ $\Phi_{d1}(0, -0.1745, -0.785)$	15.6993 4.9860	16.7616 4.3106	17.5846 4.6098	14.0480 4.7756
$P_{d2}(0, 0, 1.3)$ $\Phi_{d2}(0, -0.1745, 0)$	18.4234 3.8616	20.8449 4.3737	15.1539 4.5990	14.2637 5.1738
$P_{d3}(4, -3.6, 1)$ $\Phi_{d3}(0, 0, 0)$	22.4270 3.4101	23.7317 3.7038	23.3493 3.3140	20.0499 2.7673
$P_{d4}(-4, 3, 0.8)$ $\Phi_{d4}(0, 0, 0)$	14.4960 5.1295	14.4507 5.1235	15.6484 5.1447	17.0568 5.9435
$P_{d5}(0, -2, 1.3)$ $\Phi_{d5}(-0.1745, 0, -0.5236)$	20.1114 0.9368	24.0037 4.1603	25.1016 4.0021	21.7530 6.3743
$P_{d6}(5, 3.5, 0.5)$ $\Phi_{d6}(-0.1745, 0, -0.5236)$	14.1395 6.3748	13.6078 6.5605	14.2851 7.1813	10.2288 9.6099
$P_{d7}(-3, 2, 0.2)$ $\Phi_{d7}(0, 0, -0.6981)$	12.4303 3.1670	12.2175 3.1149	7.6817 1.8791	6.9286 3.4077
$P_{d8}(4, 0, 0.7)$ $\Phi_{d8}(0, 0, 0)$	17.6281 2.7873	17.0452 2.6624	15.5182 4.0068	13.8284 6.0516
$P_{d9}(-5, -3, 1.1)$ $\Phi_{d9}(-0.0873, 0, -0.3491)$	21.2280 5.9939	21.3024 6.1447	19.8761 6.0876	19.9265 3.6321
$P_{d10}(2, 1, -1)$ $\Phi_{d10}(0, 0, 0)$	8.4207 2.4809	8.5410 2.2692	8.1781 2.2629	5.7620 5.1441
$P_{d11}(-2, 1, 0)$ $\Phi_{d11}(0, 0, -0.8727)$	12.1749 2.4735	12.1749 2.5990	8.5239 4.6947	8.2562 2.8833
$P_{d12}(-2.5, -2, 0.8)$ $\Phi_{d12}(0, -0.0873, -0.3491)$	13.0189 2.6618	13.2190 2.8216	10.7415 4.1952	10.5490 3.9351

Conclusions

This chapter detailed an extended modeling of CDPRs. The influence of pulley kinematics, friction, thermal effect as well as cable characteristics (cable mass and elasticity) have been discussed. Indeed, these factors have a significant impact on the CDPR positioning accuracy. Depending on the method used to solve the tension distribution problem, the massless elastic cable model or simplified hefty cable models lead to the best results.

Our experiments with the CoGiRo prototype showed us that it is important to determine correctly the initial state of the CDPR at the home pose (in our case, the initial unstrained length L_{T0}). One can compute L_{T0} by using the algorithm presented in Section 3.4. After knowing the desired tension and unstrained length for each cable, a cable tensing step is needed to tune the motor of each winch so that the actual state of the CDPR is close to the theoretically computed state. To this end, it is necessary to resort to a parameter identification procedure given that we have good measurements of the CDPR geometric parameters (the positions of the fixed point on each pulley P_i , the cable anchor points B_i, \dots). Such calibration of a CDPR at the initial state must be accordant to the results obtained by using a particular tension distribution strategy.

Moreover, to improve the CDPR positioning accuracy, one should carefully address the possible changes in the environment temperature (thermal effect). There will be significant changes in the cable lengths if the CDPR is working in a very cold environment or in a very hot one. Besides, friction should also have a non-negligible impact on the CDPR performances. Periodical maintenance (e.g. lubricate pulleys, gear box, transmission belt,...) is necessary to reduce the torques (or forces) loss due to friction.

THE CDPR RECONFIGURATION PROBLEM

Summary

4.1	Introduction	93
4.2	CDPR Reconfiguration as a Single-Objective Optimization Problem	96
4.3	CDPR Reconfiguration as a Multi-Objective Optimization Problem	107

In this chapter, we discuss two case studies of CDPR reconfiguration. In the first case study, the reconfiguration of a CDPR is considered as a single-objective optimization problem which can be solved by using gradient-based optimization tools. A systematic procedure is proposed. It consists in dividing the CDPR reconfiguration problem into two optimization sub-problems. The first sub-problem aims at finding the bounds on the reconfiguration parameters in which all the nonlinear constraints including wrench feasibility and geometric constraints are satisfied. The CDPR reconfiguration is thereby transformed into a classical box-constrained problem which can be solved with standard optimization tools. Two reconfiguration strategies are considered: *offline reconfiguration* and *online reconfiguration*. Two criteria are introduced to quantify the robot performance related to energy consumption: *the sum of cable tensions* (used in offline reconfiguration) and *minimal energy consumption of the CDPR* (used in online reconfiguration). The procedure provides a straightforward approach which is familiar to engineers and could be implemented in real-time software environments.

In the second case study, the reconfiguration of a CDPR is considered as a multi-objective optimization problem. A systematic procedure to derive the reconfiguration

planning solution is presented. Two criteria are used to quantify the CDPR performances: *the sum of cable tensions* and *the normalized upper bound on the infinitesimal displacement of the mobile platform*. The first criterion is related to the CDPR energy consumption. The second one is a new performance index used here to quantify the CDPR stiffness. This multi-objective optimization approach offers the end-users a set of CDPR reconfiguration solutions where the tradeoff between different performance indices is efficiently taken into account.

The chapter is organized as follows. Section 4.1 presents the general architecture of a reconfigurable CDPR considered in this chapter. It corresponds to one of the large-dimension reconfigurable suspended CDPRs introduced in Chapter 1 as a possible means to replace the conventional methods of handling large and heavy parts across a wide workspace. Then, Section 4.2 and Section 4.3 discuss the first and second case studies of the CDPR reconfiguration, respectively.

4.1 Introduction

4.1.1 Large-Dimension Reconfigurable Suspended CDPR Architecture

Fig. 4.1 shows the general concept of large-dimension reconfigurable suspended CDPRs considered in this thesis to replace conventional cranes or telescopic platforms. The winches that drive the cables are attached onto two overhead bridge cranes to form a large-dimension CDPR. The positions of the winches or cable exit points can be changed by mobile bases moving along the crane beams. The overhead bridge cranes can move along the side walls of the workshop building. In this way, each CDPR should cover any area in the workshop. Depending on the size of the workshop, multiple CDPRs can be used to perform different tasks across wide workspaces.

In fact, this idea is derived originally from the experiences of partners involved in the CableBOT project consortium. Firstly, the general suspended architecture of the reconfigurable CDPR is similar to that of the fixed-configuration redundant suspended CDPR CoGiRo prototype [17] since CoGiRo's geometry structure has shown some great potential. Secondly, the moving cranes are adapted from the overhead bridge crane systems that carry heavy parts in workshops. By attaching the winches on the cranes, there will be mostly vertical forces acting on the two side walls of the building. Lateral force components created by cables tensions which are orthogonal to the side walls are minimized. However, horizontal force components in the cables that tend to bring the two overhead bridge cranes together may need to be avoided. One solution is to connect the two cranes

with some support beams to sustain these lateral horizontal forces. In this manner, the robot system loses one degree of redundancy but, in return, becomes more stable.

In the general scenario, the 6-DOF mobile platform of the CDPR is driven by 8 cables and two overhead bridge cranes. Each cable exit point is driven by an actuator. If all the cable exit points could move freely along the bridge cranes, the number of total actuators would be 18 (where 10 actuators are used to reconfigure the robot geometry structure). It results in a highly redundant robot system. We propose to move the cable exit points by pairs along the bridges to reduce the total number of actuator from 18 to 14. If we fix the cable exit points and also the positions of two overhead bridge cranes, the total number of actuators that drive the mobile platform is reduced to 8. In the latter case, the CDPR becomes one similar to a fixed-configuration redundantly actuated CDPR (e.g. CoGiRo prototype).

In the most complex case, the reconfigurability of the proposed CDPR is determined by a maximum of 6 actuators that drive the 4 pairs of cable exit points (r_1, \dots, r_4) and the 2 overhead bridge cranes (r_5, r_6), as shown in Fig. 4.1. Hence, (r_1, r_2, \dots, r_6) are the reconfiguration parameters. Note that the positions of the two overhead bridge cranes can be fixed

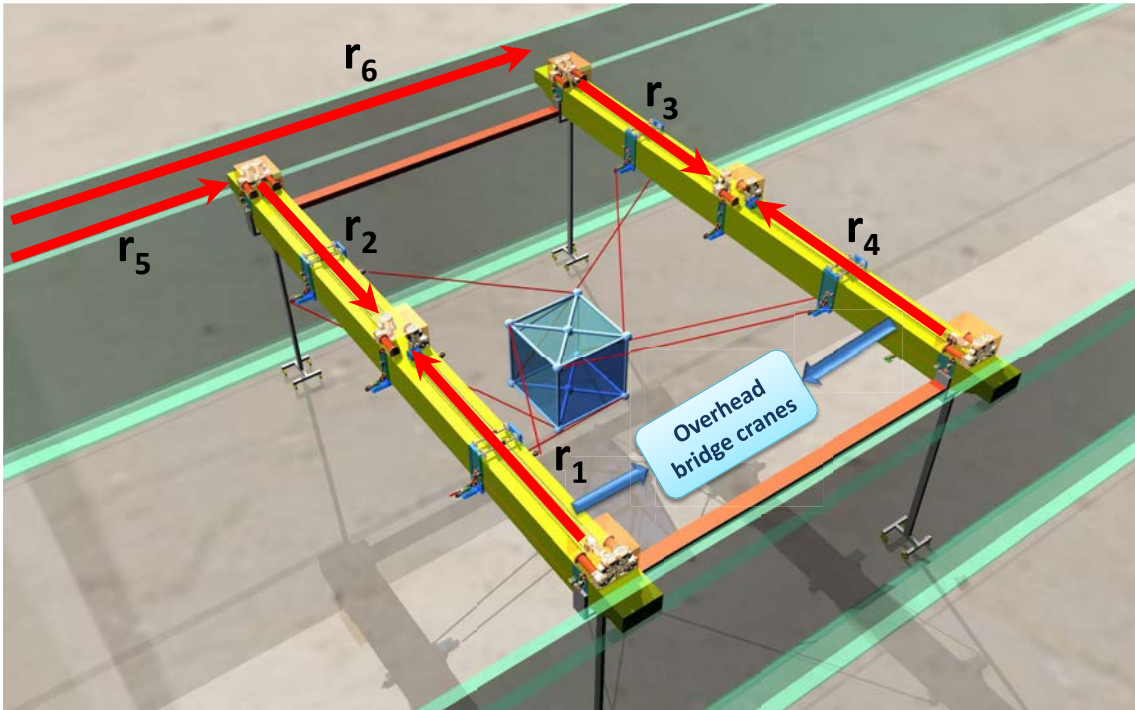


Figure 4.1: Solution using large-dimension reconfigurable suspended CDPR to replace conventional cranes

in order for the CDPR to perform at specific areas in the workshop. In such cases, there are only four reconfiguration parameters r_1, r_2, r_3 and r_4 .

It is worth noting that, by keeping the general suspended redundantly actuated architecture similar to the CoGiRo prototype [32] (using 8 cables to drive the mobile platform), the Cartesian workspace and orientation workspace of the CDPR are increased substantially, compared to 6-cable CDPRs such as the AMP [100]. Furthermore, reconfigurability should improve the CDPR performances and offers more flexible choices to the end-users (in the present work, *reconfigurability* means the ability to change the locations of the cable exit points of the CDPR).

The CDPR can operate in two modes, *offline reconfiguration* and *online reconfiguration*. In *offline reconfiguration*, appropriate positions of the cable exit points are determined offline. Thereby, the cable layout of the CDPR is adapted to a specified task. After the reconfiguration of cable exit points has been performed, the cable exit point positions are fixed and the robot starts the given tasks. Meanwhile, *online reconfiguration* consists in changing the positions of the cable exit points along a trajectory followed by the CDPR mobile platform and/or during the execution of a task.

4.1.2 The General Problem of CDPR Reconfiguration

In our view, *the reconfigurability of a CDPR is the capability of changing its cable layout to increase flexibility, i.e., obtain better performances under certain constraints*. It can be formulated as the following *nonlinear constrained optimization* problem:

"Find a set of reconfiguration parameters \mathbf{r} which minimizes several performance criteria $\mathbf{f}(\mathbf{r}) = (f_1(\mathbf{r}), f_2(\mathbf{r}), \dots)$:

$$\mathbf{r}_{opt} = \min\{f(r_1, r_2, \dots, r_p)\} \quad (4.1)$$

subjects to

$$\mathbf{r}_{\min} \leq \mathbf{r} \leq \mathbf{r}_{\max}$$

$$\mathbf{r} \in \mathbf{C}_r$$

where \mathbf{r}_{\min} and \mathbf{r}_{\max} are the lower and upper bounds on the reconfiguration parameters \mathbf{r} . Each criterion f_i is computed with respects to one or several platform poses. \mathbf{C}_r is the set of reconfiguration parameters that satisfy all nonlinear constraints including geometric constraints and wrench feasibility constraints."

In this general problem, there are two types of constraints. The first ones are *geometric constraints* which are the limitations on Cartesian workspace and orientation workspace of the CDPR. Satisfying these constraints means for instance that the CDPR pose at hand is collision free and that the cable lengths smaller than their maximum possible value. The second type are *tension based constraints* which *involve the dynamic modeling of the mobile platform* to compute the cable tensions of the CDPR.

4.2 CDPR Reconfiguration as a Single-Objective Optimization Problem

As a single-objective optimization problem, the objective function $\mathbf{f}(r_1, r_2, \dots, r_p)$ in the general problem (4.1) consists of one performance index only. In this thesis, this criterion is used to quantify the CDPR energy consumption.

Since we aim to use gradient-based optimization tools to solve the CDPR reconfiguration problem, necessary conditions must be met. In order to achieve real-time capable solving, the general problem (4.1) is divided into two optimization sub-problems. The first sub-problem is to find a feasible set of reconfiguration parameters in which all the non-linear constraints (which are time-consuming to handle) are removed. This sub-problem transforms the general problem into a standard box-constrained optimization problem which can be solved by any available standard optimization software.

In the following sub-sections, after the introduction of the two performance indices (which are used as the objective function of the optimization problem in offline reconfiguration mode and online reconfiguration mode), the procedure to solve the CDPR reconfiguration is detailed and illustrated in an example.

4.2.1 Performance Indices

Let us consider a CDPR driven by m cables in a configuration defined by \mathbf{r} . At an equilibrium pose of the mobile platform, by solving the tension distribution problem, we obtain desired cable tensions τ_i , $i = 1, 2, \dots, m$.

SUM OF CABLE TENSIONS

In **offline reconfiguration**, we choose the sum of the cable tensions as the objective function:

$$f(\mathbf{r}) = \sum_{i=1}^m \tau_i(\mathbf{r}) \quad (4.2)$$

This index directly relates to the power consumption of the CDPR. In case of the proposed *suspended CDPR architecture* (Fig. 4.1), minimizing this performance index leads generally to the optimal solution which coincides with the upper bounds on the reconfiguration parameters (an illustrating example is given in Section 4.2.5). The solution are found using Matlab optimization toolbox or NLopt package [101].

ENERGY CONSUMPTION

In **online reconfiguration**, we compute the minimal energy consumption that is needed to move the mobile platform along a given trajectory, neglecting friction between cables and pulleys or drums and between the mobile bases and the overhead bridge cranes (thus, also neglecting the energy needed to move the cable exit points):

$$E_{on}^{(s)} = \sum_{i=1}^m \tau_i^{(s)} \cdot \Delta l_i^{(s)} \quad (4.3)$$

where $\tau_i^{(s)}$ is the tension of the i -th cable (assuming that $\tau_i^{(s)} = const$ during the s -th sample time period) and $\Delta l_i^{(s)}$ is the incremental change of the i -th cable length.

To verify the results, the total energy consumption along a given trajectory of the mobile platform is computed as

$$E_{total} = \sum_{s=1}^{N_s-1} E_{on}^{(s)} \quad (4.4)$$

where N_s is the number of discrete via-points.

4.2.2 Step 1: Define Desired CDPR Performances

In practice, for a certain task, the prescribed CDPR workspace and desired performances should be defined beforehand as a set of:

- positions in Cartesian space
- orientations
- velocities

- accelerations
- wrenches

which verifies collision-free and wrench feasibility conditions.

The nonlinear constraints corresponding to $\mathbf{r} \in \mathbf{C}_r$ are defined by these desired performances.

4.2.3 Step 2: Formulate Two Optimization Sub-Problems

DETERMINE THE BOUNDS ON THE RECONFIGURATION PARAMETERS

The goal of this step is to find the lower bounds and upper bounds on the reconfiguration parameters by solving the following optimization problems:

$$\mathbf{r}_{\min} = \min\{\mathbf{r}\} \quad , \quad \mathbf{r}_{\max} = \max\{\mathbf{r}\} \quad (4.5)$$

subject to:

$$\mathbf{r} \in \mathbf{C}_r$$

This step is important since it eliminates the geometric constraints and tension based constraints, thus enabling the use of standard gradient-based optimization tools to solve the general problem (4.1) more effectively.

The method to solve this problem will be discussed later in more detail in Section 4.2.6.

BOX-CONSTRAINED OPTIMIZATION PROBLEM

Let us assume that the bounds on the reconfiguration parameters were found. Thereby, the general optimization problem (4.1) is transformed into a box-constrained optimization problem which is much simpler to solve:

$$\mathbf{r}_{opt} = \min\{f(r_1, r_2, \dots, r_p) \mid \mathbf{r} \in \mathbf{B}_r\} \quad (4.6)$$

where

$$\mathbf{B}_r = \{\mathbf{r} \mid \mathbf{r}_{\min} \leq \mathbf{r} \leq \mathbf{r}_{\max}\} \quad (4.7)$$

4.2.4 Step 3: Determining the CDPR Reconfiguration

OFFLINE RECONFIGURATION

The aim of offline reconfiguration is to find a set of reconfiguration parameters (locally) optimal with respect to a performance index over the assigned workspace and for given required performances. Let us take an example. Assume that one want the CDPR to reach any pose in a given workspace at any acceleration in a given range, while keeping the cable tensions within prescribed limits. Offline reconfiguration can consist in finding "the best" locations for the cable exit points allowing the CDPR to do so with minimal energy consumption.

To optimize the performance index with respect to the whole workspace, we discretize the latter into a finite set of N equilibrium poses. This procedure is time consuming if there are a lot of poses to be evaluated in the resulting finite set. In fact, it is generally satisfactory enough to evaluate the objective function at poses that lie on the boundary of the assigned workspace. Then, the global criterion method [102] is used to find the optimal reconfiguration according to the following steps.

- **Step 1:** Find the optimal configuration \mathbf{r}_k^* , $k = 1, 2, \dots, N$ for the k -th equilibrium pose by solving the box constrained optimization problem:

$$\mathbf{r}_k^* = \min\{f(\mathbf{r}) \mid \mathbf{r} \in \mathbf{B}_r\} \quad (4.8)$$

where \mathbf{B}_r is defined in (4.7) and f is the considered criterion. N is the total number of equilibrium poses considered in the given workspace.

- **Step 2:** Find the optimal configuration \mathbf{r}_{opt} of the following box-constrained optimization problem:

$$\text{Minimize } F(\mathbf{r}) = \frac{1}{N} \sum_{k=1}^N \left[\frac{f(\mathbf{r}_k^*) - f(\mathbf{r})}{f(\mathbf{r}_k^*)} \right]^2 \quad (4.9)$$

subject to $\mathbf{r} \in \mathbf{B}_r$

Offline reconfiguration as treated here is in fact a multi-objective optimization problem. A specificity of the problem at hand is that in usual multi-objective optimization there are more than one objective function to be evaluated at a specific pose whereas, in offline reconfiguration, there is only one objective function to be evaluated at many different poses. Furthermore, evaluating the objective function at a pose has the same priority as at any other pose which eliminates the difficulty of choosing suitable priority factors for each objective function as in the usual case of a multi-objective optimization.

ONLINE RECONFIGURATION

In online reconfiguration, we aim to find “the best” CDPR reconfigurations along a given trajectory. The locations of the cable exit points are updated at each sample time in such a way that minimizes a certain performance index.

Because of the real-time constraint, online reconfiguration should be treated as a single-objective optimization problem. At each sample time, we aim at solving the optimization problem in a few iterations. The number of iterations will be limited by the total computation time (normally, we could only allow 1, 2 or 3 iterations).

In online reconfiguration, the box constrained optimization problem (4.6) is defined as follows: At the $s - th$ sample time, find the new values of the reconfiguration parameters

$$\mathbf{r}_{opt}^{(s)} = \min\{f(r_1, r_2, \dots, r_p) \mid \mathbf{r} \in \mathbf{B}_\Delta\} \quad (4.10)$$

where

$$\mathbf{B}_\Delta = \{\mathbf{r} \mid \mathbf{r}_{opt}^{(s-1)} - \Delta_r \leq \mathbf{r} \leq \mathbf{r}_{opt}^{(s-1)} + \Delta_r\} \quad (4.11)$$

which also satisfies

$$\mathbf{B}_\Delta \subset \mathbf{B}_r \quad (4.12)$$

Δ_r is the maximum step size of the reconfiguration parameters allowed at each sample time.

One can initialize the procedure with a starting point taken as the optimal solution found from offline reconfiguration with respect to the same performance index since it reduces the probability of converging to a poor local minimum.

In online reconfiguration mode, two issues must be addressed carefully. Firstly, at each sample time, the new reconfiguration parameters $\mathbf{r}_{opt}^{(s)}$ must not exceed a certain value because of the limitations of the actuators that drive the cable exit points and the cable lengths:

$$|r_{iopt}^{(s)} - r_{iopt}^{(s-1)}| \leq \Delta_r, \quad i = \overline{1, p} \quad (4.13)$$

Secondly, the movement of the cable exit points and the changes of the cable lengths are coupled together. Because of these issues, the constraint (4.11) is added in order to help maintaining the synchronization in driving the cable exit points A_i and the cable lengths in the control system.

4.2.5 Case Study

Let us consider a situation where several CDPRs are working in a workshop. Each CDPR has to position a heavy platform in several areas which are shown in Fig. 4.2. In this situation, at each working cell, the positions of the two cranes are fixed. Support beams are used to sustain the lateral horizontal forces created by the cable tensions that tend to bring the two cranes together. The distance between the two cranes is constant and calculated with respect to the size of the working cell. It means that the number of active actuators which reconfigure the positions of the cable exit points is 4 (the 8 cable exit points are moved by pairs). After finishing its works in an area, the CDPR moves to the next area.

Assume that the CDPR is operating in a given working cell. The size of the CDPR is $22m \times 14m \times 6.4m$ ($l \times w \times h$). The distance between the two cable exit points within a pair mounted on an overhead bridge crane is $2m$. The mobile platform is a cube of size length $2m$ and weighting $2000kg$. Its center of mass C coincides with the origin of the local frame O_p (which means $d = \overrightarrow{O_p C} = 0$). The characteristics of the steel cables driving the mobile platform are:

- Young modulus $E = 120e + 09$ (Pa)
- Cross-section area $A_0 = 4.3937e - 05$ (m^2)
- Self-weight $w = 3.3955$ (N/m)

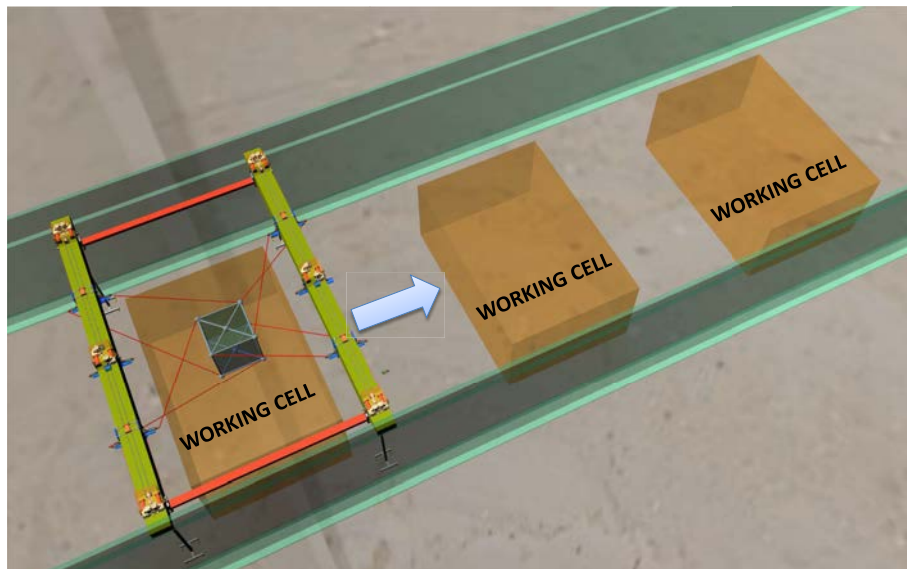


Figure 4.2: Example of a scenario in a workshop

The desired performances of the CDPR are given as:

$$\begin{aligned}
m_p &= 2000 \text{ (kg)} \\
-4 &\leq x_p \leq 4 \text{ (m)} \\
-5 &\leq y_p \leq 3 \text{ (m)} \\
0 &\leq z_p \leq 2.5 \text{ (m)} \\
\theta_x &= \text{const} = 0 \text{ (deg)} \\
-5 &\leq \theta_y \leq 0 \text{ (deg)} \\
0 &\leq \theta_z \leq 70 \text{ (deg)} \\
-0.7 &\leq a_{x,y,z} \leq 0.7 \text{ (m/s}^2\text{)} \\
-0.7 &\leq \alpha_{x,y,z} \leq 0.7 \text{ (rad/s}^2\text{)} \\
100 &\leq \tau \leq 3.1e+04 \text{ (N)}
\end{aligned}$$

The considered discretization in *position, orientation, accelerations, and angular accelerations* results in total of $18 \times 8 \times 8 \times 8 = 9216$ CDPR states to be checked to verify the cable tension constraints and collision constraints.

OFFLINE RECONFIGURATION

Fig. 4.3 shows the results of finding the bounds on the reconfiguration parameters $\mathbf{r} = (r_1, r_2, r_3, r_4)$. The equilibrium poses are selected on the edges of the assigned workspace as also shown in Fig. 4.3.

The solution of minimizing the sum of cable tensions with respect to the given workspace coincides with the upper bounds on the reconfiguration parameters:

$$\mathbf{r}_{opt} \equiv \mathbf{r}_{max} = (r_{1max}, r_{2max}, r_{3max}, r_{4max}) \quad (4.14)$$

ONLINE RECONFIGURATION

In this case, we only present the results assuming that the robot system performs under ideal conditions (e.g. without loss due to friction, perfect synchronization in the control system while updating online the cable lengths and the cable exit point positions). The starting point for online reconfiguration is \mathbf{r}_{opt} given in (4.14). The objective is to minimize the energy consumption along a trajectory. The maximum step size of the reconfiguration parameters allowed at each iteration is $\Delta_r = 0.005m$.

Smoothed trapezoidal velocity method [99] was used to generate the desired trajectory. The via-points are given in Cartesian workspace and orientation workspace (ZYX Euler angle convention) $X = (x \ y \ z, \ \theta_x \ \theta_y \ \theta_z)$ (m, deg):

$$X_1 = (-4.0 \ 1.0 \ 0.0, \ 0 \ 0 \ 0)$$

$$X_2 = (1.0 \ -5.0 \ 2.0, \ 0 \ -5 \ 30)$$

$$X_3 = (0.0 \ -2.0 \ 2.5, \ 0 \ -5 \ 70)$$

$$X_4 = (4.0 \ 3.0 \ 0.5, \ 0 \ 0 \ 0)$$

The maximum accelerations and orientation accelerations along the trajectory are $\mathbf{a}_{\max x,y,z} = (0.7 \ 0.7 \ 0.7) \ (m/s^2)$ and $\boldsymbol{\alpha}_{\max x,y,z} = (0.7 \ 0.7 \ 0.7) \ (rad/s^2)$. The time corresponding to the maximum velocity is $t_{v\max} = 0.5s$ and the sample time is $dt = 0.01s$. Fig. 4.4 shows the trajectory generated. The evolution of the reconfiguration parameters and of the energy consumptions (4.3) along the trajectory are shown in Fig. 4.5. E_{OffM} is the minimal energy consumption of the CDPR in configuration $\mathbf{r} = \mathbf{r}_{\min} = (r_{1\min}, r_{2\min}, r_{3\min}, r_{4\min})$, $E_{Offline}$ is the minimal energy consumption of the CDPR in configuration \mathbf{r}_{opt} given in (4.14) and E_{Online} is the minimal energy consumption for reconfiguration parameters updated online along the trajectory. The total

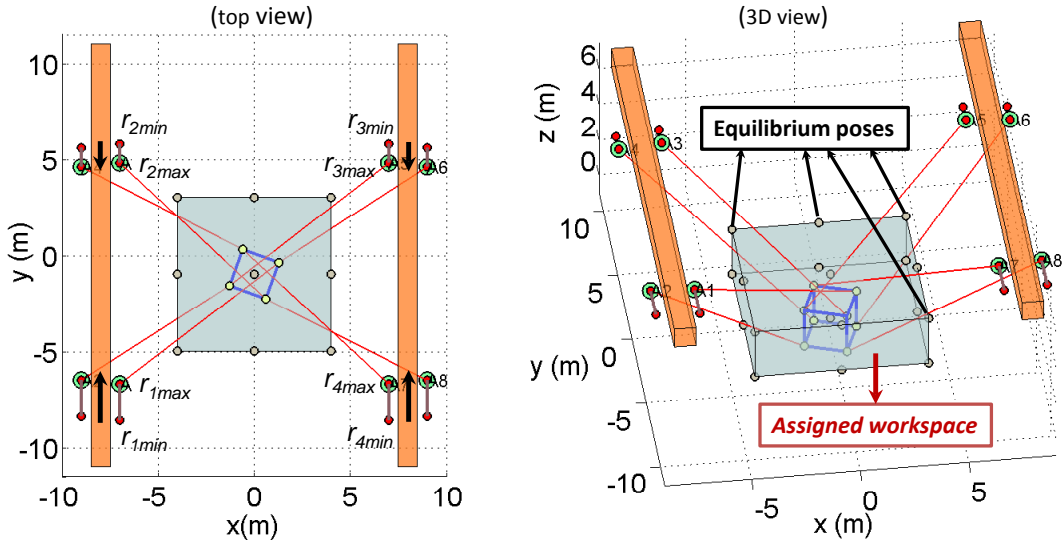


Figure 4.3: Bounds on reconfiguration parameters and desired Cartesian workspace

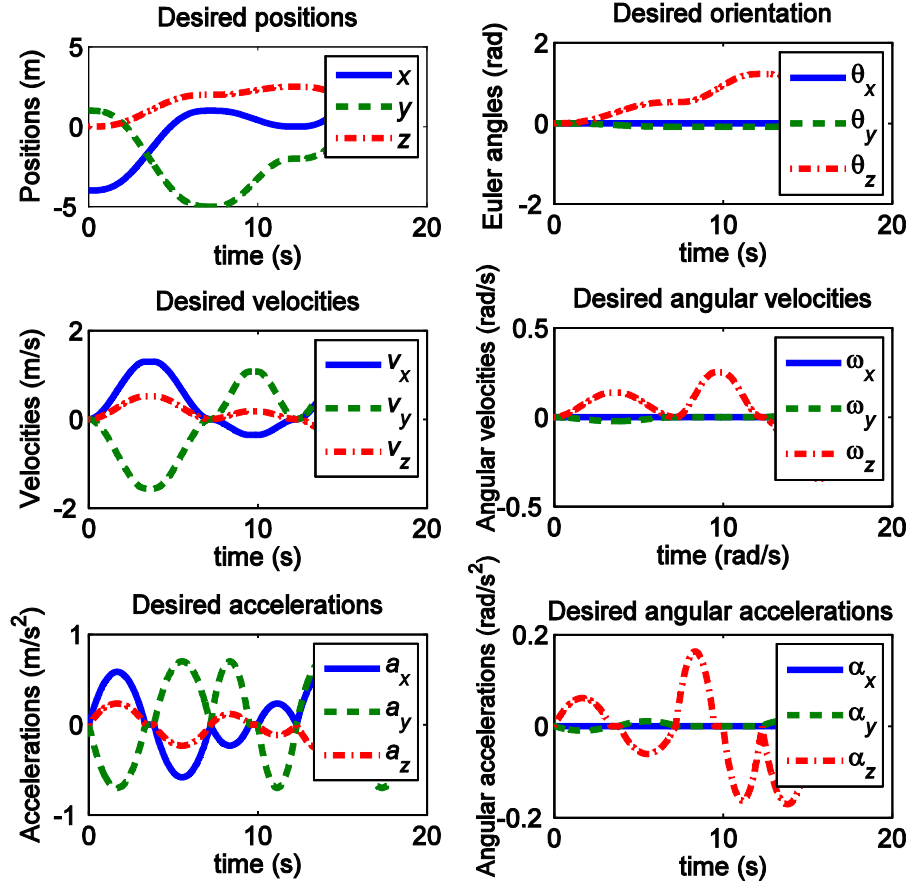


Figure 4.4: Desired trajectory

energy consumption (4.4) in the three cases is computed as:

$$E_{\Sigma OffM} = 4.5556e + 05 \text{ (J)}$$

$$E_{\Sigma Offline} = 3.8618e + 05 \text{ (J)}$$

$$E_{\Sigma Online} = 3.7955e + 05 \text{ (J)}$$

The energy saving between offline configuration at \mathbf{r}_{opt} and \mathbf{r}_{min} is 15.23%. When switching to online reconfiguration, the energy saving is 1.7187%. These results show that offline reconfiguration may provide a good solution in term of minimizing energy consumption. Under the ideal conditions considered in this case (no friction, etc.), online reconfiguration mode also reduces the total energy consumption of the CDPRE but only slightly compared to offline mode.

Note that the optimization tool LBFGS [103] in the nonlinear optimization package [101] was used to solve the boxed constrained optimization problems (4.6) - (4.7) in offline and online reconfiguration modes since this method is fast and provides stable results.

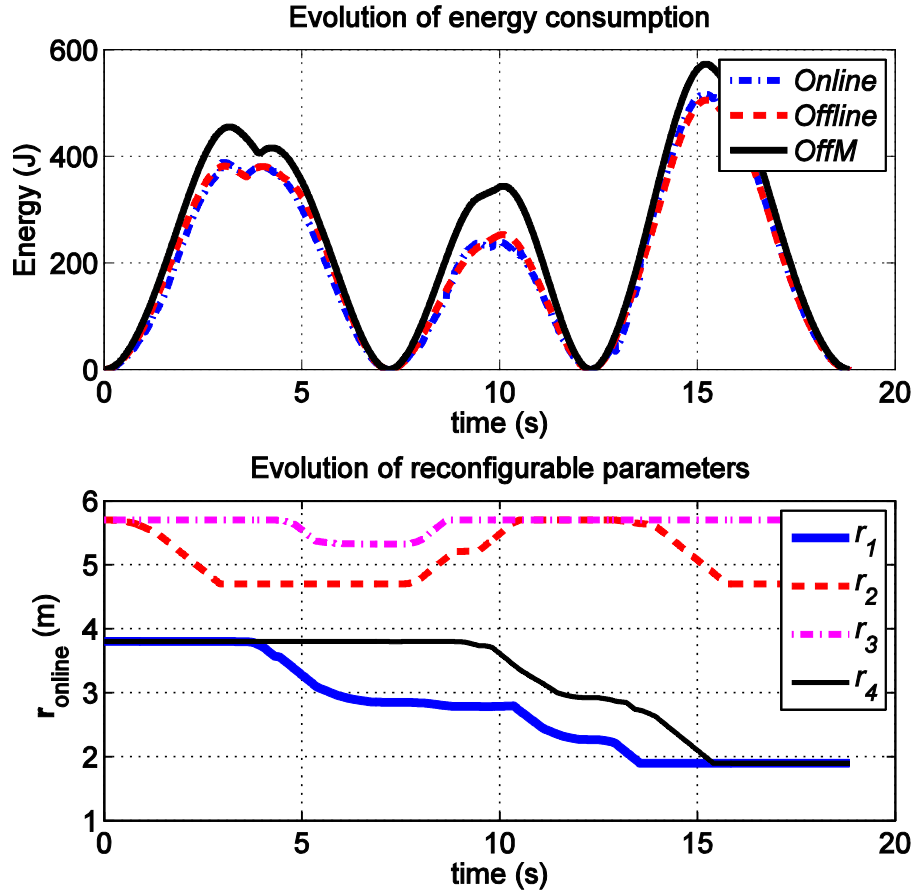


Figure 4.5: Results of online reconfiguration

4.2.6 Remark on the Methodology

In our study, we used a heuristic method to speed up the computation of the upper bounds on the reconfiguration parameters in problem (4.5). This method takes advantage of the particular characteristics of the reconfigurable CDPR family considered here. We may clarify this point as follows.

First of all, let us emphasize that:

- The cable exit points that reconfigure the CDPR cable exit points are constrained to move along the overhead bridge cranes, i.e., along only one direction.
- The considered CDPRs are suspended (all cable exit points are located above the mobile platform).

Hence, by minimizing the sum of the cable tensions, the cable exit points will tend to move to the positions where the cables are as vertical as possible while balancing the mobile platform weight. This behavior implies the fact that the optimal solution found in offline

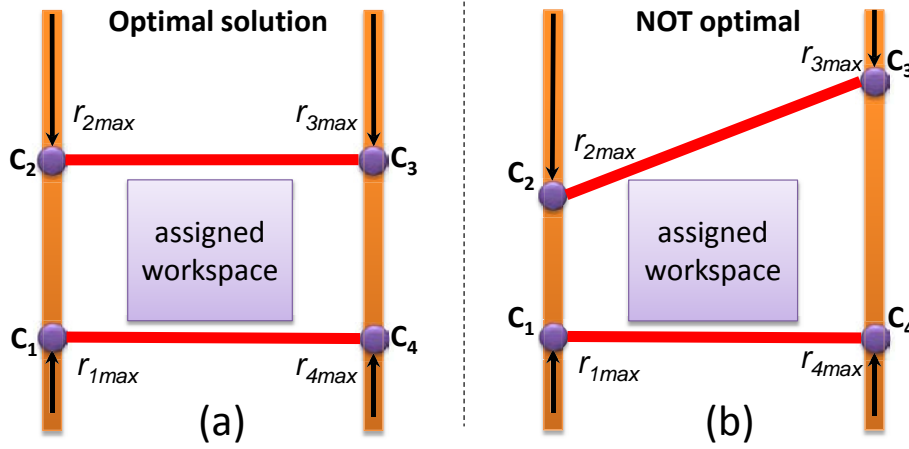


Figure 4.6: Solution for the upper bounds on the reconfiguration parameters

reconfiguration should coincide with the upper bounds on the reconfiguration parameters as shown in Fig. 4.3.

Knowing that fact beforehand, we solve the problem (4.5) as follows. We are looking for the solution that gives the minimum sum of cable tensions, which also means finding the maximum value of the upper bound vector \mathbf{r}_{\max} . Fig. 4.6a shows the optimal solution, whereas Fig. 4.6b shows a solution for the upper bound vector where we try to increase the value of $r_{2\max}$ which results in reducing the values of $r_{3\max}$ substantially. It is due to the fact that, in order to satisfy the conditions of wrench feasibility and the geometric constraints, the span of the cable exit points (the polygon $C_1C_2C_3C_4$) should cover the assigned workspace (the rectangle box). The changes in $r_{2\max}$ and $r_{3\max}$ shown in Fig. 4.6b result in increasing the value of the sum of cable tensions. Therefore, updating the values of the pairs of reconfiguration parameters (r_1, r_4) and (r_2, r_3) along the directions that keep the line C_1C_4 and C_2C_3 orthogonal to the overhead bridge cranes should lead us to the optimal solution. This heuristic helps a lot to reduce the computation time needed to solve the optimization sub-problem (4.5). In fact, in the examples shown in Section 4.2.5, while solving problem (4.5), we set the maximum displacement of updating the reconfiguration values in each iteration to $\Delta_r = 0.1 \text{ m}$. The time needed to find the sole upper bound vector \mathbf{r}_{\max} is around 2 min (which is quite fast). However, the total time needed to find the lower bound vector \mathbf{r}_{\min} (including checking all the constraints at all discretized poses) is around $40 - 50 \text{ min}$. In online reconfiguration, the time estimated for each iteration is around $30 - 40 \text{ ms}$. We use MATLAB on a PC with core $i7 - 2.7\text{GHz}$ to run the simulations.

4.3 CDPR Reconfiguration as a Multi-Objective Optimization Problem

In the previous section, we have discussed a systematic procedure to find optimal reconfigurations where the energy consumption of the reconfigurable CDPR (over a given workspace) is minimized. The reconfiguration of the CDPR is divided into two optimization sub-problems. The first one is a vector optimization problem [104] to find the bounds on the reconfiguration parameters where the nonlinear constraints include wrench feasibility constraints and non-differentiable constraints (cable interferences or geometric constraints). The general nonlinear optimization problem is then transformed into a single-objective box-constrained problem that can be solved with readily available gradient-based optimization tools [101]. This approach offers fast solution computations and can be used in both offline or online (real-time) CDPR reconfiguration. However, several issues have to be dealt with. Firstly, the vector optimization problem that aims at finding the bounds on the reconfiguration parameters is complicated. Although a heuristic approach was presented to solve it, the optimal solution greatly depends on specific use cases. Secondly, only one criterion was considered (the minimization of the energy consumption of the CDPR). In some cases, this solution may not be satisfactory enough.

In this section, we discuss the CDPR reconfiguration as a multi-objective optimization problem. The optimal reconfiguration of the robot is found by optimizing several performance indices. In this thesis, two performances indices are considered. To illustrate the proposed method, we study a use case where a CDPR carries workers in an airplane maintenance workshop. The general architecture of the CDPR is similar to the one in Fig. 4.1. The mobile platform is shown in Fig. 4.7. One drawback of this solution is that the CDPR is much more compliant than conventional telescopic platforms (which consist of rigid links). If only one performance index is used, for example, minimizing the power consumption of the CDPR as presented in the previous section, the mobile platform may become unstable at the optimal solution where all the cables tend to be as vertical as possible (like a pendulum). During operation, a strict condition is probably that the platform remains as stable as possible in order to allow the workers to work safely and efficiently. Hence, the optimal solution (found by minimizing the energy consumption) may violate this condition.

Therefore, in order to obtain appropriate CDPR reconfiguration solutions, we take into account two objectives. The first objective is to minimize the energy consumption while the second one is to maximize the stiffness of the CDPR at its mobile platform. The reconfiguration of the CDPR becomes a multi-objective (or vector) optimization problem

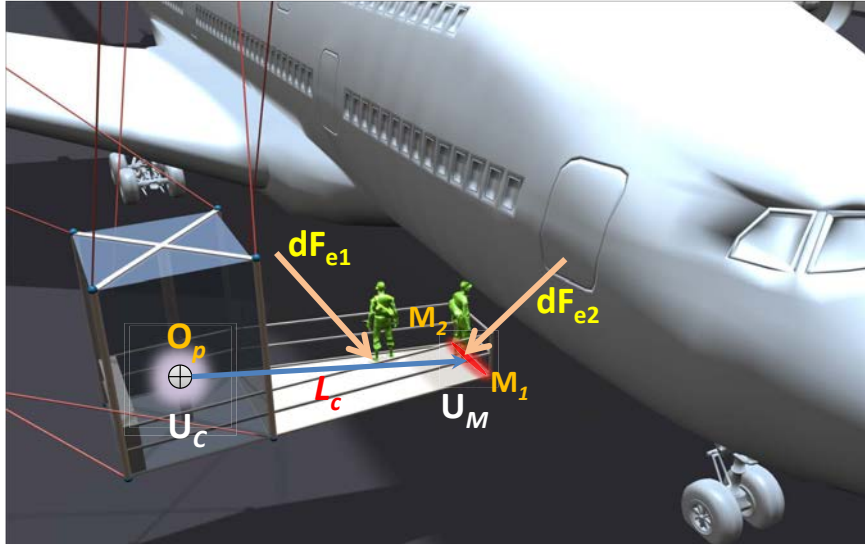


Figure 4.7: CDPR Mobile platform

with both continuous and non-differentiable nonlinear constraints. The optimal reconfiguration is a Pareto optimal point [105] among a set of possible solutions representing the tradeoff between the two considered criteria.

As the first objective function, we select the *sum of cable tensions* since this index is directly related to the energy consumption of the CDPR. As a second objective function, we introduce a new performance index which is the *normalized upper bound on the infinitesimal displacement of the mobile platform* as a means to quantify the stiffness of the CDPR. The derivation of this index is based on both the homogeneous CDPR stiffness matrix presented in [41] and the kinematic sensitivity analysis of very large-dimension CDPRs presented in [43].

Among other possible ones, there are two possible suitable optimization tools to determine the CDPR reconfiguration. If one considers the problem as a vector optimization problem, methods presented e.g. in [104] or in [106, 107] can be used to compute the Pareto front (the set of Pareto optimal solutions). However, these methods can deal efficiently with problems that have only linear constraints. Another possibility is to use efficient scalarization methods to govern all the criteria into one objective function and then use available optimization tools to solve this single-objective optimization problem. We choose the global criterion method and bounded objective function method (or ϵ -constrained method) [102] to scalarize multi-performance indices. In order to deal efficiently with the non-differentiable constraints (related to cable collisions), a derivative-free optimization tool can be used, e.g., direct search in MATLAB global optimization toolbox [107].

4.3.1 Performance Indices

SUM OF THE CABLE TENSIONS

Let us consider a CDPR driven by m cables in a configuration defined by the vector \mathbf{r} of the reconfiguration parameters. At an equilibrium pose of the mobile platform, by solving the tension distribution problem, we obtain desired cable tensions τ_i , $i = 1, 2, \dots, m$. One can compute the sum of the cable tensions at an equilibrium pose:

$$f_{\tau}(\mathbf{r}) = \sum_{i=1}^m \tau_i(\mathbf{r}) \quad (4.15)$$

To govern this criteria over a given workspace, we propose to discretized the assigned workspace into N equilibrium poses. In general, as in Section 4.2 it is enough to select N extreme points and several internal points in the workspace (e.g. divide the workspace into several boxes and only select the vertices and the center points of these boxes). The average sum of cable tensions with respect to a given workspace can be then computed as:

$$f_{\Sigma}(\mathbf{r}) = \frac{1}{N} \sum_{k=1}^N \sum_{i=1}^m \tau_{ik}(\mathbf{r}) \quad (4.16)$$

where τ_{ik} is the tension in cable i (at the end point B_i) at the equilibrium pose k .

Another way to formulate the performance index in this case is to use the global criteria method, similar to (4.9) in Section 4.2.4.

NORMALIZED UPPER BOUND ON THE INFINITESIMAL DISPLACEMENT VECTOR OF THE MOBILE PLATFORM

Let us consider again the CDPR shown in Fig. 2.4. In order to quantify the stiffness of the CDPR, a performance index meaningful to our application of interest is needed. In this work, among a set of reconfiguration solutions, the one which has the "smaller" infinitesimal displacement dX (with respect to any disturbance wrench $d\mathbf{f}_e$) is considered to lead to the highest stiffness. The disturbance wrench can be caused, e.g., by the workers on the platform (see in Fig. 4.7). From the relation:

$$\mathbf{K} \cdot dX = d\mathbf{f}_e \quad (4.17)$$

one can derive:

$$\sigma_{\min} = \frac{1}{\|\mathbf{K}^{-1}\|} \leq \frac{\|d\mathbf{f}_e\|}{\|dX\|} \leq \|\mathbf{K}\| = \sigma_{\max} \quad (\forall dX \neq \mathbf{0}) \quad (4.18)$$

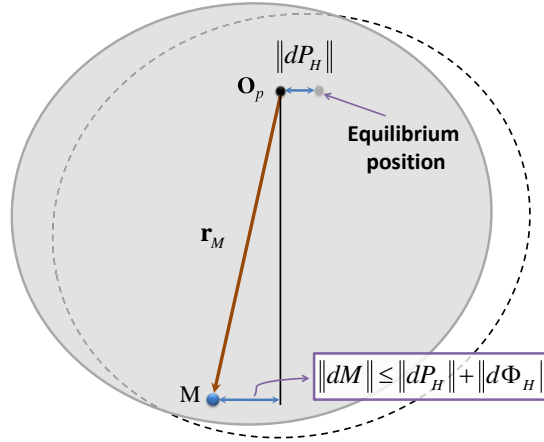


Figure 4.8: Displacements of O_p and M at the mobile platform of a CDPRE

where σ_{\min} and σ_{\max} are the minimum and maximum singular values of the stiffness matrix \mathbf{K} , and $\|\cdot\|$ denotes the 2-norm of a vector or a matrix.

In this sense, the stiffness of the CDPRE can be quantified by the singular values of the stiffness matrix (specifically σ_{\min} and σ_{\max}) regardless of the magnitude or direction of the infinitesimal wrench $d\mathbf{f}_e$. However, the term $\|d\mathbf{f}_e\|$ and $\|dX\|$ become meaningful only if $d\mathbf{f}_e$ and dX are homogeneous.

Suppose that from an equilibrium pose, a small disturbance force dF_e is applied on the mobile platform at a point M . This force creates an infinitesimal wrench at O_p , $d\mathbf{f}_e = (dF_e, \mathbf{r}_M \times dF_e)$ ($\mathbf{r}_M = \overrightarrow{O_p M}$). From (4.17), one can derive:

$$\mathbf{K}_H \cdot dX_H = d\mathbf{f}_{eH} \quad (4.19)$$

where

$$\mathbf{S}_H = \begin{bmatrix} \mathbf{1}_{3 \times 3} & \mathbf{0}_{3 \times 3} \\ \mathbf{0}_{3 \times 3} & \|\mathbf{r}_M\| \cdot \mathbf{1}_{3 \times 3} \end{bmatrix}$$

$$d\mathbf{f}_{eH} = \begin{bmatrix} dF_e \\ \mathbf{u}_M \times dF_e \end{bmatrix}$$

$$dX_H = \mathbf{S}_H \cdot dX \quad (4.20)$$

$$\mathbf{K}_H = \mathbf{S}_H^{-1} \cdot \mathbf{K} \cdot \mathbf{S}_H^{-1} \quad (4.21)$$

and \mathbf{u}_M is the unit vector $\frac{\mathbf{r}_M}{\|\mathbf{r}_M\|}$.

In (4.19), the terms dX_H and $d\mathbf{f}_{e_H}$ are homogeneous (the units are meters and Newtons, respectively). The matrix \mathbf{S}_H transforms the stiffness matrix \mathbf{K} into its homogeneous form \mathbf{K}_H . The characteristic length used in this transformation is $L_c = \|\mathbf{r}_M\|$.

Obviously, the choice of the characteristic length L_c plays an important role in providing a useful physical meaning for \mathbf{K}_H . The matrix \mathbf{K} can be considered homogeneous with the trivial characteristic length $L_c = \|\mathbf{r}_M\| = 1$ (m). One can then “safely” take the 2-norm of the infinitesimal displacement vector dX . However, even if dX_H (or dX) is homogeneous, its components $dP_H (= dO_p)$ and $d\Phi_H (= \|\mathbf{r}_M\| \cdot d\Phi)$ still represent different quantities (position and orientation). Taking the norm of the two terms together in $\|dX_H\|$ and utilize (4.18) may not be really meaningful. We shall give an interpretation for dP_H and $d\Phi_H$ as follows.

Let us consider the simple example shown in Figure 4.8. An infinitesimal wrench $d\mathbf{f}_e$ applied on the mobile platform at point M creates an infinitesimal displacement $dX_H = (dP_H, d\Phi_H)$. Let us consider the infinitesimal changes in the positions of points O_p and M under the action of $d\mathbf{f}_e$. One can write:

$$\begin{aligned}
 M &= O_p + (M - O_p) = O_p + \mathbf{r}_M \\
 \Rightarrow \|dM\| &= \|dO_p + d\Phi \times \mathbf{r}_M\| \\
 \Rightarrow \|dM\| &\leq \|dO_p\| + \|d\Phi\| \cdot \|\mathbf{r}_M\| \\
 &= \|dP_H\| + \|d\Phi_H\|
 \end{aligned} \tag{4.22}$$

The magnitude of the displacement at O_p is $\|dP_H\|$ whereas the magnitude of the displacement at M (with respect to the local mobile platform frame) is bounded by $\|d\Phi_H\|$.

With this interpretation of the homogeneous infinitesimal displacement vector dX_H , we propose to quantify separately the two terms dP_H and $d\Phi_H$. From (4.19), we can write:

$$\begin{aligned}
 dX_H &= \mathbf{K}_H^{-1} \cdot d\mathbf{f}_{e_H} \\
 \Rightarrow \begin{cases} dP_H = \mathbf{C}_P \cdot d\mathbf{f}_{e_H} \\ d\Phi_H = \mathbf{C}_\Phi \cdot d\mathbf{f}_{e_H} \end{cases}
 \end{aligned} \tag{4.23}$$

where $\mathbf{K}_H^{-1} = [\mathbf{C}_P^T, \mathbf{C}_\Phi^T]^T$.

From (4.22) and (4.23), we have:

$$\frac{\|dP_H\|}{\|d\mathbf{f}_{e_H}\|} \leq \|\mathbf{C}_P\| = \sigma_{P\max} \quad (4.24)$$

$$\frac{\|d\Phi_H\|}{\|d\mathbf{f}_{e_H}\|} \leq \|\mathbf{C}_\Phi\| = \sigma_{\Phi\max} \quad (4.25)$$

$$\Rightarrow \frac{\|dM\|}{\|d\mathbf{f}_{e_H}\|} \leq \sigma_M = \sigma_{P\max} + \sigma_{\Phi\max} \quad (4.26)$$

where $\sigma_{P\max}$ and $\sigma_{\Phi\max}$ are the maximum singular values of the matrices \mathbf{C}_P and \mathbf{C}_Φ , respectively.

The term σ_M is *the normalized upper bound on the infinitesimal displacement of the mobile platform* and can be used as a means to quantify the stiffness of the CDPR.

To govern this performance index over a given workspace (discretized into N equilibrium poses), we propose to compute the maximum value of σ_{Mk} ($k = \overline{1, N}$):

$$\sigma_M(\mathbf{r}) = \max_{1 \leq k \leq N} \{\sigma_{Mk}(\mathbf{r})\} \quad (4.27)$$

where σ_{Mk} is the normalized upper bound on the infinitesimal displacement of the mobile platform at the equilibrium pose k .

By minimizing $\sigma_M(\mathbf{r})$, one can obtain an optimal reconfiguration solution where the potential displacement of the mobile platform at the point M over a given workspace is minimized.

Note that we use the “max-norm” in this case as a fast means to compute the performance index. An alternative way (which is much more time-consuming but more reliable) is using the global criterion method to govern the criterion over the given workspace, similar to (4.9) in Section 4.2.4.

4.3.2 Scalarization of the Performance Indices

Suppose that f_Σ^* is the optimal value obtained by minimizing $f_\Sigma(\mathbf{r})$ in (4.16) (independently of minimizing $\sigma_M(\mathbf{r})$ in (4.27)) and σ_M^* is the optimal value obtained by minimizing $\sigma_M(\mathbf{r})$ in (4.27).

SCALARIZATION USING THE GLOBAL CRITERION METHOD

When the two performance indices have the same priority, we propose to use the global criterion method [102]. The reconfiguration can be classically formulated as a single-

objective optimization problem as follows:

$$\mathbf{minimize} \ f(\mathbf{r}) = [(1 - \delta_\Sigma)^s + (1 - \delta_M)^s]^{1/s} \quad (4.28)$$

subject to:

$$\begin{aligned} \mathbf{r}_{\min} &\leq \mathbf{r} \leq \mathbf{r}_{\max} \\ \mathbf{r} &\in \mathbf{C}_r \end{aligned}$$

where

$$\delta_\Sigma = \frac{f_\Sigma(\mathbf{r})}{f_\Sigma^*}, \quad \delta_M = \frac{\sigma_M(\mathbf{r})}{\sigma_M^*} \quad (4.29)$$

and \mathbf{r}_{\min} and \mathbf{r}_{\max} are the lower and upper bounds on the reconfiguration parameters. \mathbf{C}_r is the set of reconfiguration parameters that satisfy all nonlinear constraints including geometric constraints and wrench feasibility constraints. s is a normalized factor (usually one chooses $s = 2$).

In this way, the tradeoff between the two criteria is managed “automatically”.

SCALARIZATION USING THE BOUNDED OBJECTIVE FUNCTION METHOD

When the two performance indices have different priorities, we propose to use the bounded objective function method [102] to scalarize the two criteria. One criterion is kept as the objective function while the other criterion is transformed into a nonlinear constraint. For example, assume that there is a strict constraint set upon the energy consumption of the CDPR. Then, we can convert $f_\Sigma(\mathbf{r})$ into a nonlinear constraint and keep $\sigma_M(\mathbf{r})$ as the objective function. The reconfiguration problem in this case becomes:

$$\mathbf{minimize} \ \sigma_M(\mathbf{r}) \quad (4.30)$$

subject to:

$$\begin{aligned} \mathbf{r}_{\min} &\leq \mathbf{r} \leq \mathbf{r}_{\max} \\ \mathbf{r} &\in \mathbf{C}_r \\ \delta_\Sigma(\mathbf{r}) &\leq \delta \end{aligned}$$

where δ is a given value.

In this way, the tradeoff between the two criteria is managed by the term δ .

4.3.3 Systematic Procedure to Solve a Reconfiguration Problem

The procedure to find optimal CDPR reconfigurations while optimizing the two objective functions is given in the following steps.

- **Step 1:** Assign desired CDPR performances including Cartesian workspace and orientation ranges of the mobile platform and bounds on cable tensions (nonlinear constraints $\mathbf{r} \in \mathbf{C}_r$). Set the limitations of the actuators that drive the cable exit points and the two overhead bridge cranes (linear constraints).
- **Step 2:** Determine the CDPR reconfiguration parameters. The choice of the reconfiguration parameters depends on the use cases.
- **Step 3:** Determine the characteristic length L_c (which transforms the stiffness matrix into its homogeneous form) in order to compute the index σ_M in (4.27).
- **Step 4a:** Find the optimal value f_Σ^* by solving the single-objective optimization problem:

$$\mathbf{minimize} \ f_\Sigma(\mathbf{r}) = \frac{1}{N} \sum_{k=1}^N \sum_{i=1}^m \tau_{ik}(\mathbf{r}) \quad (4.31)$$

subject to:

$$\begin{aligned} \mathbf{r}_{\min} &\leq \mathbf{r} \leq \mathbf{r}_{\max} \\ \mathbf{r} &\in \mathbf{C}_r \end{aligned}$$

- **Step 4b:** Find the optimal value σ_M^* by solving the single-objective optimization problem:

$$\mathbf{minimize} \ \sigma_M(\mathbf{r}) = \max_{1 \leq k \leq N} \{\sigma_{Mk}(\mathbf{r})\} \quad (4.32)$$

subject to:

$$\begin{aligned} \mathbf{r}_{\min} &\leq \mathbf{r} \leq \mathbf{r}_{\max} \\ \mathbf{r} &\in \mathbf{C}_r \end{aligned}$$

- **Step 5a:** If the two performance indices have the same priority, solve the optimization problem (4.28) to find the Pareto optimal reconfiguration solution for the CDPR.
- **Step 5b:** If the priorities of the two performance indices are different, solve the optimization problem (4.30) to find the Pareto optimal reconfiguration solution for the CDPR. The additional nonlinear constraint (e.g., $\delta_\Sigma(\mathbf{r}) \leq \delta$) should be formulated using the relative ratios given in (4.29). In case $f_\Sigma(\mathbf{r})$ is chosen as the objective function, step 4a can be removed. In case $\sigma_M(\mathbf{r})$ is chosen as the objective function, step 4b can be removed.

Note that the nonlinear constraints $\mathbf{r} \in \mathbf{C}_r$ can be reformulated into a standard form as follows:

$$g(\mathbf{r}) = 0.5 - 1.0 * h(\mathbf{r}) \leq 0 \quad (4.33)$$

where

$$h(\mathbf{r}) = \begin{cases} 1, & \text{if } \mathbf{r} \in \mathbf{C}_r \\ 0, & \text{if } \mathbf{r} \notin \mathbf{C}_r \end{cases} \quad (4.34)$$

Here, $h(\mathbf{r})$ consists of routines that verify geometric constraints (collision detections) and wrench feasibility constraints.

4.3.4 Case Study

Let us consider the application of using large-dimension reconfigurable suspended CDPR to replace gantry nacelles in an airplane maintenance workshop, e.g., for the Airbus A380 family (Fig. 4.9). One can use 4 CDPRs to cover the workshop divided into four sections across the airplane as shown in Fig. 4.9. The desired typical trajectory of the mobile platform is to move along the airplane fuselage or along the two wings while carrying 2-3 workers to perform certain maintenance tasks. We will consider the example of one CDPR working in one section of the workshop.

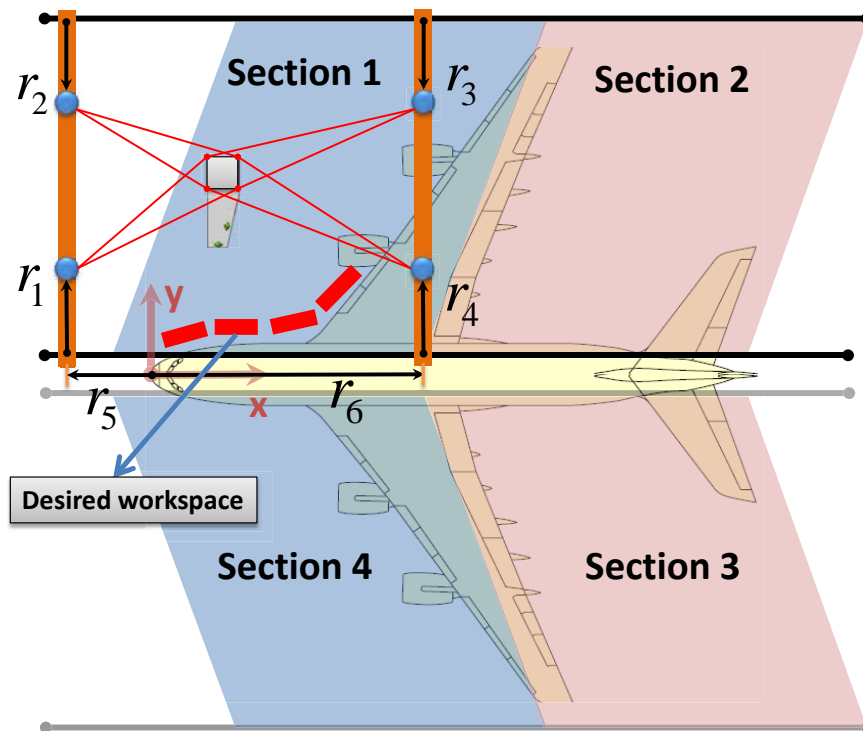


Figure 4.9: Using CDPRs to replace gantry nacelles in an airplane workshop

STEP 1: ASSIGN DESIRED CDPR PERFORMANCES

In this application, the desired Cartesian workspace consists mainly of the closed area along the airplane fuselage and its wings as shown in Fig. 4.9. This workspace can be divided into several parts in each of which the mobile platform moves with a constant orientation. We will consider one part of the workspace as shown in Fig. 4.10. Each bridge crane is of 40 m in length and 28 m in height. The distance between the two cable exit points within a pair mounted on an overhead bridge crane is 2 m. The mobile platform is shown in Fig. 4.7. Its working area (for the workers) is 4.4 m long. The mobile platform weighs 3000 kg and can carry up to 2-3 persons (total mass of 200 kg). Steel cables are used with Young's modulus $E = 120e + 09 Pa$, cross-section area $A_0 = 4.4375e - 05 m^2$ and self-weight $w = 3.3955 N/m$. The desired CDPR performances are given as (only quasi-static analysis is considered, the dynamics of the mobile platform was ignored):

$$\begin{aligned} 3000 &\leq m_p \leq 3200 \text{ (kg)} \\ 10.0 &\leq x_p \leq 20.0 \text{ (m)} \\ 6.5 &\leq y_p \leq 9.0 \text{ (m)} \\ 1.4 &\leq z_p \leq 8.8 \text{ (m)} \\ \theta_x &= \theta_y = \theta_z = 0 \text{ (deg)} \\ 100 &\leq \tau_i \leq 3.104e + 04 \text{ (N)} \end{aligned}$$

where m_p is the total carried mass (CDPR mobile platform and workers), (x_p, y_p, z_p) is the Cartesian position of the origin O_p of the mobile platform frame and τ_i is the tension in cable i at the end point B_i .

This Cartesian workspace is discretized into $N = 18$ equilibrium poses. The bounds $[r_{i\min}, r_{i\max}]$ on the parameter r_i are given in such a way that the assigned workspace lies within the span of the polygon $C_1C_2C_3C_4$:

$$\begin{aligned} 0 &\leq r_{1,4} \leq 4.5 \text{ (m)} \\ 0 &\leq r_{2,3} \leq 31 \text{ (m)} \\ -10 &\leq r_5 \leq 9 \text{ (m)} \\ 21 &\leq r_6 \leq 40 \text{ (m)} \end{aligned}$$

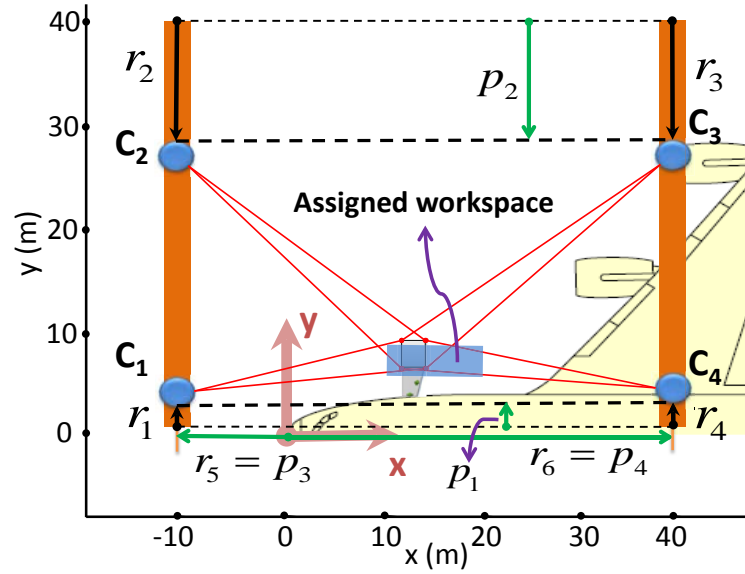


Figure 4.10: Reconfiguration parameters

STEP 2: DETERMINATION OF THE RECONFIGURATION PARAMETERS

There are a maximum of 6 parameters to configure the cable exit points A_i of the reconfigurable CDPR considered in this thesis (Fig. 4.1). Here, we consider only one use case where the number of reconfiguration parameters is $n_r = 4$. Fig. 4.10 shows the reconfiguration parameters p_1 , p_2 , p_3 and p_4 . Two pairs of cable exit points $C_1 (A_1, A_2)$ and $C_4 (A_7, A_8)$ are reconfigured by p_1 ($r_{1,4} = p_1$), while $C_2 (A_3, A_4)$ and $C_3 (A_5, A_6)$ are reconfigured by p_2 ($r_{2,3} = p_2$). The reconfiguration parameters p_3 and p_4 determine the positions of the two overhead bridges ($r_5 = p_3$, $r_6 = p_4$).

Note that after each update of p_i , a normalization of the parameters r_i is needed:

$$r_i = \min(\max(r_i, r_{i\min}), r_{i\max}) \quad (i = \overline{1,6}) \quad (4.35)$$

The corresponding bounds on the reconfiguration parameters p_i can be determined by using (4.35).

STEP 3: DETERMINATION OF THE CHARACTERISTIC LENGTH L_c

It can be seen that the homogeneous stiffness matrix \mathbf{K}_H of a CDPR presented in Section 4.3.1 depends greatly on the choices of:

- The position of the origin O_p of the local frame attached to the mobile platform.
- The characteristic length L_c (or the choice of point M to be analyzed).

We propose to choose O_p as the center of mass C of the mobile platform. In this case, because of the uncertainties on the position of C (due for example to the workers moving on the mobile platform), C falls into a set of possible points \mathbf{U}_C (Fig. 4.7), thus O_p (and also the center of mass C) is chosen as the center point of \mathbf{U}_C .

To choose L_c , we propose first to define an area of interest \mathbf{U}_M of point M which consists of the most unstable standing positions for the workers. \mathbf{U}_M can be chosen as the nearest edge of the mobile platform to the airplane fuselage (the line segment M_1M_2). Then, L_c is computed as the average distance from O_p to the points in \mathbf{U}_M as follows:

$$L_c = \int_0^1 \|M_1 + (M_2 - M_1) \cdot t\| dt \quad (4.36)$$

Here, M_1 and M_2 are expressed in the local mobile platform frame.

By solving (4.36) we obtain $L_c = 5.89021 m$.

STEPS 4 AND 5: SOLVING THE CDPR RECONFIGURATION PROBLEM

We used the pattern search algorithm in MATLAB global optimization toolbox [107] to solve the optimization problems defined in steps 4a, 4b, 5a and 5b (section 4.3.3). This method handles optimization problems with nonlinear, linear, and bound constraints, and does not require functions to be differentiable or continuous.

The mobile platform weight is 3200 *kg* (fully loaded). We only consider static equilibrium poses of the CDPR while neglecting the dynamics of the mobile platform, cables and overhead bridge cranes. In step 5b, $\sigma_M(\mathbf{r})$ is chosen as the objective function with the additional constraint $\delta_\Sigma(\mathbf{r}) \leq \delta = 1.1$. It means that the energy consumption is constrained to be less than 110% of the optimal value ($f_\Sigma(\mathbf{r}) \leq 1.1 f_\Sigma^*$).

In step 4a, we set the initial value \mathbf{r}_{init} (or \mathbf{p}_{init}) of the reconfiguration parameters in the optimization problem as the extreme values ($r_{i\max}$ or $r_{i\min}$) where the locations of the cable exit points A_i are closest to the assigned workspace [108]. In the following steps (4b, 5a, 5b) \mathbf{r}_{init} is chosen as the optimal configuration found from step 4a.

Fig. 4.11 shows the optimal reconfiguration solutions in the four steps. It is interesting to note that, in the reconfiguration solution which minimizes the sum of cable tensions, the cables tend to be as vertical as possible (Fig. 4.11a) [108]. On the contrary, by minimizing the normalized upper bound on the infinitesimal displacement index, we obtain optimal solutions where the cables tend to become horizontal (Fig. 4.11b). This fact emphasizes the reason why we considered the CDPR reconfiguration as a multi-objective optimization problem.

Table 4.1: Results obtained by solving the different optimization problems

Steps	$[p_1, p_2, p_3, p_4]$ (m)	f_Σ (N)	σ_M (m/N)	f	δ_Σ	δ_M
Step 4a	[2.20, 28.50, 6.75, 22.95]	$3.6271e+04$	$5.8890e-04$	11.4263	1.0	12.4263
Step 4b	[0, 15.80, 1.25, 34.62]	$4.5953e+04$	$4.7391e-05$	0.2669	1.2669	1.0
Step 5a	[0, 19.44, 3.38, 28.78]	$4.1947e+04$	$5.1384e-05$	0.1777	1.1564	1.0843
Step 5b	[1.97, 23.54, 4.77, 28.07]	$3.9641e+04$	$6.8734e-05$	0.4598	1.0929	1.4503

To illustrate the tradeoff between the two criteria in the four cases, we compute their values and their relative ratios given in (4.29). The results are shown in Table 4.1 (here, f is the objective function defined in (4.28)). In step 5a, the values of δ_Σ and δ_M are quite close to 1 since we assign equal priorities for the two criteria. Meanwhile, in step 5b, although we obtain a relatively large value of δ_M (because of the constraint set upon δ_Σ), this value is still much smaller than the value obtained in step 4a.

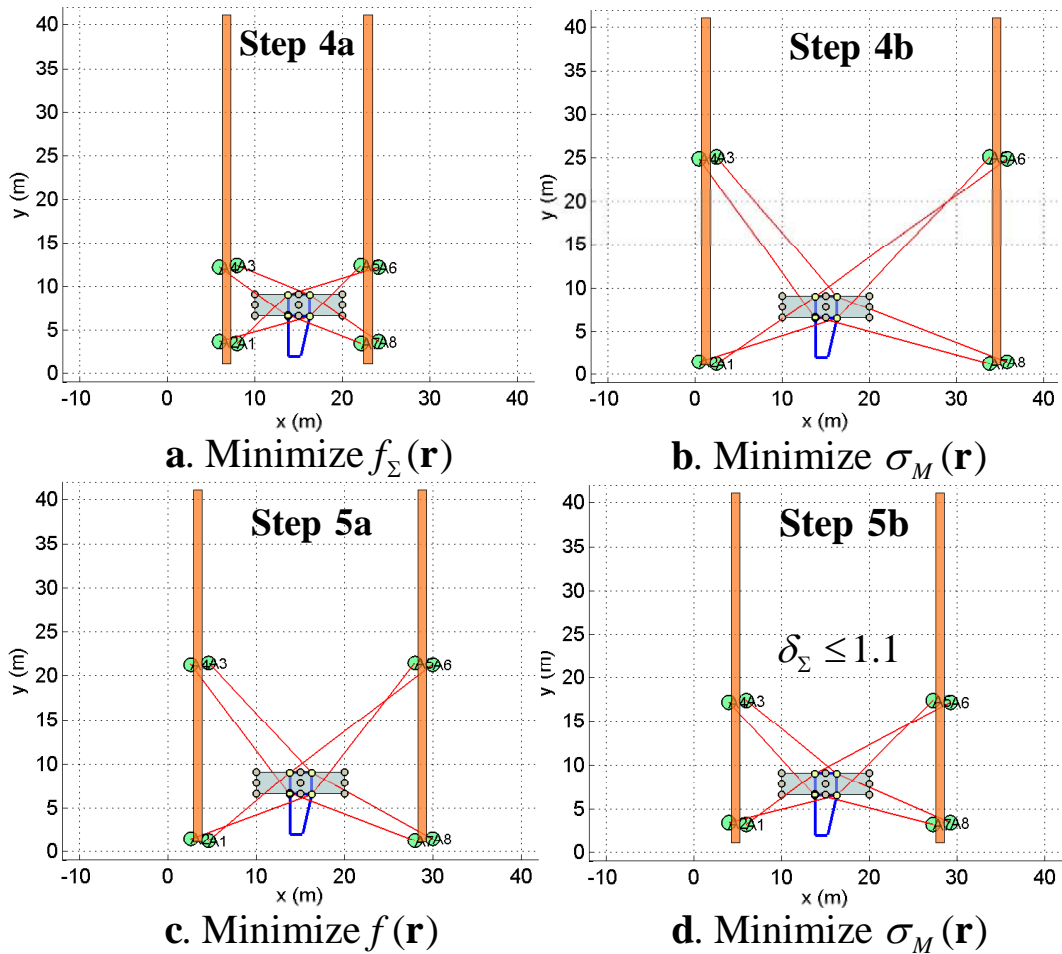


Figure 4.11: Reconfiguration solutions in case $n_r = 4$

Conclusion

This chapter discussed the CDPR reconfiguration problem. A family of large-dimension reconfigurable suspended CDPRs was considered. In a first study, the CDPR configuration problem is considered as a single-objective optimization problem. By transforming the general complex problem into more simple optimization sub-problems, one can take advantage of readily available tools to determine an optimal solution. As a benefit of using gradient-based optimization tools, real-time reconfiguration planning (online reconfiguration) of a CDPR could be achieved. In situations where there is no reliable method to handle difficult issues in online reconfiguration, offline reconfiguration offers a more reliable choice. Furthermore, the presented method to determine offline reconfigurations can be applied to specific cases such as finding the optimal solution for a given trajectory.

In a second study, the optimal reconfigurations of the considered CDPR family are found by solving a multi-objective optimization problem. A systematic procedure to determine the CDPR reconfiguration was presented and illustrated by a case study. It offers the end-users a set of possible solutions where the tradeoffs between the criteria are explicitly taken into consideration.

Although the use of derivative-free algorithms to solve the CDPR reconfiguration may be time consuming (compared to gradient-based methods), one could effectively handle non-differentiable nonlinear constraints (geometric constraints), and thus obtain more reliable solutions.

The approaches presented in this chapter could be extended to solve reconfiguration problems of other families of reconfigurable CDPRs.

CONCLUSION

In this thesis, we have developed a fundamental framework for reconfigurable cable-driven parallel robots. Several topics have been discussed in detail.

GENERAL RECONFIGURABLE ARCHITECTURES

General architectures of large-dimension reconfigurable CDPRs have been proposed. They can be used to replace conventional methods of handling large and heavy parts across a wide workspace. These solutions were illustrated in the context of two targeted industrial applications: using large-dimension reconfigurable CDPRs in a factory workshop and in an airplane maintenance workshop.

PRELIMINARY ANALYSIS TOOLS

Analysis tools that can aid the design and control of (reconfigurable) CDPRs were presented. Various problems were addressed including the kinetostatic, dynamic and elastostatic modeling, collision detections and hefty cable modeling.

CDPR kinetostatic and dynamic modeling allowed us to evaluate the CDPR performances notably by means of cable tension based criteria and to test wrench-feasibility conditions. Thanks to the derivation of the stiffness matrix of a general 6-DOF CDPR (using the elastic catenary cable model), it was possible to define a CDPR stiffness based cri-

terion. This new index quantifying the CDPR stiffness was used in the solving of the CDPR reconfiguration problem.

Two algorithms to detect cable interferences were also proposed. They can be used to verify collision free conditions for a given prescribed Cartesian workspace and a given set of orientation ranges. These tools are especially useful to deal with geometric constraints in a design problem or in a CDPR reconfiguration planning problem.

One of the main contribution of the thesis is the analysis of different cable models that could be used for large-dimension CDPRs. We have shown that among different cable models, the massless elastic cable model (taking into account only the cable elasticity) and the simplified cable model (considering both cable mass and elasticity) give the best performance for the CDPR in terms of positioning accuracy. Taking a further step, we carried out a CDPR extended modeling that takes into account various factors impacting the CDPR performances such as: the influence of pulley kinematics, thermal effect, friction, tension distribution methods and cable characteristics (Young's modulus and cable mass). The CoGiRo prototype was used to illustrate our analysis in simulation and experiments. From these results, we can conclude that all those factors may have to be considered in the modeling of a CDPR. It is suggested that the cable model used includes cable mass, elasticity and thermal effect, appropriate friction model and tension distribution method.

CDPR RECONFIGURATION PROBLEM

Moreover, systematic procedures to deal with the CDPR reconfiguration problem have been proposed. The reconfiguration problem is considered as a general nonlinear optimization problem. We focused on methods to formulate the optimization problems into standard forms in such a way that:

- It can be solved by using any available (suitable) optimization software.
- The resultant reconfiguration solutions are reasonable with respect to desired CDPR performances.

Two approaches have been proposed to formulate the reconfiguration problem. In the first approach, the CDPR reconfiguration problem is considered as a single-objective optimization problem and it is solved with fast optimization tools, which offer real-time capable reconfiguration planning solutions. Energy consumption indices were selected as the objective function to derive the optimal reconfiguration solution.

In the second approach, the CDPR reconfiguration problem is considered as a multi-objective optimization problem. The optimal planning solutions are derived by optimizing two criteria: one index (the sum of cable tension) accounts for the energy consumption,

and the other index (the normalized upper bound on the infinitesimal displacement vector of the CDPR mobile platform) accounts for the CDPR stiffness. This approach offers a more reliable resolution where the tradeoff between different criteria are efficiently taken into account.

Perspectives

Within the 3-year time frame of this thesis, I have only been able to address a number of issues related to large-dimension reconfigurable CDPRs.

In the modeling of CDPRs, I dealt mainly with static analysis. The dynamics of the cable is neglected. In fact, studying the impact of the dynamics of the cables on the CDPR performances is still an open and difficult issue. Having knowledge of dynamic behavior of the cables (e.g. natural frequency, vibration) can be useful in order to improve the CDPR performances. Besides, the deformation of the CDPR base frame structure should also be investigated.

About the control system, it would be desirable to have a more extensive study on the impact of various tension distribution methods on the CDPR performances. We have seen that it is critical to develop a good calibration procedure that includes the identification of all cable characteristics (notably the effective range of the cable Young's modulus and thermal effect), the identification of the parameters defining the CDPR initial state (which significantly impact the CDPR positioning accuracy) and the identification of friction model (friction in the winches, friction between cable and the pulley...).

Regarding the methodology to solve the CDPR reconfiguration problem, I have mainly discussed procedures to solve it as an optimization problem in the case of (continuously) positioning cable exit points. In a general case, reconfiguring a CDPR consists in changing its cable exit point positions as well as changing the positions or order of the attachment points that connect the cables to the mobile platform. The latter case is to find optimal reconfiguration of the cable layout among a finite set of configurations for the cable-platform attachment points. On the one hand, one can use the same steps proposed in our approach to deal with such integer optimization problems, specifically in the method of formulating the objective functions based on one criterion or multiple criteria. On the other hand, it would also be interesting to develop tools that could give very fast reconfiguration solutions in the cases a CDPR is used in tasks that require to carry different parts having different geometries.

Nevertheless, many unsolved problems on cable-driven parallel robots are still lying somewhere in the future, waiting for enthusiasm researchers to break through them. Hopefully, what I have done in this thesis will become a stepping stone that can aid further studies on CDPRs.

PUBLICATIONS

Conferences

1. D. Q. Nguyen, M. Gouttefarde, "*Study of Reconfigurable Suspended Cable-Driven Parallel Robots for Airplane Maintenance*," IEEE/RSJ 2014 Int. Conf. on Intelligent Robots and Systems (IROS' 14), Chicago, USA, 2014. — ICROS Best Application Paper Award Finalist —
2. D. Q. Nguyen, M. Gouttefarde, O. Company, F. Pierrot, "*On the Analysis of Large-Dimension Reconfigurable Suspended Cable-Driven Parallel Robots*," IEEE Int. Conf. Robotics and Automation (ICRA' 14), Hong Kong, China, 2014.
3. D. Q. Nguyen, Marc Gouttefarde, O. Company, F. Pierrot, "*On the Simplifications of Cable Model in Static Analysis of Large-Dimension Cable-Driven Parallel Robots*," IEEE/RSJ 2013 Int. Conf. on Intelligent Robots and Systems (IROS' 13), Tokyo, Japan, 2013.
4. D. Q. Nguyen, M. Gouttefarde, "*Stiffness Matrix of 6-DOF Cable-Driven Parallel Robots and its Homogenization*," Advances in Robot Kinematics (ARK), J. Lenarcic and O. Khatib eds., Springer, pp. 181-191, 2014 (14th ARK International Symposium).
5. D. Q. Nguyen, M. Gouttefarde, "*On the Improvement of Cable Collision Detection Algorithms*," Cable-Driven Parallel Robots, T. Bruckmann and A. Pott eds., Springer, pp. 29-40, 2014 (Second international conference on cable-driven parallel robots, Duisburg, Germany).
6. M. Gouttefarde, D. Q. Nguyen, C. Baradat, "*Kinetostatic Analysis of Cable-Driven Parallel Robots with Consideration of Sagging and Pulleys*," Advances in Robot Kinematics (ARK), J. Lenarcic and O. Khatib eds., Springer, pp. 213-221, 2014 (14th ARK International Symposium).
7. M. Michelin, C. Baradat, D. Q. Nguyen, M. Gouttefarde, "*Simulation and Control with XDE and Matlab/Simulink of a Cable-Driven Parallel Robot (CoGiRo)*," Cable-Driven

Parallel Robots, T. Bruckmann and A. Pott eds., Springer, pp. 29-40, 2014 (Second international conference on cable-driven parallel robots, Duisburg, Germany).



COMPLEMENTARY MODELING

A.1 Extended Modeling: a General Case

In a general case, there are several segments of the cable that connect the cable exit point to the drum, passing through several pulleys. Fig. A.1 shows an example of a cable routing system including three transmission pulleys. The pulleys are aligned in such order that any two consecutive pulleys are horizontally aligned or vertically aligned. For the sake of simplification, we will consider only the cable routing system shown in Fig. A.1 (the method can be easily adapted to any N -pulley cable routing system). The total cable unstrained length (from the drum to the cable anchor point B) is computed as follows:

$$\begin{aligned}
 L_T = & O(L_0) + L_0^{(D,P_{1a})} + L_0^{(P_{1a},P_{1b})} \\
 & + \dots + L_0^{(P_{k-1b},P_{ka})} + L_0^{(P_{ka},P_{kb})} \\
 & + L_0^{(P_{kb},P_{k+1a})} + \dots + L_0^{(P_{Nb},B)} \quad (k = 2, \dots, N)
 \end{aligned} \tag{A.1}$$

where $O(L_0)$ is the cable deformation due to undetermined uncertainties (e.g., temperature). $L_0^{(D,P_{1a})}$ is the cable unstrained length between the drum and the first pulley. $L_0^{(P_{kb},P_{(k+1)a})}$ is the cable unstrained length between the two pulleys k and $(k+1)$. $L_0^{(P_{ka},P_{kb})}$ is the cable unstrained length of the cable segment that mount on the pulley k . $L_0^{(P_{Nb},B)}$ is the cable unstrained length of the cable segment between the last pulley N and the cable anchor point B .

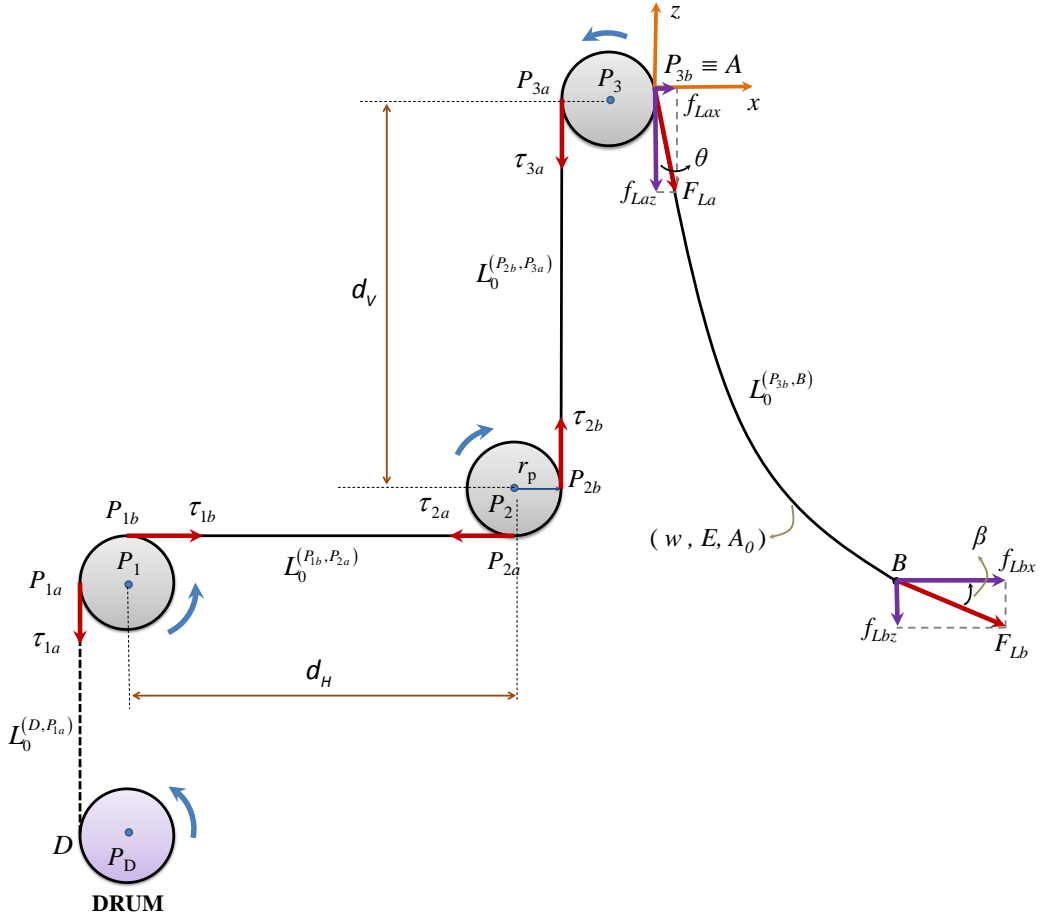


Figure A.1: Drum and cable transmission components: a general case

The total cable unstrained length of each cable is a constant value (L_D is the unstrained length of the part of the cable wound on the drum):

$$L_T + L_D = L_{total} = const \quad (A.2)$$

The cable segment mounted on each pulley is computed as follows:

$$L_0^{(P_{ka}, P_{kb})} = \widehat{P_{ka}P_{kb}} = r_p \theta_k \quad (A.3)$$

where θ_k is the angle of the arc $\widehat{P_{ka}P_{kb}}$.

The computation of the term $L_0^{(D, P_{1a})}$ depends on the design of the winch/drum. The approach to compute $L_0^{(P_{Nb}, B)}$ is similar to the one presented in Section 3.3.2.

In the following sections, we will detail the computation of the unstrained length of the cable segments in additional cases (which have not been discussed before).

A.1.1 Cable Segment between Two Vertically Aligned Pulleys

Fig. A.2 shows the cable segment between two pulleys 2 and 3 which are vertically aligned. In this case, the two tangent points P_{2b} and P_{3a} have the same x-coordinate. The lateral horizontal force components in the cable at points P_{2b} and P_{3a} are zero ($f_{Lx} = 0$), and the cable tensions at these points satisfy $\tau_{2b} = \tau_{3a} - wL_0^{(P_{2b}, P_{3a})}$. The vertical distance between the two tangent points is d_V .

From the catenary equations (3.15), one can derive the analytical expression for the cable unstrained length:

$$\begin{aligned}
 z_{P_{3a}} &= z_{P_{2b}} - \frac{f_{Lz} L_0}{EA_0} + \frac{w L_0^2}{2EA_0} + \frac{C_T}{w} (\tau_{3a} - \tau_{2b}) \\
 \Rightarrow \frac{w}{2EA_0} L_0^2 + \frac{\tau_{3a} - w L_0}{EA_0} L_0 + C_T L_0 + z_{P_{2b}} - z_{P_{3a}} &= 0 \\
 \Rightarrow \frac{w}{2EA_0} L_0^2 - \left(C_T + \frac{\tau_{3a}}{EA_0} \right) L_0 + d_V &= 0 \\
 \Rightarrow L_0^{(P_{2b}, P_{3a})} &= \frac{2d_V}{C_T + \frac{\tau_{3a}}{EA_0} + \sqrt{\left(C_T + \frac{\tau_{3a}}{EA_0} \right)^2 - \frac{2w d_V}{EA_0}}} \quad (A.4)
 \end{aligned}$$

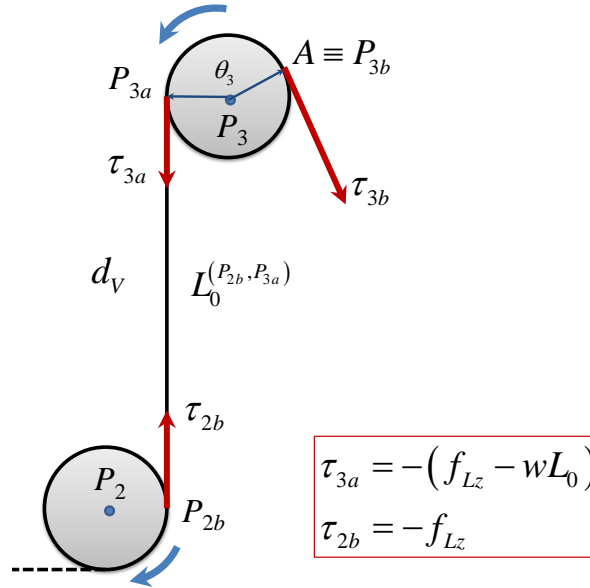


Figure A.2: Cable segment between two vertically aligned pulleys

If the massless elastic cable model is used then:

$$L_0^{(P_{2b}, P_{3a})} = \frac{d_V}{C_T + \frac{\tau_{3a}}{EA_0}} \quad (\text{A.5})$$

Note that the cable tension at point P_{3a} is computed from the belt friction equation:

$$\tau_{3a} = \tau_{3b} e^{\mu_s \theta_3} \quad (\text{A.6})$$

The difference in unstrained length of the vertical cable segment using (A.4) and (A.5) is very small, thus we can use (A.5) to compute $L_0^{(P_{2b}, P_{3a})}$ as described in Section 3.3.1.

A.1.2 Cable Segment between Two Horizontally Aligned Pulleys

Fig. A.3 shows the cable segment between two pulleys 1 and 2 which are horizontally aligned. In this case, the two tangent points P_{1b} and P_{2a} have the same z-coordinate. Assume that the cable frame is attached to the point P_{1b} . From the catenary cable equations, one can derive:

$$\begin{aligned} \tau_{1b} &= \tau_{2a} \\ x_{P_{1b}} - x_{P_{2a}} &= -\frac{f_{Lx} L_0}{EA_0} + \frac{C_T f_{Lx}}{w} \ln \left(\frac{\tau_{2a} - w L_0/2}{\tau_{2a} + w L_0/2} \right) \\ \Rightarrow d_H &= \frac{f_{Lx} L_0}{EA_0} + \frac{C_T f_{Lx}}{w} \ln \left(\frac{\tau_{2a} + w L_0/2}{\tau_{2a} - w L_0/2} \right) \end{aligned} \quad (\text{A.7})$$

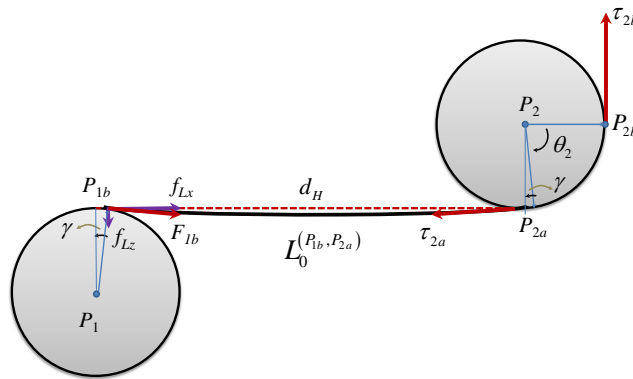


Figure A.3: Cable segment between two horizontally aligned pulleys

where

$$\begin{aligned} L_0 &= L_0^{(P_{1b}, P_{2a})} \\ \gamma &= \text{atan2}(f_{Lz}, f_{Lx}) \\ f_{Lz} &= \frac{w L_0}{2} \\ f_{Lx} &= \sqrt{\tau_{2a}^2 - \frac{w^2 L_0^2}{4}} \end{aligned}$$

and d_H is the distance between the two pulleys ($d_H = P_1 P_2$).

The cable tension at point P_{2a} can be computed from the belt friction equation:

$$\tau_{2a} = \tau_{2b} e^{\mu_s \theta_2} \quad (\text{A.8})$$

There is no analytical expression for L_0 from (A.7). One can use iterative method to get $L_0^{(P_{1b}, P_{2a})}$, e.g. initialize with $L_0 = d_H$ and use the Newton-Raphson method to compute L_0 . Although the method is quite fast, there is no guarantee that the algorithm will converge within a few iterations in all the cases. In fact, we can alternatively use the massless elastic cable model to compute the unstrained length of the cable horizontal segment (since the difference in the cable unstrained length is very small compared to the numerical solution obtained with the catenary cable model):

$$L_0^{(P_{1b}, P_{2a})} = \frac{d_H}{C_T + \frac{\tau_{2a}}{EA_0}} \quad (\text{A.9})$$

with

$$\begin{aligned} \tau_{2a} &= \tau_{2b} e^{\mu_s \pi/2} \quad (\theta_2 = \pi/2 - \gamma \approx \pi/2) \\ \tau_{2b} &= \tau_{3a} - w L_0^{(P_{2b}, P_{3a})} \end{aligned}$$

A.1.3 Cable Segment between the Drum and the First Pulley

Fig. A.4 shows the cable segment between the drum and the first pulley. c is the step of the helix of the part of the cable wound on the drum and t (rad) is the total rotation angle of the helix. r_D is the radius of the drum. D is the tangent point between the cable and the drum.

As mentioned before, the computation of the unstrained length of the cable segment in this case depends on the design of the winch. In this section, we consider again the winch

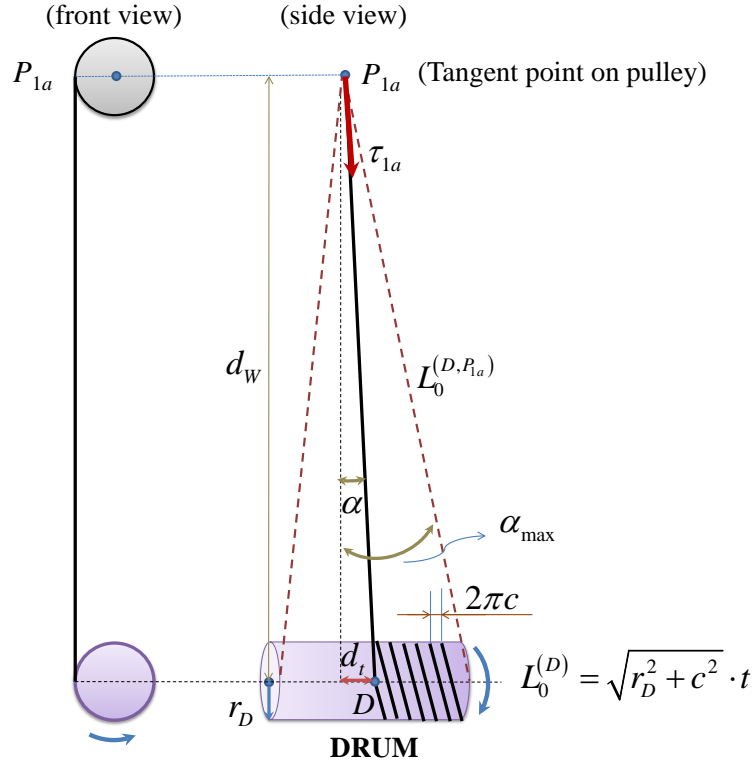


Figure A.4: Cable segment between the drum and the first pulley

design of the CoGiRo prototype. The case when the maximum tilt angle of the cable α_{\max} is less than a small value was discussed in Section 3.3.1. However, when the tilt angle α is non-negligible (the cable segment is not in a vertical position), the modeling becomes more complicated.

Let us assume that at the initial pose of the mobile platform (the home pose), we know the unstrained length L_{T0} of the cable from the drum to the anchor point B . At a sample time k , a desired motor angular displacement q_d is generated. We have:

$$\begin{aligned}
 L_{T0} + r_q q_d &= L_0^{(D, P_1)}(k) + L_0^{(P_1, B)}(k) \\
 &= \frac{\sqrt{d_w^2 + d_t^2}}{C_T + \frac{\tau_{1a}}{EA_0}} + L_0^{(P_1, B)}(k)
 \end{aligned} \tag{A.10}$$

Let us define $L_{0d} = L_0^{(P_1, B)}(k)$ and $M = C_T + \frac{\tau_{1a}}{EA_0}$.

The value of L_{0d} can be computed from the corresponding unstrained lengths of all the cable segments between any two consecutive pulleys, wound on each pulley, and between the last pulley and the cable anchor point B .

In (A.10):

$$d_t = d_0 + r_L q_d \quad (\text{A.11})$$

where d_0 is the distance from the cable tangent point D to the vertical axis position when the mobile platform is at the home pose and r_L is a conversion ratio. In the case of the CoGiRo CDPR we have:

$$r_q = \frac{2\pi\sqrt{r_D^2 + c^2}}{3000} \quad (\text{A.12})$$

$$r_L = \frac{2\pi c}{3000} \quad (\text{A.13})$$

Substituting (A.11) into (A.10) we have:

$$\begin{aligned} (L_{T0} + r_q q_d) M &= \sqrt{d_w^2 + (d_0 + r_L q_d)^2} + L_{0d} M \\ \Rightarrow (M^2 r_q^2 - r_L^2) q_d^2 &+ 2[r_q(L_{T0} - L_{0d})M^2 - d_0 r_L] q_d \\ &+ M^2(L_{T0} - L_{0d})^2 - (d_w^2 + d_0^2) = 0 \end{aligned} \quad (\text{A.14})$$

Solving (A.14), we obtain two possible solutions for q_d :

$$q_d = \frac{r_L d_0 - r_q(L_{T0} - L_{0d})M^2 \pm \sqrt{\Delta}}{M^2 r_q^2 - r_L^2} \quad (\text{A.15})$$

where $\Delta = M^2 [r_L(L_{T0} - L_{0d}) - r_q d_0]^2 + (M^2 r_q^2 - r_L^2) d_w^2$.

When $d_0 = 0$ and $r_L = 0$ (the cable segment is assumed to be in a vertical position), we get the same solution as the one obtained with the massless elastic cable model:

$$\begin{aligned} L_{T0} + r_q q_d &= \frac{d_w}{M} + L_{0d} \\ \Rightarrow q_d &= \frac{-(L_{T0} - L_{0d})}{r_q} + \frac{d_w}{M r_q} \end{aligned} \quad (\text{A.16})$$

This solution corresponds to the general case:

$$q_d = \frac{r_L d_0 - r_q(L_{T0} - L_{0d})M^2 + \sqrt{\Delta}}{M^2 r_q^2 - r_L^2} \quad (\text{A.17})$$

To implement (A.17) in a control scheme, it is important to "precisely" determine the values of d_0 and L_{T0} at the initial state of the CDPR (when the mobile platform is at the home pose).

A.2 Tangent Point between a Line and a Circle

Fig. A.5 shows the tangent point between a straight line and a circle. The problem is to find the coordinates of the tangent point $A(x_a, z_a)$ being given the coordinates of the point $B(x_b, z_b)$ in the local frame attached to the origin P and the radius of the circle. The coordinates of the point A must satisfy the circle equation and the tangent line equation:

$$(x_A - r_p)^2 + z_A^2 = r_p^2 \quad (\text{A.18})$$

$$(x_A - r_p)(x_b - r_p) + z_A z_b = r_p^2 \quad (\text{A.19})$$

$$\Rightarrow x_A - r_p = \frac{r_p^2 - z_A z_b}{x_b - r_p} \quad (\text{A.20})$$

Substituting (A.20) into (A.18) we have:

$$\begin{aligned} & \left(\frac{r_p^2 - z_A z_b}{x_b - r_p} \right)^2 + z_A^2 = r_p^2 \\ \Rightarrow & \left[z_b^2 + (x_b - r_p)^2 \right] z_A^2 - 2 z_b r_p^2 \cdot z_A + r_p^4 - r_p^2 (x_b - r_p)^2 = 0 \\ \Rightarrow & z_A = \frac{z_b r_p^2 \pm \sqrt{\Delta}}{z_b^2 + (x_b - r_p)^2} \end{aligned} \quad (\text{A.21})$$

where $\Delta = \left[z_b^2 + (x_b - r_p)^2 - r_p^2 \right] r_p^2 (x_b - r_p)^2$.

In Fig. A.5, $z_A > 0$, thus we obtain the solution:

$$z_A = \frac{z_b r_p^2 + r_p |x_b - r_p| \sqrt{z_b^2 + (x_b - r_p)^2 - r_p^2}}{z_b^2 + (x_b - r_p)^2} \quad (\text{A.22})$$

$$x_A = r_p + \sqrt{r_p^2 - z_A^2} \quad (\text{A.23})$$

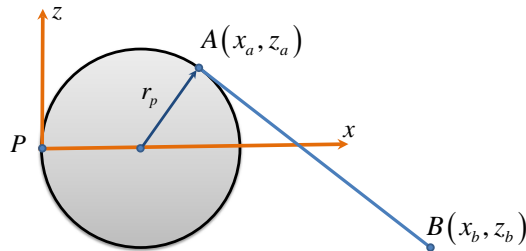


Figure A.5: Tangent line from a fixed point to a circle

BIBLIOGRAPHY

- [1] P. Bosscher, R. L. Williams II, L. S. Bryson, and D. Castro-Lacouture. “Cable-suspended robotic contour crafting system”. *Automation in Construction*, 17(1):45–55, 2007. Cited pages 3 and 5.
- [2] A. Pott, C. Meyer, and A. Verl. “Large-scale assembly of solar power plants with parallel cable robots”. *Proceedings of the 41st International Symposium on Robotics and the 6th German Conference on Robotics (ROBOTIK’ 10)*, pages 1–6, 2010. Cited pages 3 and 9.
- [3] P. Bosscher, R. L. Williams II, and M. Tummino. “A concept for rapidly-deployable cable robot search and rescue systems”. *Proceedings of the ASME International Design Engineering Technical Conferences and Computers and Information in Engineering Conference (DETC/CIE ’05)*, pages 589–598, 2005. Cited page 3.
- [4] J.-P. Merlet, D. Daney. “A portable, modular parallel wire crane for rescue operations”. *IEEE International Conference on Robotics and Automation (ICRA)*, pages 2834 – 2839, May 2010. Cited pages 3, 12, and 47.
- [5] D. Surdilovic, R. Bernhardt. “STRING-MAN: a new wire robot for gait rehabilitation”. *2004 IEEE International Conference on Robotics and Automation (ICRA)*, pages 2031 – 2036, May 2004. Cited page 3.
- [6] G. Rosati, P. Gallina, S. Masiero. “Design, implementation and clinical tests of a wire-based robot for neurorehabilitation”. *IEEE Transactions on Neural Systems and Rehabilitation Engineering*, 15(4):560–569, 2007. Cited page 3.
- [7] X. Lin, D. I. Jun, X. Jin, J. Seon, A. Pott, S. Park, J.-O. Park and S. Y. Ko. “Upper Limb Rehabilitation Using a Planar Cable-Driven Parallel Robot with Various Rehabilitation Strategies”. *Cable-Driven Parallel Robots*, pages 307–322, 2014. Cited page 3.

- [8] Q. Jiang, V. Kumar. “*Determination and stability analysis of equilibrium configurations of objects suspended from multiple aerial robots*”. *Journal of Mechanisms and Robotics*, 4(2), 2012. Cited page 3.
- [9] Q. Jiang, V. Kumar. “*The inverse kinematics of cooperative transport with multiple aerial robots*”. *IEEE Transactions on Robotics*, 29(1):136–145, 2013. Cited page 3.
- [10] X. Tang, W. Zhu, C. Sun, and R. Yao. “*Similarity model of feed support system for FAST*”. *Experimental Astronomy*, 29(3):177–187, 2011. Cited page 3.
- [11] A. Ming, T. Higuchi. “*Study on multiple degree-of-freedom positioning mechanism using wires-concept, design and control*”. *International Journal of the Japan Society for Precision Engineering*, 28(2):131–138, 1994. Cited page 3.
- [12] R. Verhoeven. “*Analysis of the workspace of tendon-based Stewart platforms*”. *PhD Thesis, University of Duisburg-Essen, Germany*, 2004. Cited page 3.
- [13] M. Gouttefarde. “*Characterizations of fully constrained poses of parallel cable-driven robots: a review*”. *Proceedings of the ASME International Design Engineering Technical Conferences and Computers and Information in Engineering Conference (DETC '08)*, pages 21–30, 2008. Cited page 4.
- [14] S. Kawamura, W. Choe, S. Tanaka, and S. R. Pandian. “*Development of an ultra-high speed robot FALCON using wire drive system*”. *IEEE International Conference on Robotics and Automation (ICRA)*, 1:215–220, 1995. Cited pages 4 and 6.
- [15] T. Bruckmann, L. Mikelsons, M. Hiller, and D. Schramm. “*A new force calculation algorithm for tendon-based parallel manipulators*”. *Proceedings of the IEEE/ASME International Conference on Advanced Intelligent Mechatronics (AIM '07)*, pages 1–6, 2007. Cited pages 4, 5, and 6.
- [16] J. Albus, R. Bostelman, and N. Dagalakis. “*The NIST robocrane*”. *Journal of Robotic Systems*, 10(5):709–724, 1993. Cited pages 4, 6, and 47.
- [17] J. Lamaury, M. Gouttefarde. “*Control of a Large Redundantly Actuated Cable-Suspended Parallel Robots*”. *Proceedings of the IEEE International Conference on Robotics and Automation (ICRA)*, 2013. Cited pages 4, 5, 9, 61, 85, and 93.
- [18] L. Mikelsons, T. Bruckmann, D. Schramm, and M. Hiller. “*A real-time capable force calculation algorithm for redundant tendon-based parallel manipulators*”. *IEEE International Conference on Robotics and Automation*, pages 3869–3874, 2008. Cited pages 4, 6, 33, 36, and 41.

- [19] A. Pott, T. Bruckmann, and L. Mikelsons. "Closed-form force distribution for parallel wire robots". *Computational Kinematics, Springer, Berlin, Germany*, pages 25–34, 2009. Cited pages 4, 6, 9, and 33.
- [20] J.-P. Merlet. "The kinematics of the redundant N-1 wire driven parallel robot". *IEEE International Conference on Robotics and Automation*, 2012. Cited page 4.
- [21] M. Carricato. "Direct Geometrico-Static Problem of Underconstrained Cable-Driven Parallel Robots With Three Cables". *Journal of Mechanisms and Robotics*, 5, 2013. Cited page 4.
- [22] M. Carricato, G. Abbasnejad. "Direct Geometrico-Static Analysis of Under-Constrained Cable-Driven Parallel Robots with 4 Cables". *Cable-Driven Parallel Robots*, 12:269–285, 2013. Cited page 4.
- [23] M. Gouttefarde, J. Collard, N. Riehl, C. Baradat. "Simplified static analysis of large-dimension parallel cable-driven robots". *IEEE International Conference on Robotics and Automation*, pages 2299–2305, 2012. Cited pages 4, 32, 33, 36, 37, 38, 41, 42, 84, and 85.
- [24] K. Kozak, Q. Zhou, and J. Wang. "Static analysis of cable-driven manipulators with non-negligible cable mass". *IEEE Transactions on Robotics*, 22(3):325–433, 2006. Cited pages 4, 32, 33, and 40.
- [25] E. Ottaviano, G. Castelli. "A Study on the Effects of Cable Mass and Elasticity in Cable-Based Parallel Manipulator". *Proc. of the 18th CISM-IFTOMM Symp. On Robot Design, Dynamics and Control, Springer Ed. Udine*, pages 149–156, 2010. Cited page 4.
- [26] X. Diao, O. Ma. "Force-closure analysis of 6-DOF cable manipulators with seven or more cables". *Robotica*, 27(2):209–215, 2009. Cited page 4.
- [27] A. Ghasemi, M. Eghtesad, M. Farid. "Workspace analysis of planar and spatial redundant cable robot". *Proceedings of the American Control Conference (ACC' 08)*, pages 2389–2394, 2009. Cited pages 4 and 5.
- [28] T. Bruckmann, A. Pott, and M. Hiller. "Calculating force distributions for redundantly actuated tendon-based Stewart platforms". *Advances in Robot Kinematics*, pages 403–412, 2006. Cited pages 4 and 6.
- [29] P. H. Borgstrom, B. L. Jordan, G. S. Sukhatme, M. A. Batalin, and W. J. Kaiser. "Rapid computation of optimally safe tension distributions for parallel cable-driven robots". *IEEE Transactions on Robotics*, 25(6):1271–1281, 2009. Cited pages 4 and 6.

- [30] A. Pott. "An algorithm for real-time forward kinematics of cable-driven parallel robots". *Advances in Robot Kinematics: Motion in Man and Machine*, Springer, Dordrecht, The Netherlands, pages 529–538, 2010. Cited pages 4, 6, and 9.
- [31] W. B. Lim, S. H. Yeo, G. Yang, S. K. Mustafa, and Z. Zhang. "An algorithm for real-time forward kinematics of cable-driven parallel robots". *Proceedings of the IEEE/ASME International Conference on Advanced Intelligent Mechatronics (AIM '11)*, pages 73–78, 2011. Cited pages 4 and 6.
- [32] J. Lamaury, M. Gouttefarde. "A tension distribution method with improved computational efficiency". *Cable-Driven Parallel Robots, Mechanisms and Machine Science*, Springer, 12:71–85, 2013. Cited pages 4, 5, 6, 9, 12, 33, 36, 41, 47, 75, 78, 79, 81, 84, 85, 88, and 95.
- [33] K. Müller, C. Reichert and T. Bruckmann. "Analysis of a Real-Time Capable Cable Force Computation Method". *Cable-Driven Parallel Robots, Mechanisms and Machine Science*, Springer, 32:227–238, 2014. Cited pages 4, 5, 6, and 41.
- [34] C. Gosselin, M. Grenier. "On the determination of the force distribution in overconstrained cable-driven parallel mechanisms". *Meccanica*, 46(1):3–15, 2011. Cited page 4.
- [35] C. B. Pham, S. H. Yeo, G. Yang, M. S. Kurbanhusen, and I.-M. Chen. "Force-closure workspace analysis of cable-driven parallel mechanisms". *Mechanism and Machine Theory*, 41(1):53–69, 2006. Cited page 5.
- [36] C. B. Pham, S. H. Yeo, G. Yang, and I.-M. Chen. "Workspace analysis of fully restrained cable-driven manipulators". *Robotics and Autonomous Systems*, 57(9):901–912, 2009. Cited page 5.
- [37] D. Lau, D. Oetomo, and S. K. Halgamuge. "Wrench-closure workspace generation for cable driven parallel manipulators using a hybrid analytical-numerical approach". *Journal of Mechanical Design*, 133(7), 2011. Cited page 5.
- [38] A. Berti, J.-P. Merlet and M. Carricato. "Workspace Analysis of Redundant Cable-Suspended Parallel Robots". *Cable-Driven Parallel Robots*, pages 41–54, 2014. Cited page 5.
- [39] M. Gouttefarde, D. Daney, J.-P. Merlet. "Interval-Analysis-Based Determination of the Wrench-Feasible Workspace of Parallel Cable-Driven Robots". *IEEE Transactions on Robotics*, 27(1):1–13, 2011. Cited pages 5 and 38.

- [40] A. M. Hay, J. A. Snyman. "Optimization of a planar tendon-driven parallel manipulator for a maximal dextrous workspace". *Engineering Optimization*, 37(3):217–236, 2005. Cited page 5.
- [41] P. Lafourcade, Y.-Q. Zheng, Xi.-W. Liu. "Stiffness Analysis of Wire-Driven Parallel Kinematic Manipulators". *Proceedings of the 11th World Congress in Mechanism and Machine Science, IFToMM, Tianjin, China*, page April, 2004. Cited pages 5 and 108.
- [42] X. Tang, L. Tang, J. Wang, and D. Sun. "Workspace quality analysis and application for a completely restrained 3-Dof planar cable-driven parallel manipulator". *Journal of Mechanical Science and Technology*, 27(8):2391–2399, 2013. Cited page 5.
- [43] S. Bouchard, C. Gosselin. "Kinematic sensitivity of a very large cable-driven parallel mechanism". *ASME International Design Engineering Technical Conferences*, 2006. Cited pages 5 and 108.
- [44] J. Du, W. Ding and H. Bao. "Cable Vibration Analysis for Large Workspace Cable-Driven Parallel Manipulators". *Cable-Driven Parallel Robots, Mechanism and Machine Science, Springer*, 12:437–449, 2013. Cited page 5.
- [45] H. Yuan, E. Courteille and D. Deblaise. "Elastodynamic Analysis of Cable-Driven Parallel Manipulators Considering Dynamic Stiffness of Sagging Cables". *IEEE International Conference on Robotics and Automation (ICRA)*, 2014. Cited page 5.
- [46] X. Weber, L. Cu villon and J. Gangloff. "Active vibration canceling of a cable-driven parallel robot using reaction wheels". *IEEE International Conference on Intelligent Robots and Systems (IROS)*, 2014. Cited page 5.
- [47] S. Fang, D. Franitza, M. Torlo, F. Bekes, and M. Hiller. "Motion control of a tendon-based parallel manipulator using optimal tension distribution". *IEEE/ASME Transactions on Mechatronics*, 9(3):561–568, 2004. Cited page 5.
- [48] R. L. Williams II, P. Gallina, and J. Vadia. "Planar translational cable-direct-driven robots". *Journal of Robotic Systems*, 20(3):107–120, 2003. Cited page 5.
- [49] S. Kawamura, H. Kino, and C. Won. "High-speed manipulation by using parallel wire-driven robots". *Robotica*, 18(1):13–21, 2000. Cited pages 5 and 6.
- [50] H. Kino, T. Yahiro, T. Fumiaki, and T. Morizono. "Robust PD Control Using Adaptive Compensation for Completely Restrained Parallel Wire-Driven Robots". *IEEE Transactions on Robotics*, 23:803–812, 2007. Cited page 5.

- [51] G. S. Natal, A. Chemori, and F. Pierrot. “*Dual-Space Adaptive Control of Redundantly Actuated Parallel Manipulators for Extremely Fast Operations With Load Changes*”. *IEEE International Conference on Robotics and Automation (ICRA)*, 2012. Cited page 5.
- [52] T. Dallej, M. Gouttefarde, N. Andreff, M. Michelin, and P. Martinet. “*Towards vision-based control of cable-driven parallel robots*”. *IEEE International Conference on Intelligent Robots and Systems (IROS)*, pages 2855–2860, 2011. Cited page 6.
- [53] R. Chellal, L. Cuillon and E. Laroche. “*A Kinematic Vision-Based Position Control of a 6-DOF Cable-Driven Parallel Robot*”. *Cable-Driven Parallel Robots*, pages 213–226, 2014. Cited page 6.
- [54] A. B. Alp and S. K. Agrawal. “*Cable suspended robots: feedback controllers with positive inputs*”. *Proceedings of the American Control Conference*, 1:815–820, 2002. Cited page 6.
- [55] S. R. Oh and S. K. Agrawal. “*Nonlinear sliding mode control and feasible workspace analysis for a cable suspended robot with input constraints and disturbances*”. *Proceedings of the American Control Conference*, 5:4631–4636, 2004. Cited page 6.
- [56] S.-R. Oh and S. K. Agrawal. “*A reference governor-based controller for a cable robot under input constraints*”. *IEEE Transactions on Control Systems Technology*, 13(4): 639–645, 2005. Cited page 6.
- [57] A. Alikhani and M. Vali. “*Modeling and robust control of a new large scale suspended cable-driven robot under input constraint*”. *IEEE Proceedings of the 8th International Conference on Ubiquitous Robots and Ambient Intelligence (URAI '11)*, pages 238–243, 2011. Cited page 6.
- [58] M. A. Khosravi and H. D. Taghirad. “*Experimental performance of robust PID controller on a planar cable robot*”. *Cable-Driven Parallel Robots*, pages 337–352, 2013. Cited page 6.
- [59] <http://www.nist.gov/el/isd/ms/robocrane.cfm>. Cited page 6.
- [60] N. G. Dagalakis, J. S. Albus, B.-L. Wang, J. Unger, and J. D. Lee. “*Stiffness study of a parallel link robot crane for shipbuilding applications*”. *Journal of Offshore Mechanics and Arctic Engineering*, 111(3):183–193, 1989. Cited page 6.
- [61] R. Bostelman, J. Albus, N. Dagalakis, A. Jacoff, and J. Gross. “*Applications of the NIST RoboCrane*”. *Proceedings of the 5th International Symposium on Robotics and Manufacturing*, pages 14–18, 1994. Cited page 6.

- [62] W. G. Rippey and J. A. Falco. "The NIST automated arc welding testbed". *Proceedings of the 7th International Conference on Computer Technology in Welding, NIST Special Publication SP*, pages 203–212, 1997. Cited page 6.
- [63] E. Amatucci, R. Bostelman, N. Dagalakis, and T. Tsai. "Summary of modeling and simulation for NIST robocrane applications". 1997. Cited page 6.
- [64] A. M. Lytle, K. S. Saidi, R. V. Bostelman, W. C. Stone, and N. A. Scott. "Adapting a tele-operated device for autonomous control using three-dimensional positioning sensors: experiences with the NIST RoboCrane". *Automation in Constructiog*, 13(1):101–118, 2004. Cited page 6.
- [65] <http://www.aemksystems.com>. Cited page 6.
- [66] S. Fang. "Design, Modeling and Motion Control of Tendon Based Parallel Manipulators". VDI-Verlag, 2005. Cited page 6.
- [67] M. Hiller, S. Fang, S. Mielczarek, R. Verhoeven, and D. Franitza. "Design, analysis and realization of tendon-based parallel manipulators". *Mechanism and Machine Theory*, 40(4):429–445, 2005. Cited page 6.
- [68] A. Pott. "Influence of Pulley Kinematics on Cable-Driven Parallel Robots". *Proceedings of the 13th International Symposium on Advances in Robot Kinematics, Springer*, pages 197–204, 2012. Cited pages 9 and 60.
- [69] D. Q. Nguyen, M. Gouttefarde, O. Company and F. Pierrot. "On the simplifications of cable model in static analysis of large-dimension cable-driven parallel robots". *IEEE International Conference on Intelligent Robots and Systems (IROS)*, pages 928–934, 2013. Cited pages 9, 33, and 82.
- [70] M. Michelin O. Tempier C. Baradat J. Izard, M. Gouttefarde. "A Reconfigurable Robot for Cable-Driven Parallel Robotic Research and Industrial Scenario Proofing". *Cable-Driven Parallel Robots, Mechanisms and Machine Science*, 12:135–148, 2013. Cited page 9.
- [71] J.-P. Merlet. "Kinematics of the wire-driven parallel robot marionet using linear actuators". *IEEE International Conference on Robotics and Automation*, pages 3857–3862, 2008. Cited pages 9 and 47.
- [72] B. Duan, Y. Qiu, F. Zhang, B. Zi. "On design and experiment of the feed cable-suspended structure for super antenna". *Mechatronics*, 19:503–509, 2009. Cited page 9.

- [73] X. Duan, Y. Qiu, J. Mi, and Z. Zhao. "Motion prediction and supervisory control of the macro-micro parallel manipulator system". *Robotica*, 29(7):1005–1015, 2011. Cited page 9.
- [74] Q. J. Duan, J. L. Du, and X. C. Duan. "Kinematic analysis of a hybrid structure". *International Journal of Advanced Robotic Systems*, 9, 2012. Cited page 9.
- [75] <http://www.spidercam.org>. Cited page 11.
- [76] <http://www.skycam.tv>. Cited page 11.
- [77] G. Rosati, D. Zanotto and S. K. Agrawal. "On the Design of Adaptive Cable-Driven Systems". *Journal of Mechanisms and Robotics, Transactions of the ASME*, 3, May 2011. Cited page 12.
- [78] X. Zhou, C.P. Tang, and V. Krovi. "Analysis Framework for cooperating Mobile Cable Robots". *IEEE International Conference on Robotics and Automation*, pages 3128–3133, May 2012. Cited page 12.
- [79] X. Zhou, C.P. Tang, and V. Krovi. "Cooperating Mobile Cable Robots: Screw Theoretic Analysis". *Lecture Notes in Electrical Engineering, Springer Berlin Heidelberg*, 57:109–123, May 2013. Cited page 12.
- [80] M. Irvine. "Cable Structures". *Cambridge, MA: MIT Press*, 1981. Cited pages 30, 32, 34, 43, 60, and 67.
- [81] H.-T. Thai, S.-E. Kim. "Nonlinear static and dynamic analysis of cable structures". *Finite Elements in Analysis and Design*, 47(3):237–246, 2011. Cited pages 30, 43, and 60.
- [82] H. Li, X. Zhang, R. Yao, J. Sun, G. Pan and W. Zhu. "Optimal Force Distribution based on slack rope model in the incompletely constrained cable-driven parallel mechanism of FAST telescope". *Cable-Driven Parallel Robots, Mechanism and Machine Science, Springer*, 2:87–102, 2013. Cited pages 33 and 36.
- [83] R. Yao, X. Tang, J. Wang, P. Huang. "Dimensional Optimization Design of the Four-Cable-Driven Parallel Manipulator in FAST". *IEEE/ASME Transaction on Mechatronics*, 15(6):932–941, 2010. Cited page 33.
- [84] K. Maeda, S. Tadokoro, T. Takamori, M. Hiller, R. Verhoeven. "On Design of a Redundant Wire-Driven Parallel robot WARP manipulator". *IEEE International Conference on Robotics and Automation*, pages 895–900, 1999. Cited pages 47 and 49.

- [85] J.-P. Merlet. "Analysis of the Influence of Wires Interference on the Workspace of Wire Robots". *On Advances in Robot Kinematics*, pages 211–218, 2004. Cited pages 47 and 48.
- [86] Y. Wischnitzer, N. Shvalb, M. Shoham. "Wire-driven Parallel Robot: Permitting Collisions Between Wires". *The International Journal of Robotics Research*, 27(9):1007–1026, 2008. Cited page 47.
- [87] M. Otis, S. Perreault, T.-L. Nguyen-Dang, P. Lambert, M. Gouttefarde, D. Laurendeau, and C. Gosselin. "Determination and Management of Cable Interferences Between Two 6-DOF Foot Platforms in a Cable-Driven Locomotion Interface". *IEEE Transactions on Systems, Man, and Cybernetics - Part A: Systems and Humans*, 39(3):528–544, 2009. Cited pages 47 and 49.
- [88] S. Perreault, C. Gosselin. "Cable-Driven Parallel Mechanisms: Application to a Locomotion Interface". *Journal of Mechanism Design*, 130, 2008. Cited page 47.
- [89] S. Perreault, P. Cardou, C. Gosselin, M. J.-D. Otis. "Geometric Determination of the Interference-Free Constant-Orientation Workspace of Parallel Cable-Driven Mechanisms". *Journal of Mechanisms and Robotics*, 2, 2010. Cited pages 47, 48, and 49.
- [90] S. Lahouar, E. Ottaviano, S. Zeghoul, L. Romdhanec, M. Ceccarelli. "Collision free path-planning for cable-driven parallel robots". *Robotics and Autonomous Systems*, 57:1083–1093, 2009. Cited page 47.
- [91] C. Ericson. "Real-Time Collision Detection". Morgan Kaufmann, 2005. Cited pages 47, 48, 49, and 51.
- [92] Meshlab. <http://meshlab.sourceforge.net/>. Cited page 54.
- [93] V. Schmidt, A. Pott. "Implementing Extended Kinematics of a Cable-Driven Parallel Robot in Real-Time". *Cable-Driven Parallel Robots, Mechanisms and Machine Science*, Springer, 12:287–298, 2013. Cited page 60.
- [94] F. Ju, Y.S. Choo. "Super element approach to cable passing through multiple pulleys". *International Journal of Solids and Structures*, 42:3533–3547, 2005. Cited page 62.
- [95] B. Armstrong-Hélouvry. "Control of Machines with Friction". Kluwer Academic, 1991. Cited page 64.
- [96] F. Al-Bender, V. Lampaert, and J. Swevers. "The Generalized Maxwell-Slip Model: A Novel Model for Friction Simulation and Compensation". *IEEE Transactions on Automatic Control*, 50(11), 2005. Cited pages 64 and 65.

- [97] M. Lepidi, V. Gattulli. “*Static and dynamic response of elastic suspended cables with thermal effects*”. *International Journal of Solids and Structures*, 49:1103–1116, 2012. Cited page 67.
- [98] M. Gouttefarde, D. Q. Nguyen, C. Baradat. “*Kinetostatic Analysis of Cable-Driven Parallel Robots with Consideration of Sagging and Pulleys*”. *Advances in Robot Kinematics (ARK)*, pages 213–221, 2014. Cited page 70.
- [99] W. Khalil, Étienne Dombre. “*Modeling, Identification And Control of Robots*”. Hermes Penton, 2002. Cited pages 83 and 103.
- [100] MHS. “*Aerial Multi-axis Platform (AMP)*”. <http://www.mhs-llc.com/custom-multi-axis-positioning-material-handling-system>. Cited page 95.
- [101] S. G. Johnson. “*The NLopt nonlinear-optimization package*”. <http://ab-initio.mit.edu/nlopt>. Cited pages 97, 104, and 107.
- [102] S. S. Rao. “*Engineering Optimization: Theory and Practice*”. John Wiley & Sons, 2009. Cited pages 99, 108, 112, and 113.
- [103] L. Luksan. “*Low-storage BFGS algorithm*”. <http://www.uivt.cas.cz/luksan/subroutines.html>. Cited page 104.
- [104] A. Löhne. “*Vector Optimization with Infimum and Supremum*”. Springer, 2011. Cited pages 107 and 108.
- [105] Y. Censor. “*Pareto Optimality in Multiobjective Problems*”. *Appl. Math. Optimiz.*, 4: 41–59, 1977. Cited page 108.
- [106] K. Deb. “*Multi-Objective Optimization using Evolutionary Algorithms*”. John Wiley & Sons, Ltd, Chichester, England, 2001. Cited page 108.
- [107] MATLAB. “*Global Optimization Toolbox*”. <http://www.mathworks.com>. Cited pages 108 and 118.
- [108] D. Q. Nguyen, M. Gouttefarde, O. Company and F. Pierrot. “*On the Analysis of Large-Dimension Reconfigurable Suspended Cable-Driven Parallel Robots*”. *IEEE International Conference on Robotics and Automation (ICRA)*, 2014. Cited page 118.

Résumé

Cette thèse propose un cadre d'étude des robots parallèles à câbles (RPC) reconfigurables. Sa contribution se décompose en trois parties.

1. Proposition d'architectures de RPC reconfigurables de grande dimension - Ces architectures sont destinées à remplacer certains moyens classiques de manipulation de pièces lourdes et/ou volumineuses au travers d'un vaste espace de travail, par exemple dans un atelier d'usine ou dans un hangar de maintenance d'avions.
2. Outils d'analyse utiles à la conception et à la commande de RPC (reconfigurables) - Diverses problématiques sont abordées tels que les modélisations cinématique, dynamique et élasto-statique des RPC et la détection de collisions de câbles.
3. Méthodes et outils de résolution efficace du problème de la reconfiguration d'un RPC - Considéré comme un problème d'optimisation non linéaire, l'étude se concentre sur des méthodes de reformulation du problème sous des formes standards. Les reconfigurations optimales du RPC peuvent alors être déterminées à l'aide de méthodes classiques d'optimisation.

Mots clefs : *Robots parallèles à câbles, reconfiguration, modélisation*

Abstract

In this thesis, a fundamental framework for reconfigurable cable-driven parallel robots (CDPR) is developed. It consists of three main parts:

1. Propositions of general architectures of large-dimension reconfigurable CDPRs which can be used to replace conventional means of handling large and heavy parts across a wide workspace, e.g., in a factory workshop or in an airplane maintenance workshop.
2. Analysis tools that can aid the design and control of a general (reconfigurable) CDPR. Various issues are addressed including kinematic, dynamic and elastostatic modeling, collision detections and cable modeling.
3. Methods and tools to solve the CDPR reconfiguration problem efficiently. This problem is considered as a general nonlinear optimization problem. The thesis focuses on methods to formulate this optimization problem into standard forms which can be solved by using available (suitable) optimization software in order to obtain optimal CDPR reconfigurations.

Keywords: *Cable-driven parallel robots, reconfiguration, kinetostatic models*
